

A MAGNETOTELLURIC INVESTIGATION OF
PEMBERTON AREA, BRITISH COLUMBIA

by
PETER O. SULE

B. Sc., Ahmadu Bello University, 1973

A THESIS SUBMITTED IN PARTIAL FULFILMENT
OF THE REQUIREMENTS FOR THE DEGREE OF
MASTER OF SCIENCE

in the Department
of
Geophysics and Astronomy

We accept this thesis as conforming
to the required standard

THE UNIVERSITY OF BRITISH COLUMBIA
October, 1976

© Peter O. Sule, 1976

In presenting this thesis in partial fulfilment of the requirements for an advanced degree at the University of British Columbia, I agree that the Library shall make it freely available for reference and study.

I further agree that permission for extensive copying of this thesis for scholarly purposes may be granted by the Head of my Department or by his representatives. It is understood that copying or publication of this thesis for financial gain shall not be allowed without my written permission.

Department of GEOPHYSICS AND ASTRONOMY

The University of British Columbia
2075 Wesbrook Place
Vancouver, Canada
V6T 1W5

Date December 6, 1976

ABSTRACT

The magnetotelluric method has been used in the determination of the electrical conductivity structure of the Pemberton area of British Columbia. Meager Mountain, which is at the junction of the Garibaldi volcanic belt and the Pemberton volcanic belt, is the focus of a detailed geothermal resource evaluation. The aim of this project is to determine whether there is a resistivity structural change across the Pemberton volcanic belt. A knowledge of this will give some information about the structural control. This will aid in the investigation of any correlation between the electrical conductivity structure and the hot springs which almost circumscribe Meager Mountain.

The temporal variations in the electric and magnetic components of the earth's field were recorded at Alta Lake (ALT), Pemberton (PEM) and D'Arcy (DAR) from July to September 1975. This profile runs across the Pemberton volcanic belt. Selected sections of the analogue data were converted to digital form and power spectral analyses were made on the latter. The computed apparent resistivity curves show a discrepancy between the EX/D and EY/H which indicates the presence of a resistivity anisotropy/inhomogeneity in the region. Since there is some power in the vertical magnetic component (Z) in the region, it can be concluded that there is inhomogeneity in the conductivity structure. Also the computed Z power attenuation ratios between stations infer that any lateral conductivity change does not persist to large depths. It is also deduced that Z power increases slightly from ALT towards DAR.

Some of the difference between the EX/D and EY/H apparent resistivity curves may be due to near surface inhomogeneities and the physical topography of the region. However, the bulk of this difference can be explained by considering a vertical fault zone near PEM, with ALT and PEM on the up-fault and DAR on the down-fault structure. The wider displacement between the EX/D and EY/H curves at DAR as compared to ALT can then be due to the fact that ALT is nearer the fault zone than DAR. On the basis of this interpretation one would expect a more pronounced change in the vertical magnetic component than observed.

Apparent resistivity type curves for several theoretical layered earth models were computed and matched with the experimental curves. The results thus obtained indicate that the electrical resistivity structure in the Pemberton area fits the following layered earth model. The upper crustal layer has a resistivity of the order of 300 ohm-m and a thickness of about 40 km under ALT and PEM and about 60 km under DAR. At ALT and PEM, this layer is underlain by a more conductive material of resistivity about 30 ohm-m and a thickness of approximately 20 km. There is no trace of this layer at DAR. The resistivity value of this second layer is of the same order of magnitude as those usually reported from regions of geothermal investigations. The next layer at all the stations is highly resistive (greater than 2000 ohm-m) and has a thickness of about 500 km. This is underlain by a highly conductive basement having a resistivity of about 10 ohm-m or less.

From the overall result, it is evident that there is a resistivity change across the structural boundary of the volcanic belt near Pemberton. In this work, this change has been designated as a vertical fault. However, the nature of the variation of Z and H powers with frequency indicates a more complex structural change, for example, a sloping interface. We have thus delineated some of the structural control in the Pemberton area.

TABLE OF CONTENTS

	page
ABSTRACT	i
TABLE OF CONTENTS	iv
LIST OF TABLES	v
LIST OF FIGURES	vi
ACKNOWLEDGEMENTS	ix
CHAPTER ONE	1
INTRODUCTION	1
1.1 General objective	1
1.2 Brief geology of the area of investigation	5
1.3 Brief outline of the thesis	12
CHAPTER TWO	15
REVIEW OF THE MAGNETOTELLURIC METHOD	15
2.1 General background	15
2.2 Source fields of MT variations	22
CHAPTER THREE	26
INSTRUMENTATION	26
3.1 General introduction	26
3.2 Field installation	29
CHAPTER FOUR	32
DATA ACQUISITION AND ANALYSIS	32
4.1 Data acquisition	32
4.2 Data reduction	33
4.3 Data analysis	47
CHAPTER FIVE	59
INTERPRETATION AND CONCLUSIONS	59
5.1 General introduction	59
5.2 Determination of resistivity distribution	60
5.3 Conclusions	103
Suggestions for further work	110
BIBLIOGRAPHY	111
APPENDICES	
A Basic magnetotelluric theory	118
B MT fields over an n-layered, homogeneous and isotropic earth	123
C MT curve matching technique	131
D Brief note on Hasegawa's MT program (1962)	133

LIST OF TABLES

Table		Page
1	Coordinates of the magneto-telluric stations	13
2	Depths of penetration (km) at various values of resistivity, ρ (ohm-m) and periods, T (seconds)	18
3	Classification of geomagnetic micropulsations	23
4	Model curve parameters	84

LIST OF FIGURES

<u>Figure</u>		<u>Page</u>
1	Schematic map showing the distribution of late Tertiary and Quaternary volcanic and plutonic rocks, oceanic ridges and earthquake epicentres (after Souther, 1976)	2
2	Locations of the magnetotelluric stations: Alta Lake, Pemberton and D'Arcy in southwestern British Columbia	6
3	Sketch map of the North American Cordillera (after King, 1969)	8
4	A chart of the depth of penetration (km) of EM waves as a function of resistivity (ohm-metre) and period (seconds)	19
5	Block diagram of the instrumentation	27
6	Sample of the total noise (recorded, playback and digitising noise) at a magnetically quiet period	34
7	Samples of the natural variations in the magnetic and the electric components at Alta Lake	36
8	Samples of the natural variations in the magnetic and the electric components at Pemberton	38
9	Samples of the natural variations in the magnetic and the electric components at D'Arcy	40
10	Block diagram representation of the digitisation process	42
11	Diagrammatic representation of the digitiser	45
12	Mean smoothed power spectra of the electric and magnetic components at Alta Lake	51
13	Mean smoothed power spectra of the electric and magnetic components at Pemberton	53

<u>Figure</u>		<u>Page</u>
14	Mean smoothed power spectra of the electric and magnetic components at D'Arcy	55
15	Mean coherence between the orthogonal electric and magnetic components at each station	57
16	Two-layer standard resistivity curves (after Yungul, 1961)	61
17	Two-layer standard phase angle curves (after Cagniard, 1953)	63
18	Phase angles between the orthogonal electric and magnetic components at Alta Lake	65
19	Phase angles between the orthogonal electric and magnetic components at Pemberton	67
20	Phase angles between the orthogonal electric and magnetic components at D'Arcy	69
21	Apparent resistivity curves at Alta Lake	71
22	Apparent resistivity curves at Pemberton	73
23	Apparent resistivity curves at D'Arcy	75
24	Computed apparent resistivity model curves drawn on the experimental data at Alta Lake	78
25	Computed apparent resistivity model curves drawn on the experimental data at Pemberton	80
26	Computed apparent resistivity model curves drawn on the experimental data at D'Arcy	82
27	The derived MT model for the Pemberton area	90
28	Z-transfer function at Alta Lake	92
29	Z-transfer function at Pemberton	94
30	Z-transfer function at D'Arcy	96
31a	Power ratios, Z/H at each station	98
31b	Power attenuation (standard impedance) ratios	100
31c	Ratios of the power in the Z component at Alta Lake and D'Arcy to that at Pemberton	104

<u>Figure</u>		<u>Page</u>
32	(A) MT structural model of Western Canada by Caner et al. (1969)	106
	(B) MT structural model for Victoria by Caner and Auld (1968)	
33	Model of source-free, homogeneous and isotropic half-space	119
34	Isotropic n-layered earth model showing layer thickness and resistivity notation used in the theoretical formulation.	124

ACKNOWLEDGEMENTS

I would like to express my sincere thanks to Dr. H. Dragert who supervised this project from the beginning until the end of June 1976 when he left the university to work for the government in Ottawa. The computer programs he generously made available to me are highly appreciated. My special thanks to Dr. R. M. Ellis who supervised the completion and write-up of the thesis. I am greatly indebted to Dr. L. K. Law of the Victoria Geophysical Observatory for his help and stimulating discussions during the course of this project.

The effort of R. D. Meldrum, H. Verwoerd and C. West in repairing the fault in the digitising system is greatly appreciated. My thanks are extended to fellow graduate students in the department who have provided help, particularly W. B. Cumming whose demultiplexing program I used.

I would also like to express my sincere gratitude to all others who have in any way helped in the successful completion of this work.

The Study Fellowship award by Ahmadu Bello University, Zaria is greatly appreciated. Throughout the entire duration of this work, I have been supported by the Canadian International Development Agency Scholarship.

The reported research has been supported by a National Research Council of Canada grant to Dr. H. Dragert. Field program assistance has been rendered by Victoria Geophysical Observatory.

CHAPTER ONE

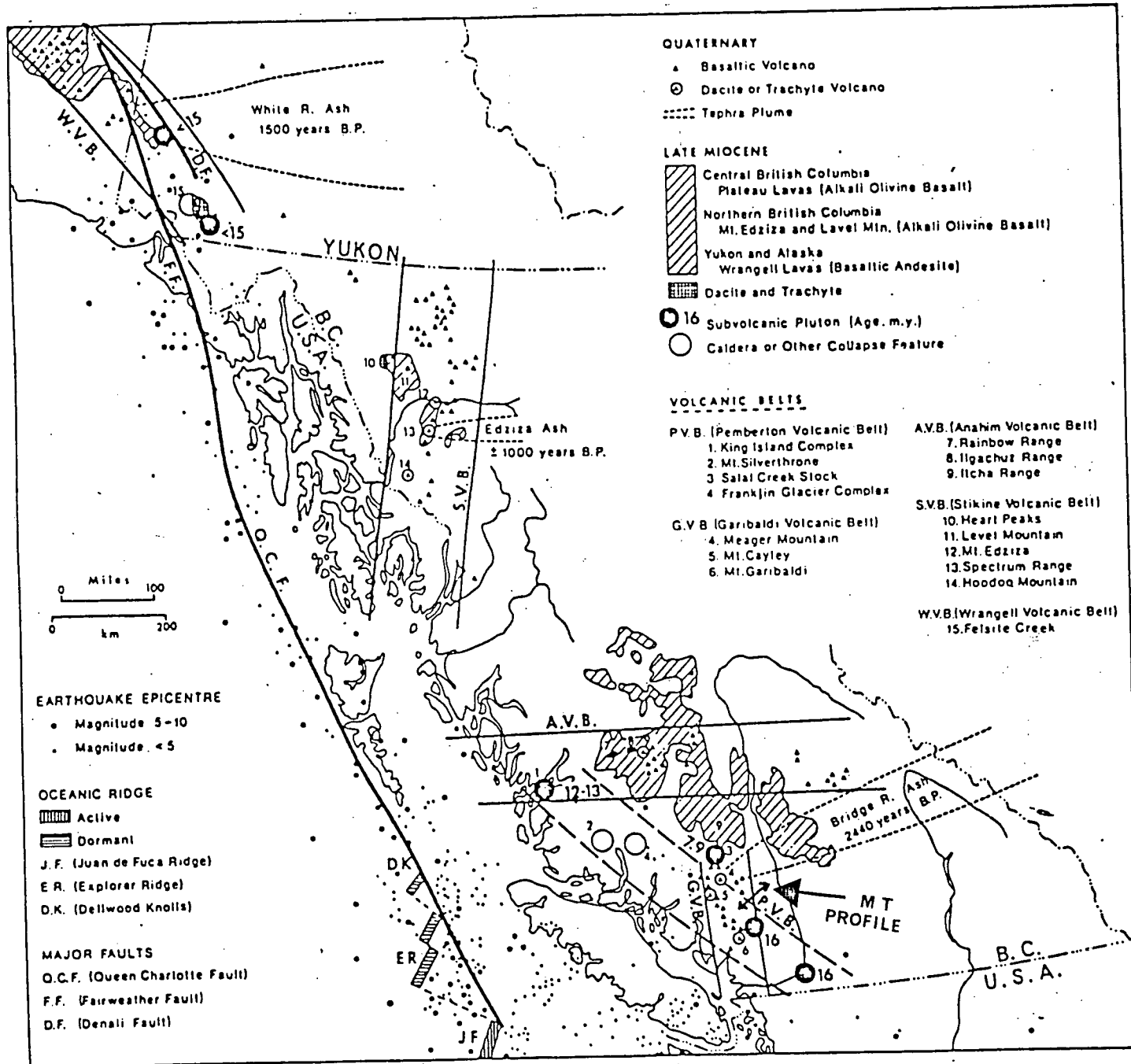
INTRODUCTION

1.1 GENERAL OBJECTIVE

In the search for alternative sources of energy to supplement the fossil fuels, it has been recognized that geothermal power (the production of electricity using the natural heat of the earth) has a promising potential. Consequently, an investigation of the geothermal resource potential of western Canada was begun in 1972 by the Department of Energy, Mines and Resources. From this investigation of the Canadian Cordillera, five broad thermal anomalies extending through the west-central British Columbia and Southern Yukon have been delineated. These anomalies correspond to well-defined belts of Quaternary volcanoes including more than 100 post-glacial eruptive centres (Souther, 1976). Fig. 1 shows the distribution of these volcanic belts. Meager Mountain, which is the junction of the Garibaldi volcanic belt and the Pemberton volcanic belt (Fig. 1), has been the focus of a detailed geothermal resource evaluation by the British Columbia Hydro and Power Authority since 1974. On the Garibaldi and Pemberton volcanic belts, six groups of thermal springs lie along the same lineament as the Miocene plutons. The hottest of these springs issues from fractured granodiorite at several points around the periphery of Meager Mountain, a Quaternary dacite and andesite volcano from which the 2000-years-old Bridge River ash was erupted (Souther, 1976).

A joint plan to run a magnetotelluric and geomagnetic depth sounding (MT/GDS) profile at Meager Creek, across the Pemberton volcanic belt and across the Garibaldi volcanic belt was made by the Victoria Geophysical Observatory and the University of British Columbia in 1974. The MT/GDS profile at Meager Creek and across the Pemberton volcanic belt

FIG. 1 Schematic map showing the distribution of late Tertiary and Quaternary volcanic and plutonic rocks, oceanic ridges and earthquake epicentres (after Souther, 1976). The profile used in this project is indicated by an arrow.



was done in 1975, but that across the Garibaldi volcanic belt will be done in the future. A preliminary interpretation of the data obtained from the profile across the Pemberton volcanic belt is presented in this thesis. The interpretation of the Meager Creek data is in progress at Victoria.

The presently observable natural heat of the earth arises mainly from the decay of radioactive elements in the crust and the mantle. Most of this heat is too diffuse to ever be economically exploited by man. Generally, the earth's temperature increases by only a few degrees centigrade per kilometre of depth (10-30°C per km) but locally in some areas of the crust where hot or molten rock is present, the thermal gradient may be many times higher than normal. Only these rare anomalous regions where abnormally high temperatures exist at shallow enough depths to be reached by drilling constitute potential geothermal resources. The two most commonly used geophysical techniques of investigating these anomalous regions are heat flow measurements and the resistivity method. The latter has been used in this project. The MF method has been used instead of the ordinary electrical resistivity methods because this is a broad scale preliminary investigation and hence the need to take advantage of the much greater depths of penetration of the MF method.

Regions of high thermal gradient give rise to high conductivity values (that is, low resistivity values). How high the value of the conductivity is, depends on the temperature increase of the rock, its permeability and its environment, that is, whether hot water, brine or steam is present.

Thus, the objective of this work is to determine the regional electrical conductivity structure of the Lillooet valley in the Pemberton area using the MF method. A knowledge of the electrical conductivity structure will aid in understanding the fault systems associated with the volcanic belts and thus give information about the structural control.

This will help in the investigation of any correlation between the electrical conductivity structure and the hot springs which almost circumscribe Meager Mountain.

1.2 BRIEF GEOLOGY OF THE AREA OF INVESTIGATION

The area investigated in this work is the Pemberton area and the observing stations used in the project are at Alta Lake, Pemberton and D'Arcy (Fig. 2). In as far as this project is concerned, the Pemberton area refers to the region lying roughly between latitude 50 and 51 degrees North and longitude 122 and 123 degrees West.

Detailed geological studies of the Pemberton area have not been published and consequently only a brief regional geological description, extracted mainly from the work on the Canadian Cordillera will be presented.

The Pemberton area lies within the Coast Range Plutonic Complex of the Canadian Cordillera which forms part of the Circum-Pacific orogenic belt. This belt is the main potential geothermal source region of the world as a result of the recent and ongoing volcanic activities. Fig. 3 shows a sketch map of the Cordillera.

The Coast Range Plutonic Complex, which underlies almost the entire Coast Mountains, is one of the world's largest Phanerozoic granitic masses. It comprises a mosaic of coalescing, northwesterly elongate granitic plutons that are younger and more potassic eastward and subordinate narrow belts of metamorphic rocks (Price and Douglas, 1972).

The oldest known rocks in the Coast Range Plutonic Complex are Mississippian. In the Coast Mountains are basalt, andesite, acid volcanic rock, sandstone, conglomerate, pelite and carbonate of Mississippian, Pennsylvanian and Permian ages. These assemblages are possibly remnants of island arcs with no positive information on the

FIG. 2 Locations of the magnetotelluric stations:
Alta Lake, Pemberton and D'Arcy in southwestern
British Columbia. The numbers on the map show
elevations in metres and the scale of the map
is 1:1,000,000.

123°W

122°W

51°N

50°

49°N

COAST MOUNTAINS

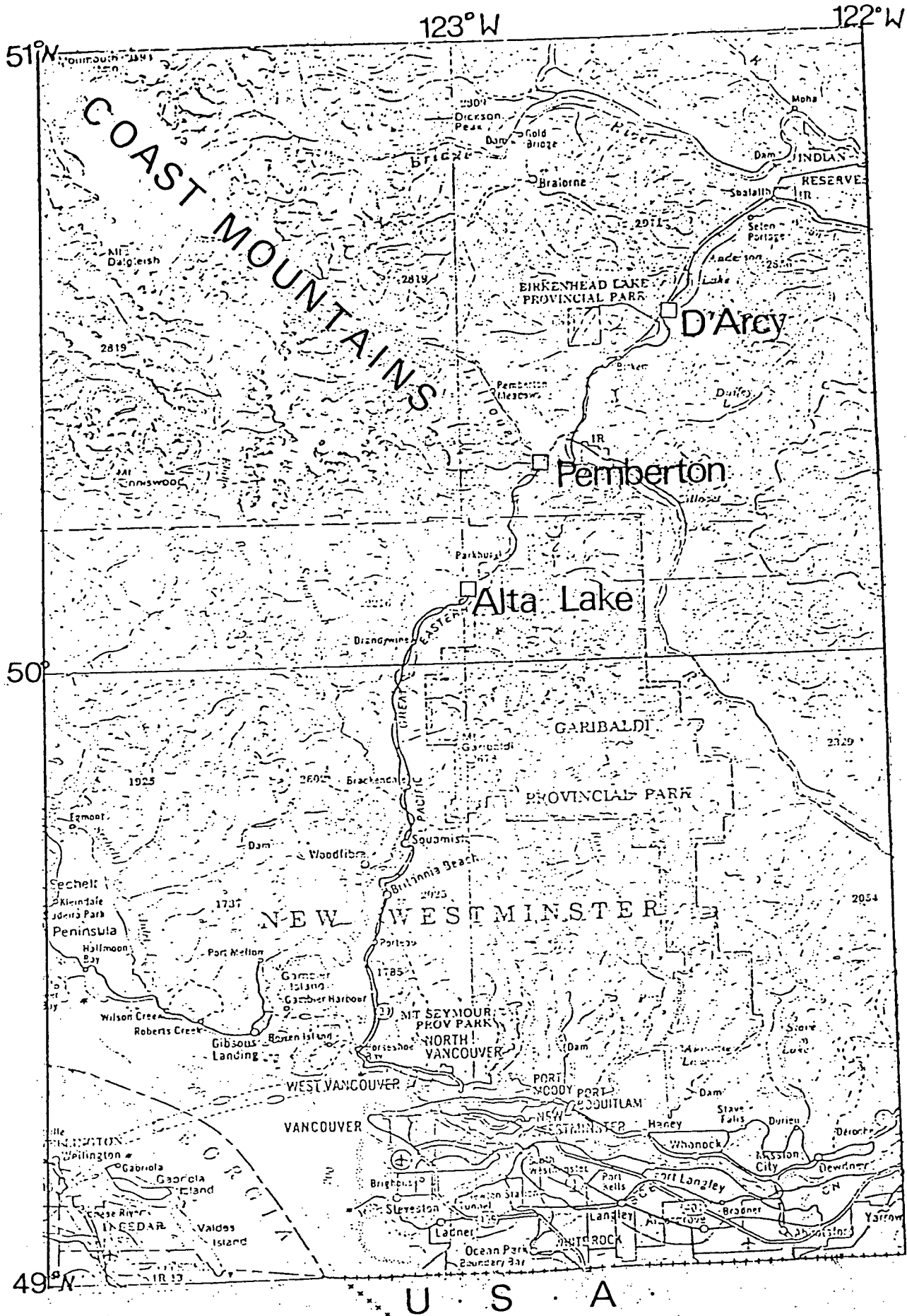
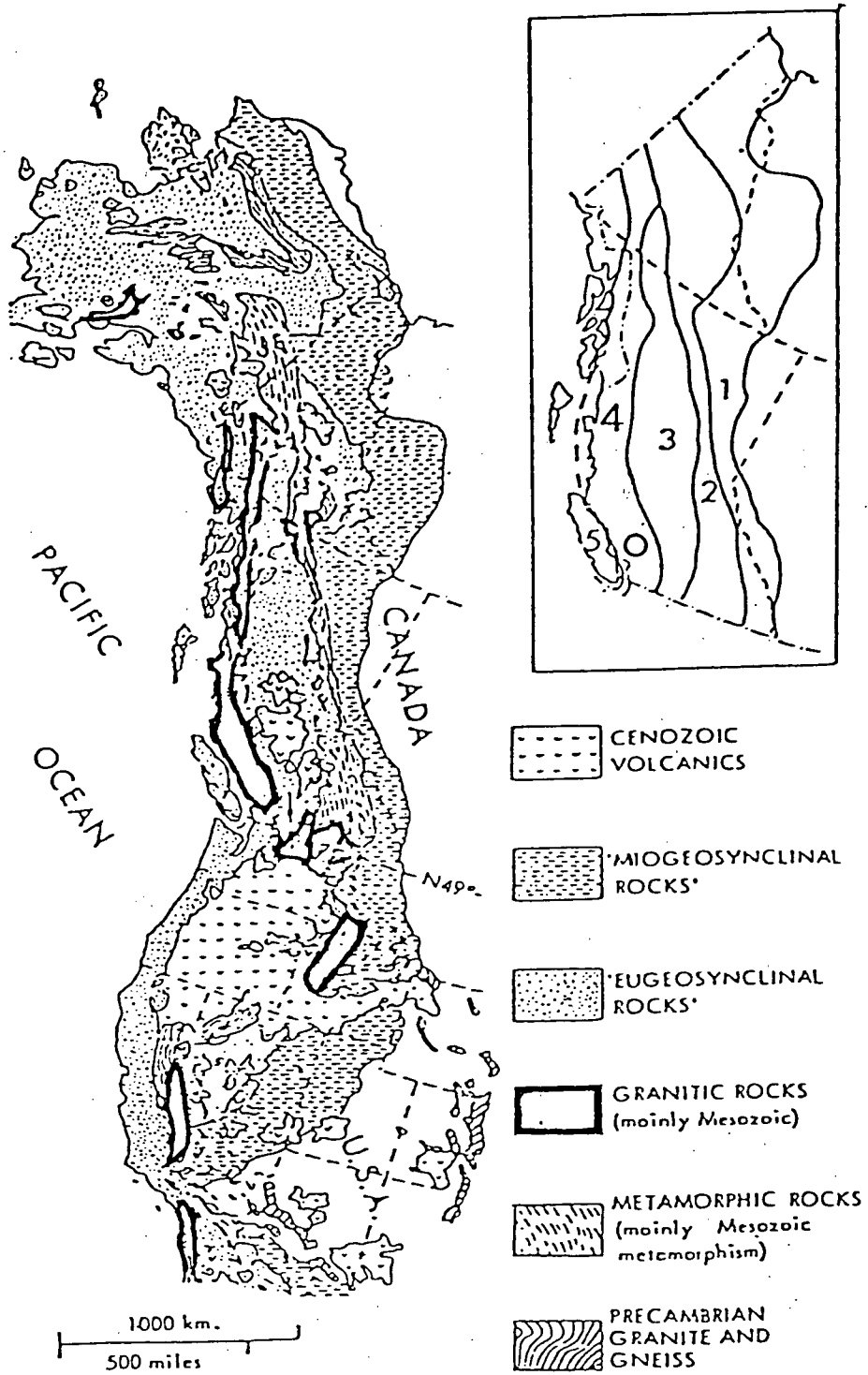


FIG. 3 Sketch map of the North American Cordillera (after King, 1969). "Eugeosynclinal" and "Miogeosynclinal" rocks refer to the stratified assemblages respectively with and without volcanic rocks. The inset map shows the location of the geological and physiographic belts of the Canadian Cordillera. These are (1) Rocky Mountain Belt, (2) Omineca Crystalline Belt, (3) Intermontane Belt, (4) Coast Plutonic Complex and (5) Insular Belt. (Taken from Monger, et al., 1972). The circle on the inset shows the Pemberton area.



polarity of the arcs and little precise information on when they were active (Monger et al., 1972). The Coast Range Plutonic Complex of granitic and subordinate metamorphic rocks has evolved from a terrane which may include pre-Devonian crystalline basement; this was probably the site of a late Paleozoic volcanic arc (Price and Douglas, 1972).

In the late Cretaceous and Eocene time, the Cordillera with the exception of the Rocky Mountain Belt was the site of extensive, continental explosive acidic to intermediate volcanism (Souther, 1967, 1970b). North of latitude 52 degrees North, the Coast Plutonic Complex was the site of early Mesozoic volcanism and late Mesozoic plutonism and uplift, whereas to the south, sedimentation prevailed until terminated by late Mesozoic plutonism and uplift (Price and Douglas, 1972). Granitic plutons of Tertiary ages make up 80 per cent of the Coast Range Plutonic Complex.

Miocene and later volcanism in the Cordillera was generally very different in character from that of the Eocene. Although the style of volcanism changed by the late Pliocene and through the Quaternary, most lavas still appear to belong to the alkali-olivine basalt suite.

In contrast to the Miocene lava sheets, these are mainly small separate centres. Some of these are merely isolated cinder cones active as recently as about 200 years ago. Others comprise large composite volcanoes, such as Mount Edziza in northwestern British Columbia, where volcanics range from picrite basalt to rhyolite (Monger et al., 1972). In southwestern British Columbia, the Mount Garibaldi Centre (Mathews, 1958) is more andesitic in overall composition and is an intraglacial dacite dome that erupted about 10,000 years ago.

The change from Eocene calcalkaline lavas associated with the sub-volcanic plutonic rocks to the Miocene and younger alkaline olivine basalts is quite fundamental. The Eocene (and older) volcanics are

interpreted as having formed above an east-dipping offshore subduction zone (Souther, 1970a). The Miocene and younger lavas show no change in composition with distance from the continental margin and hence, may be quite unrelated to any subduction zone (Monger et al., 1972).

The geological formations in the Pemberton area include highly deformed volcanic and sedimentary rocks of Upper Triassic age, sediments which may be of Cretaceous age, batholithic rocks intruded in the Upper Jurassic - Cretaceous periods and unconsolidated glacial and stream deposits (Cairnes, 1924). Although no conclusive evidence has been obtained, the batholithic intrusives are believed to have resulted from two different periods of intrusion, one before and the other after the deposition of the Cretaceous sediments.

Upper Triassic rocks form a broad belt, extending northwesterly across the central parts of the region and this belt is referred to as the Pemberton band (Camsell, 1917). The members of this band include both volcanic and sedimentary rocks which are often indistinguishable in most cases and in this locality, fossils have not been found.

The N - NW trending Pemberton volcanic belt (Fig. 1) is a late Miocene volcanic front related to an early stage of spreading from Juan de Fuca - Explorer ridge system and subduction of Juan de Fuca plate (Souther, 1976). This volcanic belt is defined by a group of epizonal plutons and two deeply eroded cauldron complexes, Mt. Silverthron and Franklin Glacier complexes (Ney, 1968). The plutons are believed to be subvolcanic bodies associated with a Miocene volcanic front that was active during the early stages of subduction of Juan de Fuca plate. With the notable exception of King Island, all the plutons and eruptive rocks are calc-alkaline, mainly granodioritic bodies and dacite ejecta, whereas the coeval plateau lavas are uniformly alkaline basalts, suggesting a paired relationship analogous to an arc, back-arc association (Souther,

1976). The Miocene volcanic front is crossed at an acute angle by a line of approximately 32 Quaternary centres that comprise the Garibaldi volcanic belt (Fig. 1). Dacite and andesite are the predominant rock types, associated with minor rhyolite and high-alumina basalt. The youngest activity occurred less than 2500 years ago from a vent near Meager Mountain. Explosive eruption of dacitic pumice produced a thick welded ash flow in the upper Lillooet valley and a plume of air-fall pumice that settled over a wide area of southern British Columbia. The latter, called the Bridge River ash, is dated at 2440 ± 140 years B.P. (Nasmith et al., 1967).

1.3 BRIEF OUTLINE OF THE THESIS

The main objective of this work, as stated earlier, is to determine the electrical conductivity structure of the Pemberton area using the MT method. To accomplish this, the temporal variations in the magnetic and electric components of the earth's field (3 magnetic and 2 electric components) were recorded at Alta Lake (ALT), Pemberton (PEM) and D'Arcy (DAR) (Fig. 2) from July to September, 1975. The coordinates of these stations are given in Table 1. Selected portions of the analogue data were digitised at 1 second intervals. A data section of 60 minutes duration constituted a data file. The digital data were analysed using the power spectral technique. The apparent resistivities were calculated using Cagniard's MT theory (1953). The phase angles and the coherence between the orthogonal electric and the magnetic components were also calculated. The phase angles were used in a qualitative interpretation at the stations. In finding the averages of all the data files at each station, only those points showing a coherence of 0.7 or higher were used. By matching the experimental apparent resistivity curves with calculated mathematical models (curve matching

Table 1 Location of the MT stations

Station	Geographic Latitude	Coordinates Longitude	Geomagnetic Latitude	Coordinates Longitude	Distance from Vancouver (km)
Alta Lake (ALT)	50.1°N	123.0°W	55.8°N	67.3°W	114
Pemberton (PEM)	50.3°N	122.8°W	56.0°N	67.3°W	138
D'Arcy (DAR)	50.6°N	122.5°W	56.4°N	67.1°W	176

technique), the earth parameters - layer thickness and resistivity - at the stations were estimated.

In order to determine whether the region is characterised by any strong anisotropy and inhomogeneity, the ratio of the power in the vertical magnetic component to that in the horizontal magnetic components (Z/H) and the Z-transfer function at each station and the relative Z power attenuation ratios between stations were calculated.

The general principles of the MT method are reviewed (chapter 2). Following this, the instrumentation used in this project is briefly described (chapter 3), the data acquisition and analysis are discussed (chapter 4) and finally, the interpretation and conclusions are presented (chapter 5).

CHAPTER TWO

REVIEW OF THE MAGNETOTELLURIC METHOD

2.1 GENERAL BACKGROUND

The magnetotelluric (MT) method, as the name implies, is a combination of the magnetic and telluric methods. By this technique, the conductivity distribution of the subsurface is determined from a comparison at the earth's surface of the orthogonal horizontal magnetic and electric components of the transient fields associated with the telluric current flows resulting from naturally occurring electromagnetic (EM) disturbances.

The recognition that the transient geomagnetic variations and the telluric currents flowing in the ground are closely related stemmed from the early work of Tikhonov (1950), Rikitake (1950, 1951) and Kato and Kikuchi (1950). However, the MT method of prospecting did not actually develop rapidly until after the 1953 classic paper of Cagniard in which the basic concepts of the MT method were treated. In addition, Cagniard presented master curves (phase and apparent resistivity) for the two layer case. These curves were normalised so that they were applicable to different geological models.

The assumptions encompassed in Cagniard's MT theory can be summarised as follows:

(i) The field quantities (magnetic and electric) vary harmonically or can be decomposed into harmonic form.

(ii) A plane EM wave is incident on the earth's surface. This implies that the horizontal space variations in the magnetic field are negligible compared to the vertical ones.

(iii) The earth is horizontally stratified. This implies that the vertical component of the magnetic field is negligible compared

to the horizontal components.

Under the above conditions, Cagniard showed (refer to Appendix A) that the variation of resistivity with depth can be determined from the apparent resistivity given by

$$\rho_a = 0.2 T \frac{|\underline{E}|^2}{|\underline{H}|^2} \quad (2.1)$$

where \underline{E} and \underline{H} are functions of period,

ρ_a = apparent resistivity expressed in ohm metres (ohm-m),

T = period of the EM wave disturbance in seconds,

$|\underline{E}|$ = amplitude of the variation in the horizontal electric field expressed in millivolt per kilometre (mv/km),

$|\underline{H}|$ = amplitude of the variation in the horizontal magnetic field expressed in gammas (γ).

Berdichevsky (1960) extended Cagniard's formulae to an n-layer case (see Appendix B). Yungul (1961) has presented a catalogue of standard resistivity curves for the three-layer earth models, while Srivastava (1967) has presented two - and three - layer master curves for the interpretation of the MT field data. The solutions of the vertical fault problem for the case when the magnetic field is everywhere parallel to the trace of the fault (H polarisation) have been obtained by d'Erceville and Kunetz (1962) and extended to the case of a dike discontinuity by Rankin (1962). From a consideration of a non-homogeneous two dimensional structure representing a conductive sediment-filled graben surrounded by crystalline rocks, Wright (1970) has shown that the failure of the apparent resistivity curves to converge at long periods does not necessarily indicate anisotropy or inhomogeneity at depth, but that it is equally possible to arise from a near-surface distortion of the telluric currents.

The ability to distinguish one layer from another is termed the resolving power. The resolving power of the MT method depends on the thickness and the resistivity contrast of the different layers. Lack of resolving power for very high resistivity layers is inherent in almost all MT data. The effect of each layer appears gradually rather than abruptly so that a very thin layer would not be detected unless it has a very high conductivity. However, this tendency to average together minor features makes it possible to detect weakly systematic variations which would otherwise be lost with a higher resolving power. Thus, it can be viewed that gross structural features are emphasised at the expense of the finer details. This characteristic carries over to the two dimensional case, so that structural features may show up even though traverses do not directly cross over them and thus justifying large traverse spacings (Vozoff, 1972).

The fundamental advantage of the MT method over conventional electrical resistivity methods is the greater depth of penetration. The conventional resistivity methods are limited by the inverse square law for point sources, while the penetration of plane EM waves in a uniform conductor is given by the skin depth

$$P = \left(\frac{1}{2\pi} \right) \sqrt{10 \rho T} \quad (2.2)$$

where

P = depth of penetration (in km),

ρ = resistivity (in ohm-m),

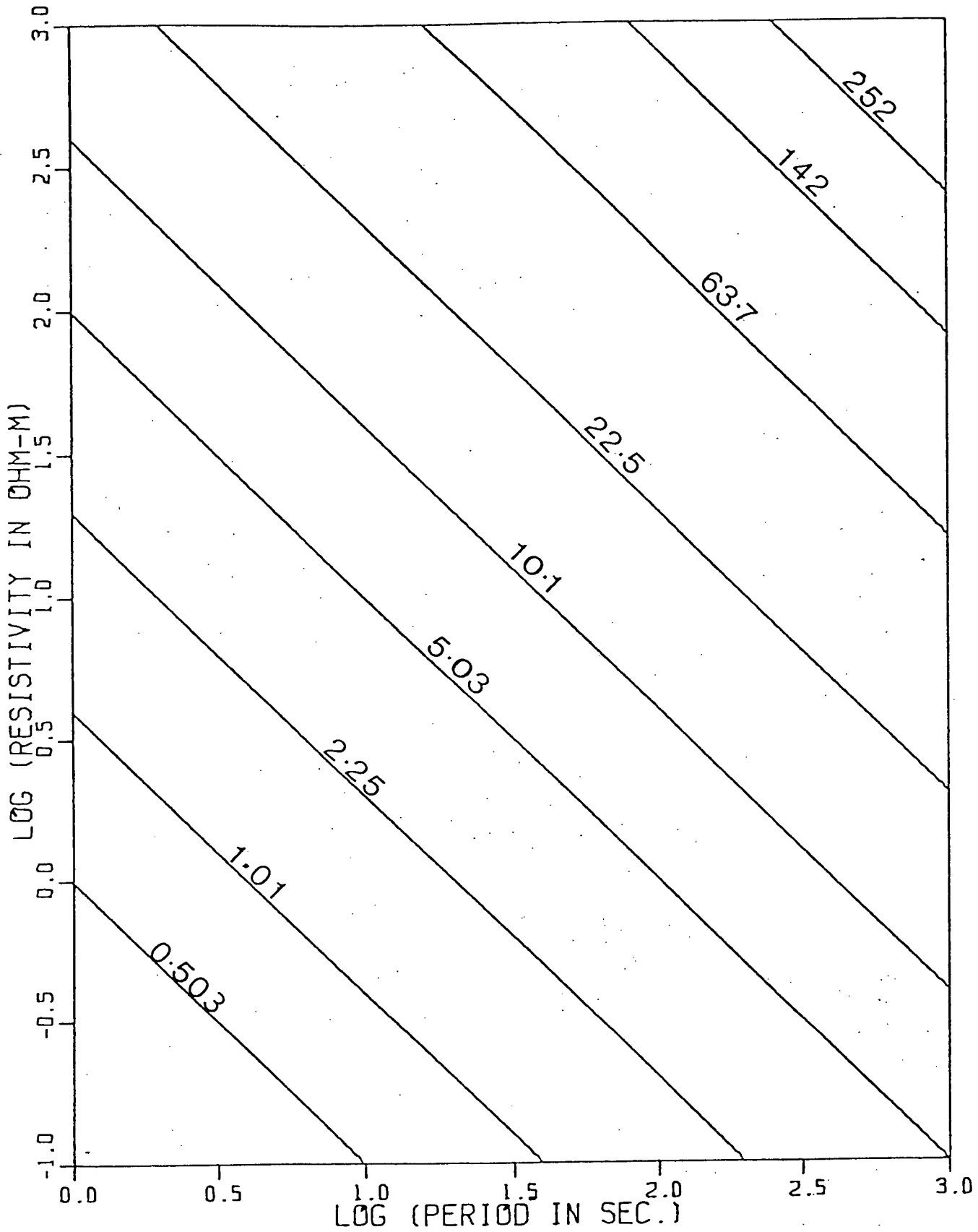
T = period (in seconds).

To illustrate how the order of magnitude of P varies with ρ and T , Table 2 shows calculated values of P for different chosen values of ρ and T and Fig. 4 shows a chart of P as a function of ρ and T . Thus, the exploration of any depth of the earth would be attainable if the wealth of frequencies in the spectrum of the EM waves could be suitably utilized. Another advantage of the MT method is that it makes possible a

Table 2 Depths of penetration (in km) at various values of resistivity, ρ (in ohm-m) and periods, T (in seconds)

ρ (ohm-m) ↓	T(sec.) →								
	1	5	10	20	60	100	200	600	1000
0.2	0.225	0.503	0.712	1.01	1.74	2.25	3.18	5.51	7.12
0.4	0.318	0.712	1.01	1.42	2.47	3.18	4.50	7.80	10.1
0.5	0.356	0.796	1.13	1.59	2.76	3.56	5.03	8.72	11.3
1	0.503	1.13	1.59	2.25	3.90	5.03	7.12	12.3	15.9
2	0.712	1.59	2.25	3.18	5.51	7.12	10.1	17.4	22.5
10	1.59	3.56	5.03	7.12	12.3	15.9	22.5	39.0	50.3
20	2.25	5.03	7.12	10.1	17.4	22.5	31.8	55.1	71.2
40	3.18	7.12	10.1	14.2	24.7	31.8	45.0	78.0	101
50	3.56	7.96	11.3	15.9	27.6	35.6	50.3	87.2	113
80	4.50	10.1	14.2	20.1	34.9	45.0	63.7	110	142
250	7.96	17.8	25.2	35.6	61.6	79.6	113	195	252
400	10.1	22.5	31.8	45.0	78.0	101	142	247	318
1000	15.9	35.6	50.3	71.2	123	159	225	390	503
5000	35.6	79.6	113	159	276	356	503	872	1130

FIG. 4 A chart of the depth of penetration (km) of EM waves as a function of resistivity (ohm-metre) and period (seconds).



single-station interpretation in the case of a uniform or horizontally layered earth. Finally, nature provides the signal source.

The interpretation of the MT data is usually subject to a number of ambiguities among which are: surface layer effects, inhomogeneities/anisotropies and to a limited extent source field wavelengths (dimensions). Its logistics (long lines, ground contacts, etc.) are fairly complicated. It is often difficult to obtain consistent results from several stations. The latter difficulty is partly due to the above mentioned ambiguities and to some extent because of lack of coherent energies (contamination by noise) at all frequencies of interest. MT signals in the higher frequency (greater than 0.1 Hz) spectrum are often of low coherence and are probably generated by local sources and thus inhibiting the usefulness of the MT method at these frequencies (Price, 1962).

From an investigation of the effect of non-plane wave sources on the MT theory, Wait (1954) has pointed out some limitations of Cagniard's plane wave analysis and has shown that corrections for second and higher order spatial derivatives of the source fields must be applied in the cases where the tangential electric and magnetic fields vary appreciably in a horizontal distance comparable with the skin depth in the ground. Price has shown that the limitations mentioned by Wait (1954) become more stringent when the dimensions and distribution of the source field are considered and that this is true even if the field is on a global scale and the depths being probed are quite moderate. The modifications which occur when the source dimensions are taken into account in the case of MT fields over an n-layered earth are indicated in Appendix B. Madden and Nelson (1964), Srivastava (1965), Caner (1969) and others, from a consideration of realistic earth models in their MT data interpretations with and without source effects, have shown that Cagniard's wave assumption

is valid in the vast majority of geological situations for MT periods less than 1000 seconds. Thus, it would appear that the source effect on the MT theory becomes significant only at the very long periods. In the present work, the influence of the source dimension has been neglected. This seems reasonable because of the similarity of the power spectra of the horizontal magnetic components at the stations which is probably indicative of the uniformity of the source fields in the region of investigation. Also, the distance separations of the stations used in this project are small compared with the height of the source fields.

Analog model studies for two and three dimensional bodies have been conducted by Rankin et al. (1965) and Dosso (1966a, b). Investigations of this type are particularly useful in problems which are not amenable to analytical solutions. An excellent review of the MT theory for a layered medium has been given by Wait (1962).

2.2 SOURCE FIELDS OF MT VARIATIONS

Geomagnetic micropulsations in the frequency range 0.001 to 1 Hz are the usual MT source fields. Continuous variations (fluctuations) of the earth's magnetic field with periods of the order of 10 minutes or less are collectively termed geomagnetic micropulsations. These represent fine structures in the geomagnetic variations. Unlike the main magnetic field and secular variations which are of internal origin, micropulsations are of solar origin. While micropulsations with periods of a few minutes may have a few hundred gammas amplitude in the auroral zones, those of periods of about a second have much smaller amplitudes of the order of one-hundredth of a gamma or less. This indicates that the physical processes involved in the generation of micropulsations may differ greatly from one type to another.

From experimental knowledge, it has been recognised that micropulsations may be divided into two main classes — those of a

regular and mainly continuous nature called Pc-type and those with an irregular pattern termed Pi-type. The Pc group is further subdivided into five subgroups (Pc1 to Pc5) and Pi group into two subgroups (Pi1, Pi2) (Jacobs et al., 1964). The following table shows the various subgroups along with their period ranges.

Table 3 Classification of geomagnetic micropulsations

Type	Range of periods
Continous pulsations	
Pc1	0.2 - 5
Pc2	5 - 10
Pc3	10 - 45
Pc4	45 - 150
Pc5	150 - 600
Irregular pulsations	
Pi1	1 - 40
Pi2	40 - 150

The exact theories of the origin of geomagnetic micropulsations are not yet understood. However, the current idea about micropulsations is that they are caused by hydromagnetic (hm) waves which can be generated on the boundary of and within the magnetosphere (e.g. during plasma injection). It is generally agreed that suitable conditions for generating hm resonances exist in the upper atmosphere. These hm waves propagate in the magnetosphere both along the lines of force (toroidal pulsations) and across the lines of force (poloidal pulsations). On reaching the lower limits of the ionosphere, hm waves are observed on the earth's surface as pulsations of the magnetic field and earth currents (Jacobs, 1970). Recently, a correlation between geomagnetic micropulsations and the magnetic fluctuations in the solar wind has been observed and from this, it is inferred that some Pc3 and 4 pulsations may be of a solar wind

origin (Nourry, 1976).

It is presently believed that the Pc1 emissions constitute wave packets propagating along the field lines between conjugate points. On account of dispersion, the wave packets will spread, the low-frequency components travelling faster than the high-frequency ones, so that the observed signal on the earth's surface will be a rising tone (Troitskaya, 1967). Pi2 pulsations are believed to originate from the resonance of Alfvén waves in the magnetospheric cavity in the region of the beginning of the neutral sheet (Raspopov, 1968).

Pc2 - 4 pulsations are predominantly dayside phenomena, while Pc5 series have occurrence peaks in the morning and evening hours (Jacobs and Sinno, 1960a, b). However, Campbell (1967) has stated that the apparent duration of the pulsation signals is related to the sensitivity of the recording device. They are probably always present, but sometimes too small to detect. Pi2 pulsations have been observed to predominate in the night-time and have a maximum around local midnight. They have also been detected in the daytime (Volker, 1968). Pi1 pulsations often appear as riders on the long period Pi2 pulsations.

The simplifying assumptions usually made in MT interpretations with respect to the source fields are:-

- (i) stationarity of source;
- (ii) infiniteness of source;
- (iii) uniformity of source.

Some limitations of these assumptions have already been referred to in the last section (Wait, 1954 and Price, 1962). It is now generally accepted that as a working MT theory, the signals can be treated as plane EM waves.

When the magnetic fluctuations reach the earth's surface, most of the incident energy is reflected and a small portion is refracted into the earth. The latter travels downwards through the rocks as a magnetic field which is varying with time and hence gives rise to induced electric fields and currents, called telluric (eddy) currents, flow as a result. On account of the high conductivity of the earth relative to air, all currents, electric and magnetic fields are practically horizontal in a uniform or horizontally layered earth, irrespective of the directions of the incident fields. This is analogous to Snell's law in optics, with the velocity in the earth being orders of magnitude smaller than in the air. At each point, the currents and the electric fields are orthogonal to the associated magnetic fields in the case of isotropic media.

CHAPTER THREE

INSTRUMENTATION

3.1 GENERAL INTRODUCTION

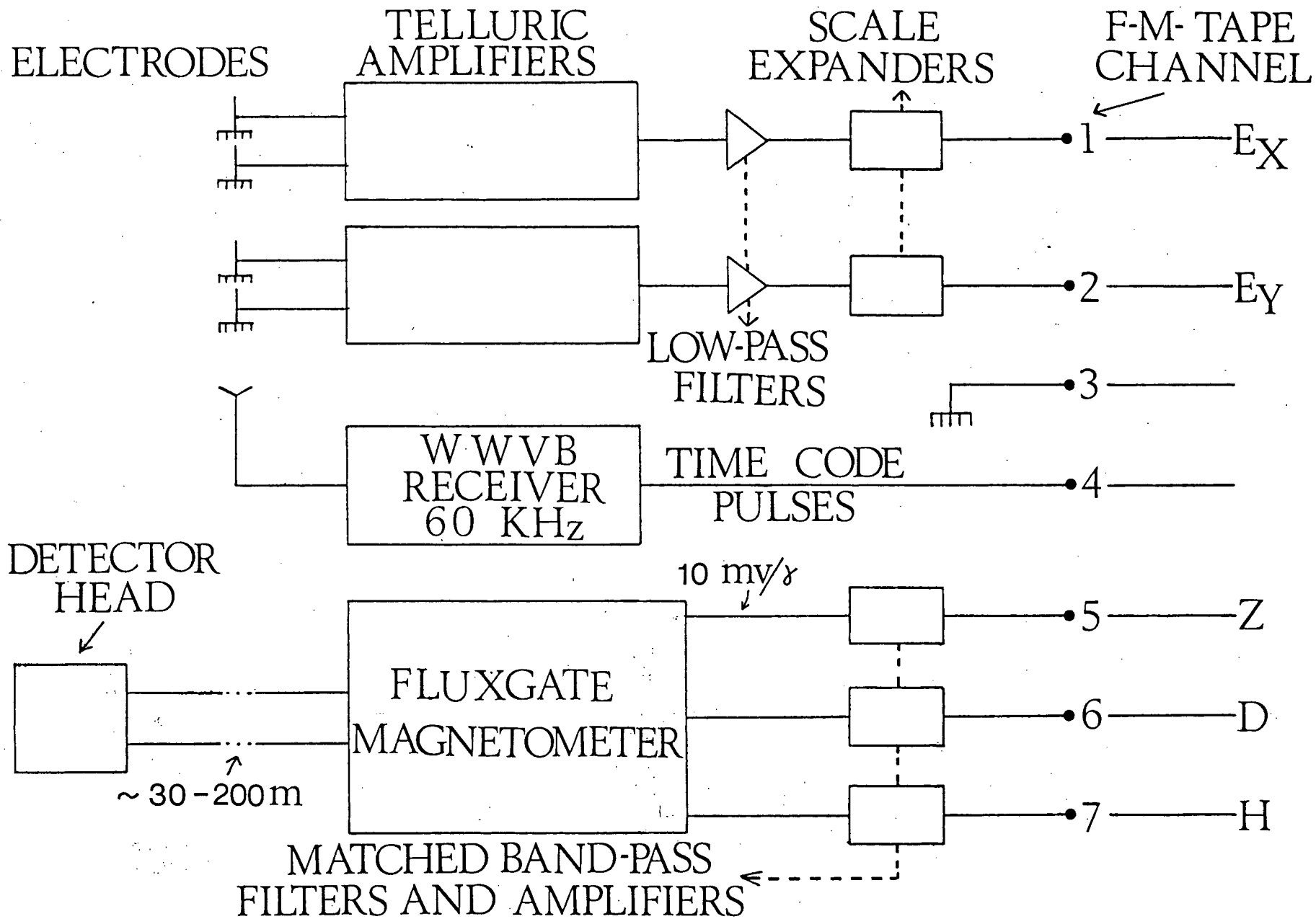
The instrumentation used in this project is a magnetotelluric adaptation of the geomagnetic depth sounding (GDS) system developed by Caner and Dragert (1972) and used for GDS field studies by Dragert (1973). Since a detailed description of this instrumentation has been published (Caner and Dragert, 1972 and Dragert, 1974), only a very brief discussion of the instrumentation will be given in this thesis.

Fig. 5 shows the block diagram of the instrumentation used in this project. The instrumentation basically consists of a fluxgate magnetometer and a telluric system. The magnetometer measures the vertical magnetic component (Z) and the two horizontal magnetic components (D and H) - these components can also be referred to as H_z , H_y and H_x respectively.

The instrumentation is suitable for geomagnetic induction data recording over a wide range of frequencies (0.1 to 100 millihertz) and uses a commercially available, saturable-core (fluxgate) magnetometer (Trigg et al., 1971) as the basic element. The frequency response (in both amplitude and phase) of the system is flat within the frequency range of interest thus permitting data analysis without frequency-dependent instrument-response corrections. For the response curves, refer to Caner and Dragert (1972).

The fluxgate magnetometer consists of a 3-component fluxgate sensing head and electronic circuitry which includes an automatic zero suppression circuit and a 3-component control unit. The sensing head, which is designed for post mounting, has appropriate levels and adjustment

FIG. 5 Block diagram of the instrumentation.



screws for correct orientation. The automatic zero suppression circuit, which was originally developed by Trigg (1970), applies a baseline shift whenever the input signal reaches a preselected limiting value. This circuit is capable of "stepping" seven times in either direction and consequently resulting in an extended dynamic range (about 18 db increase).

The telluric system consists of four galvanised steel electrodes, band pass filters and an amplifier which also includes an automatic zero suppression circuit and a 2-component control unit.

The whole electronic circuitry of the MT system is built into a single compact and portable unit mounted in a water-proof aluminium carrying-case, the inside of which is well padded to prevent any damage to the components while in transit and to serve as insulation. All connections to the system can be made externally through the appropriate terminals at the side of the aluminium case.

With this unit, three basic outputs can be obtained for each of the magnetic components - a direct output from the detecting head, a filtered output and a filtered stepped output - while for the telluric components only a filtered stepped output is available. The direct output from the detecting head was filtered (band-pass) and amplified before it was recorded on FM tape along with the amplified telluric components.

The system can either be powered by a 115V 60 Hertz power line or by two 12-volt car batteries. For this project, AC power was used but with the batteries connected as a back-up power supply.

3.2 FIELD INSTALLATION

For this project, the MT electronic circuitry and the tape recorders at the Alta Lake and D'Arcy stations were protected by a permanent shelter, while at Pemberton they were kept inside a well insulated temporary aluminium hut.

At each station, a suitable location for the fluxgate sensing head was found. Such a location, as much as possible, should be free from any disturbances by moving magnetic objects, for example, train, truck, etc. and far from stationary magnetic objects, for example, magnetic construction and steel pipe lines. The location should also be far from power transmission lines and from streams.

Since a slight tilt of the sensing head will cause a large change in the total H and D field readings and the field variations in Z will be contaminated by changes in H and D, it is necessary to support firmly in the ground the aluminium pipe on which the sensing head is mounted. It is also essential that the pipe is supported vertically in the ground to ensure that the head can be levelled using the adjustment screws and levels on it. The ideal method is to install the sensing head in a hole about 2 feet by 2 feet and 6 feet deep. The five-foot aluminium pipe is set vertically in concrete leaving about 2 feet exposed. This technique virtually eliminates the effects of temperature variation and wind vibrations and unnecessary human interference with the sensing head. However, if the ground conditions are such as to render this method impracticable, then it will suffice to simply drive the aluminium pipe into the ground leaving about 2 feet exposed. Both methods were used in this project. To prevent any vibration of the sensing head, it is essential that the length of unsupported pipe below the head does not exceed 2 feet. The head is next securely fastened to the top of the pipe. The head is properly oriented, levelled and then connected to the MF circuitry about 30 to 200 metres away using a shielded cable. After adjusting the H, D and Z baselines to zero, the hole is covered at the top with a piece of plywood which is then covered with sand for insulation. The essence of setting the H, D and Z baselines to read zero is to buck out the prevailing dc values of these components so that thereafter only variations from these dc values are recorded.

Next the telluric lines are laid out. A "north" galvanised steel electrode (2 to 3 feet in length) is driven into the ground at any suitable spot on the site leaving about 6 inches exposed. At a distance of 100 metres south (geomagnetic) of the north electrode, the south electrode is driven into the ground. Similarly, the east and west electrodes are installed at a separation of 100 metres. Each of the electrodes is then connected to the appropriate terminals on the system by means of a well insulated copper wire. The required electric field variations are obtained by dividing the observed potential differences by the electrode spacing.

CHAPTER FOUR

DATA ACQUISITION AND ANALYSIS

4.1 DATA ACQUISITION

The data recording was carried out at three stations in British Columbia - Alta Lake (ALT), Pemberton (PEM) and D'Arcy (DAR) - from July to September, 1975. The locations of these stations are shown in Fig. 2 and the station coordinates are summarised in Table 1. All stations were accessible by road and AC power was available. Due to equipment limitations, simultaneous data recording was limited to PEM and one other station.

All recordings were made on FM tapes using either a seven-channel Geotech (Model 17373) or Precision Instruments (Model PI-5100) tape recorder at a recording speed of 15/160 inches per second and within a recording band of dc to 17 Hz. Tapes 3600 feet in length allowed continuous runs for 5-1/3 days without operator attention. Throughout the duration of the recording, no major breakdown of the systems occurred. Several minor problems, such as MT line breakages, did interrupt recording.

On the first two channels of the FM tape, the electric components were recorded. The third channel was grounded so that it recorded tape noise resulting from any changes in the tape speed. The latter allowed automatic "flutter" compensation on playback which resulted in a lower noise level. WWVB coded time signal was recorded on the fourth channel and the magnetic components were recorded on the remaining channels (Fig.5).

During the project, there was a total of about 64 days of actual data recording (37 days at PEM, 16 at ALT and 11 at DAR). However, less than 5% of the total recorded data was useful since the data were generally noisy, particularly the electric components. The exact cause of

this noise is unknown, but may arise from atmospheric electric discharges, human and industrial interference, wind, AC power noise and possibly amplifier and filter noise. As an estimate of the overall accuracy of the MT system including reading errors, playback and digitising noise, all the recorded FM tapes have been searched and a section which appears to be relatively very quiet (that is, a period of very little geomagnetic activity) has been digitised and a plot of this is shown in Fig. 6. Some signal still appears to be present and the peak-to-peak noise level can be estimated to be about 2 to 3 mv/km for the electric components and about 0.3 γ for the magnetic components.

4.2 DATA REDUCTION

Each recorded FM tape was edited in a fast playback mode using the Sanborn (Model 3900) tape recorder and displaying the signals on chart paper by means of a Gould Brush 480 chart recorder. Next, sections with minimum noise contamination were selected and played back in detail and from these, the best one-hour sections showing good variations (amplitude and frequency content) were digitised using a digitising interval of 1 second. Figs. 7 to 9 show analogue plots of samples of the analysed data at each station.

Fig. 10 shows a block diagram of the equipment configuration for the digitising process. The Sanborn plays back the FM tape and the signals are passed through the Rockland filters set at zero db gain and low pass with a real-time cut-off frequency of 0.5 Hz. The latter is to minimise "aliasing" upon digitisation. The outputs of the filters are fed simultaneously to the Gould Brush and the digitiser. The former serves principally as a monitor, while from the digitiser, the signals are written onto a 9-track digital tape. The digitising rate is controlled by the pulse generator which in turn is triggered by the highly stable signal generator.

FIG. 6 Sample of the total noise (recorded, playback and digitising noise) at a magnetically quiet period.

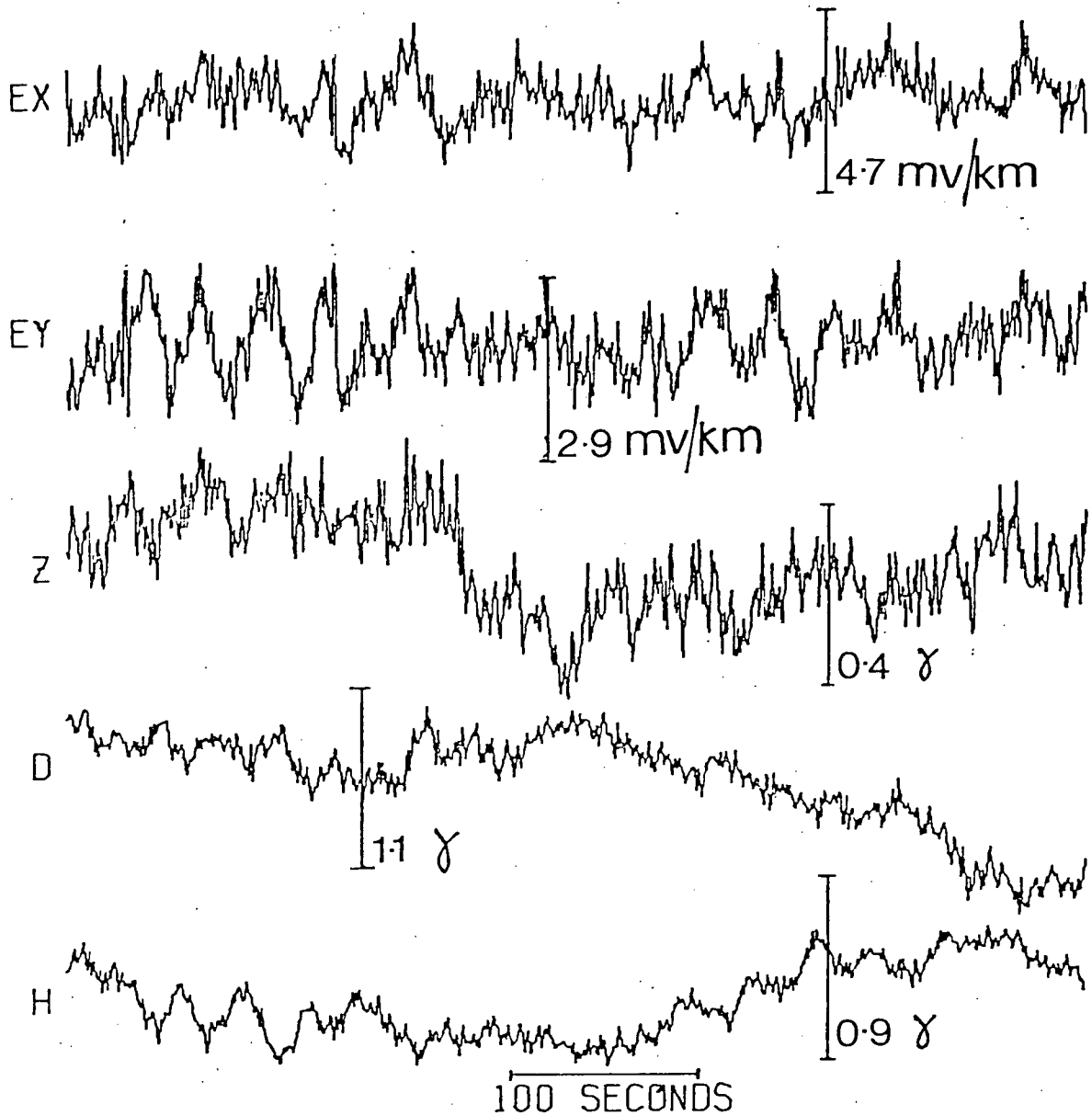
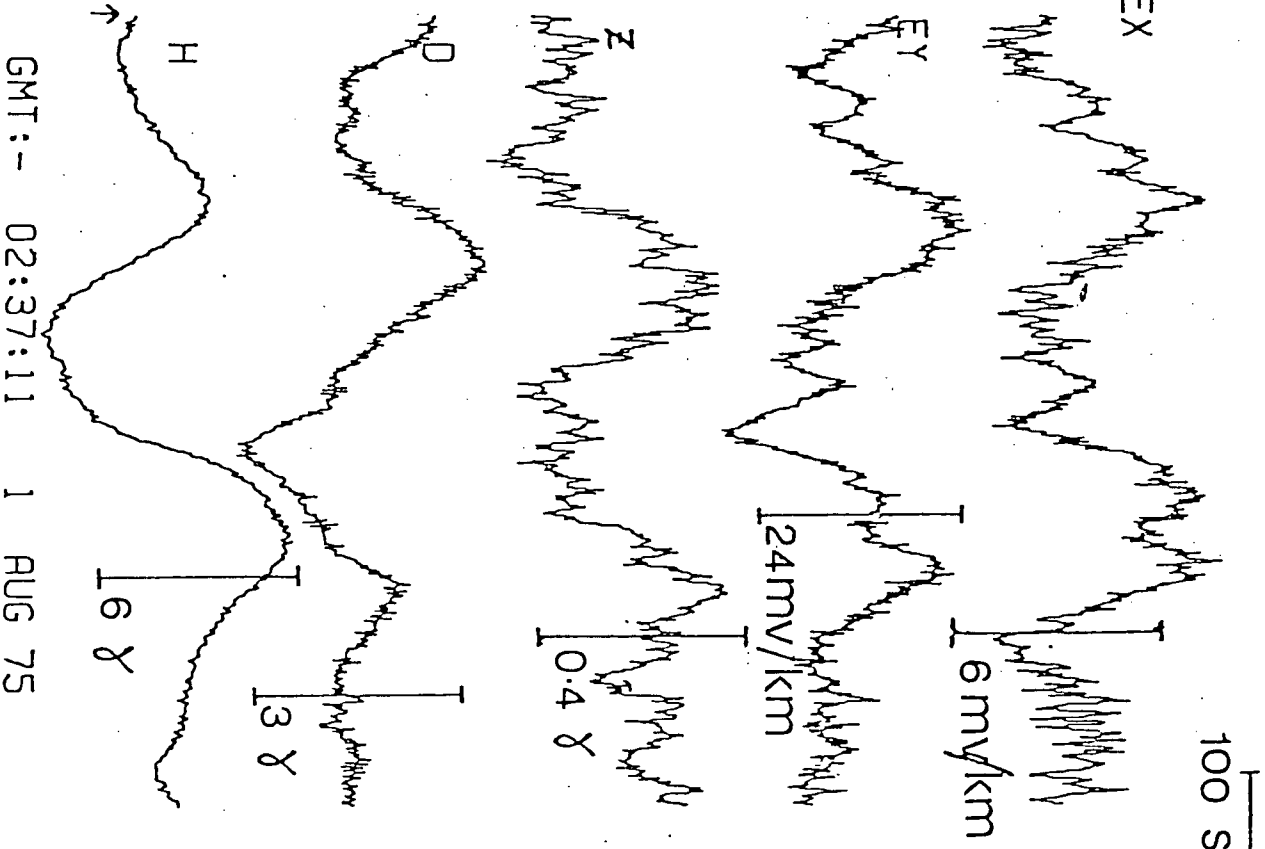


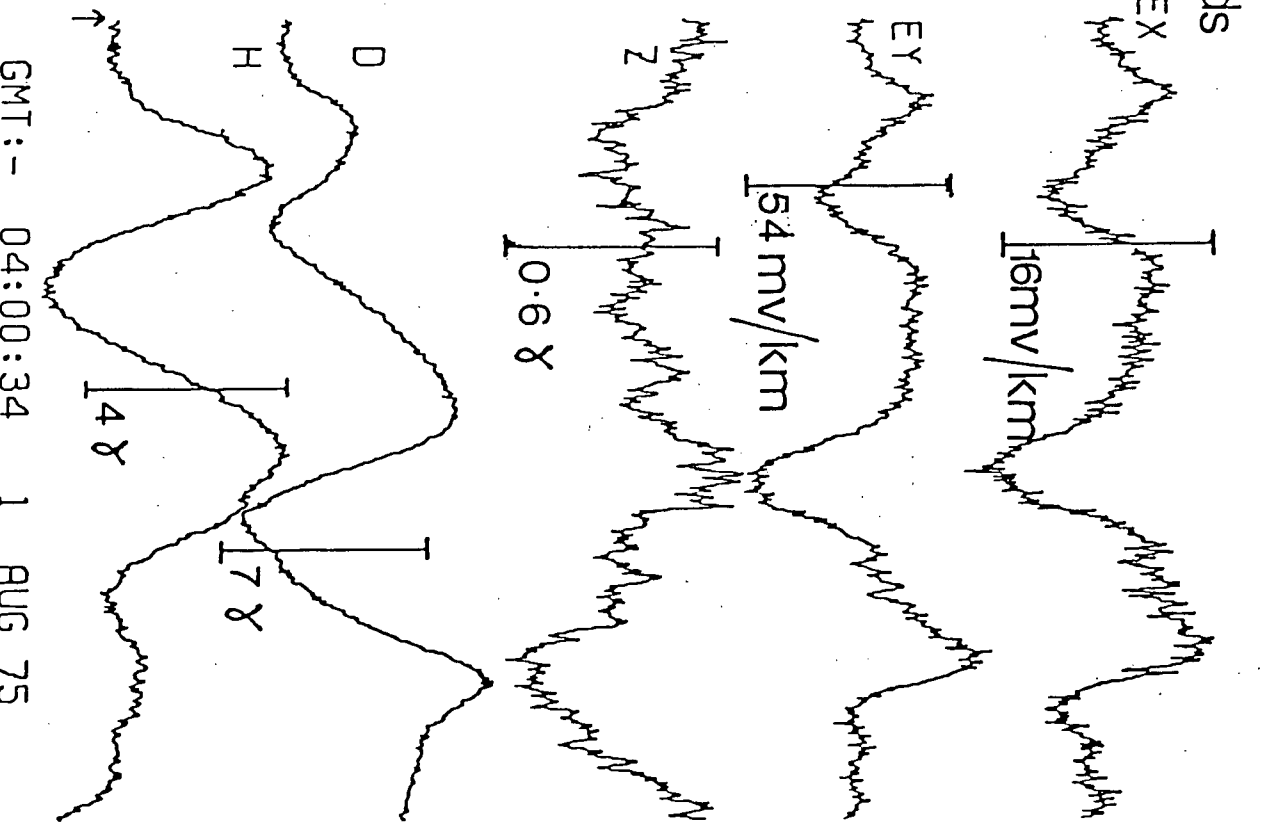
FIG. 7 Samples of the natural variations in the magnetic and the electric components at Alta Lake. The beginning of the traces is indicated by the arrow and the time corresponding to it is given in GMT. The event number is arbitrary.

STATION: ALT : EVENT: 204



GMT:- 02:37:11 1 AUG 75

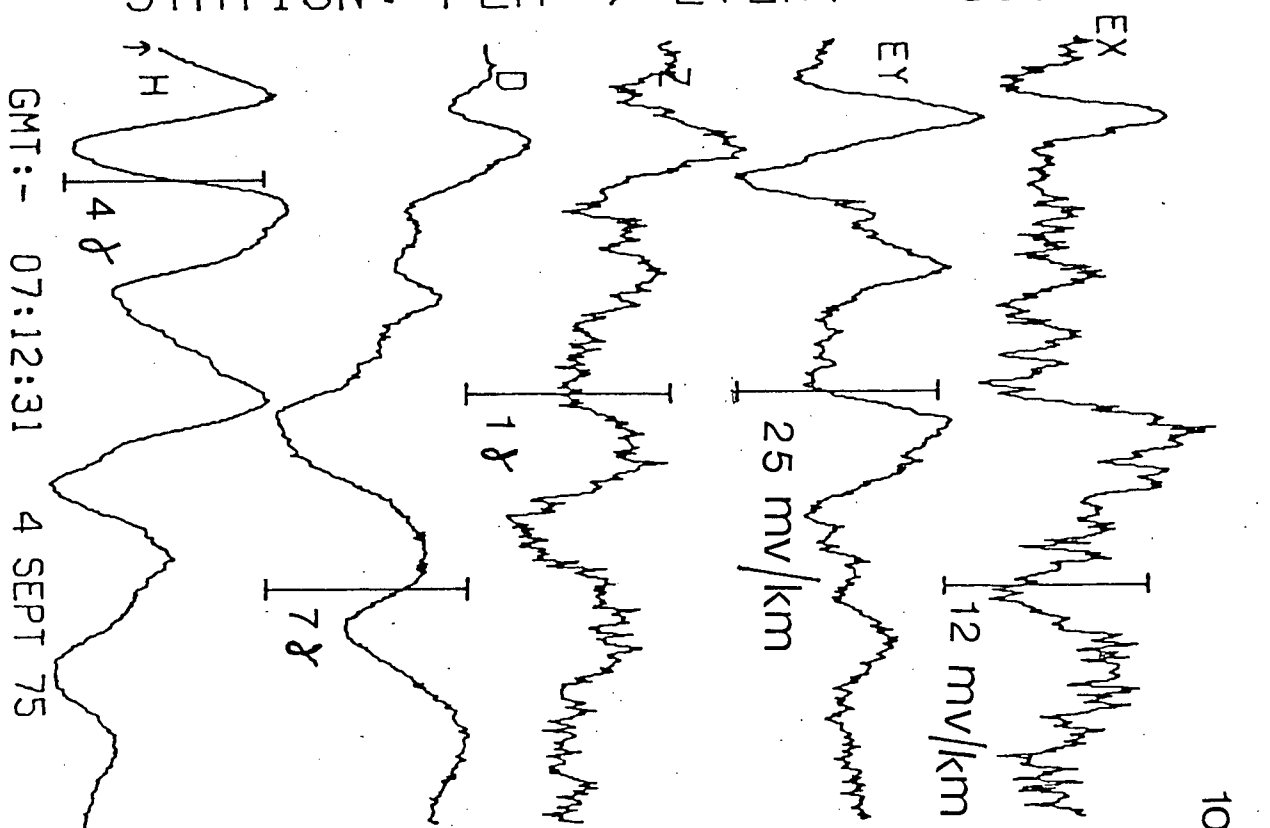
STATION: ALT : EVENT: 205



GMT:- 04:00:34 1 AUG 75

FIG. 8 Samples of the natural variations in the magnetic and the electric components at Pemberton. The beginning of the traces is indicated by the arrow and the time corresponding to it is given in GMT. The event number is arbitrary.

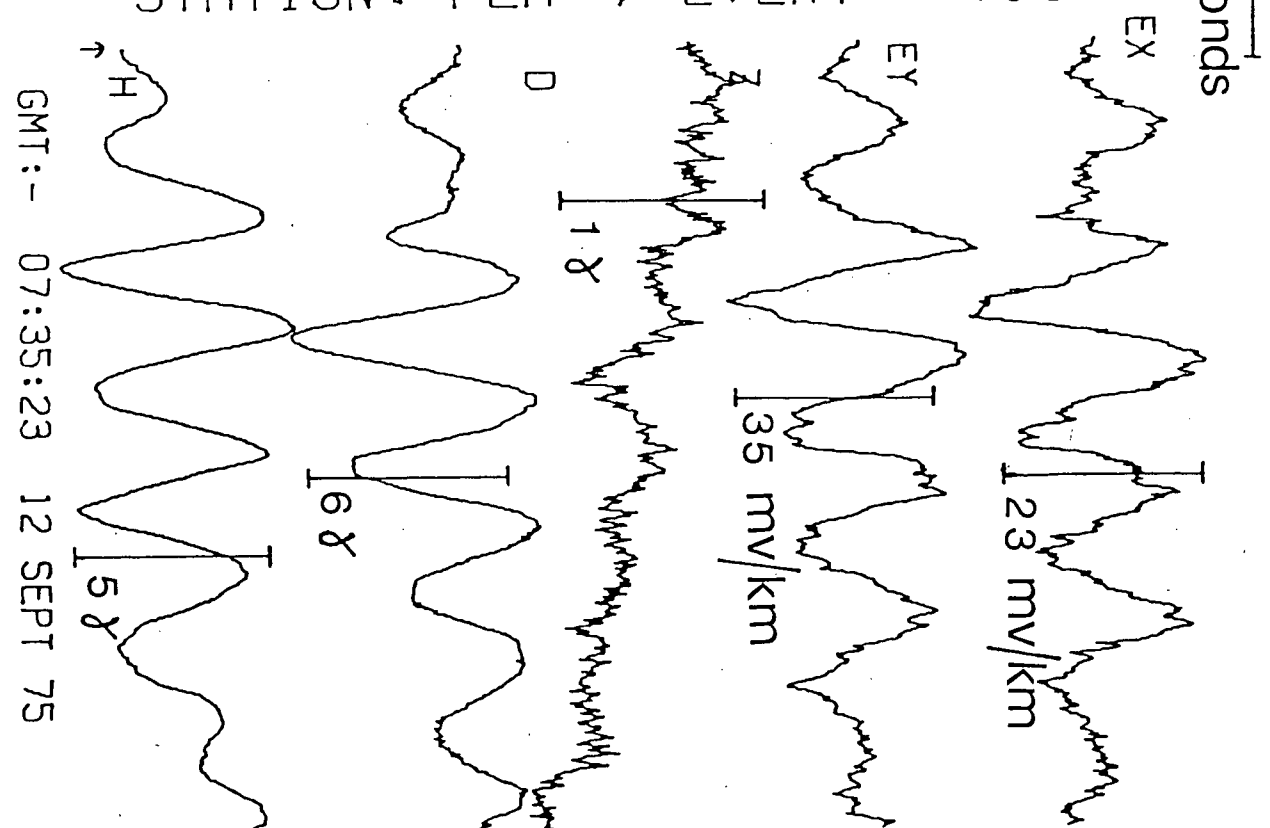
STATION: PEM : EVENT: 601



GMT: - 07:12:31

4 SEPT 75

STATION: PEM : EVENT: 703

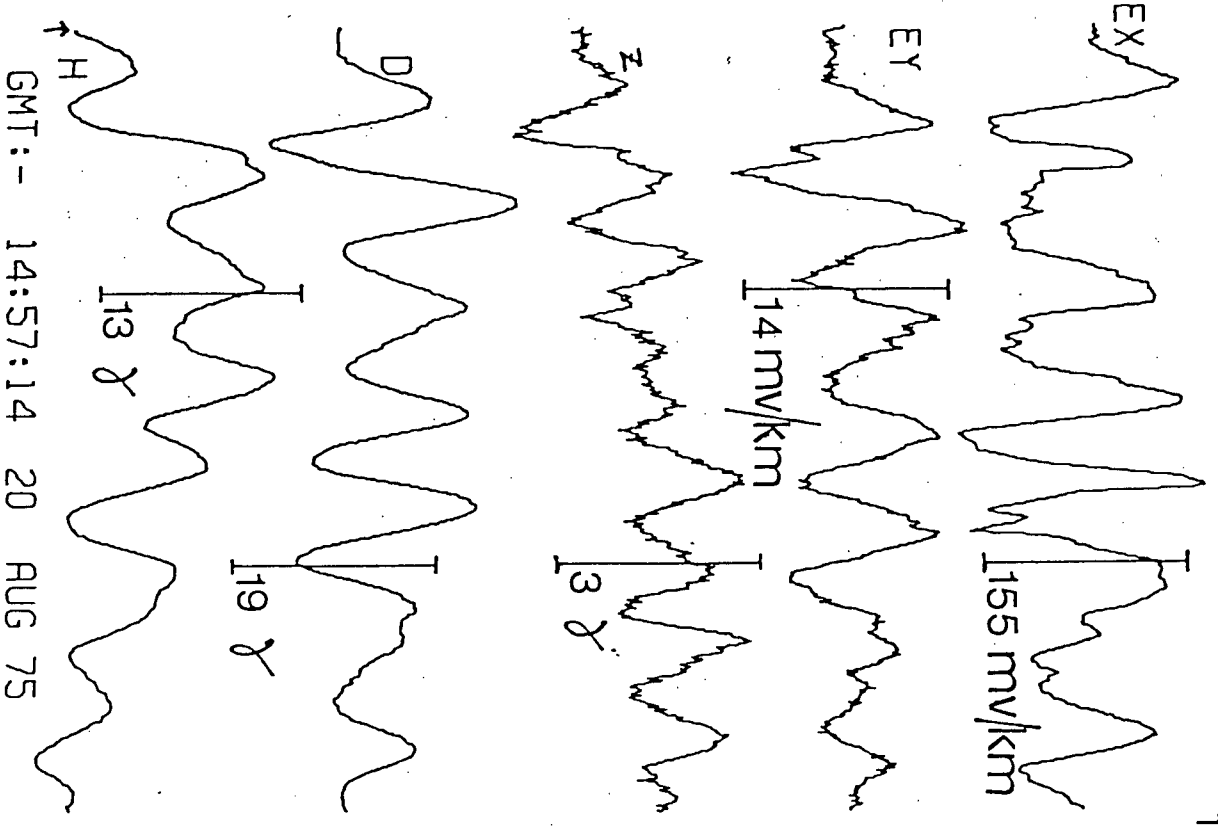


GMT: - 07:35:23

12 SEPT 75

FIG. 9 Samples of the natural variations in the magnetic and the electric components at D'Arcy. The beginning of the traces is indicated by the arrow and the time corresponding to it is given in GMT. The event number is arbitrary.

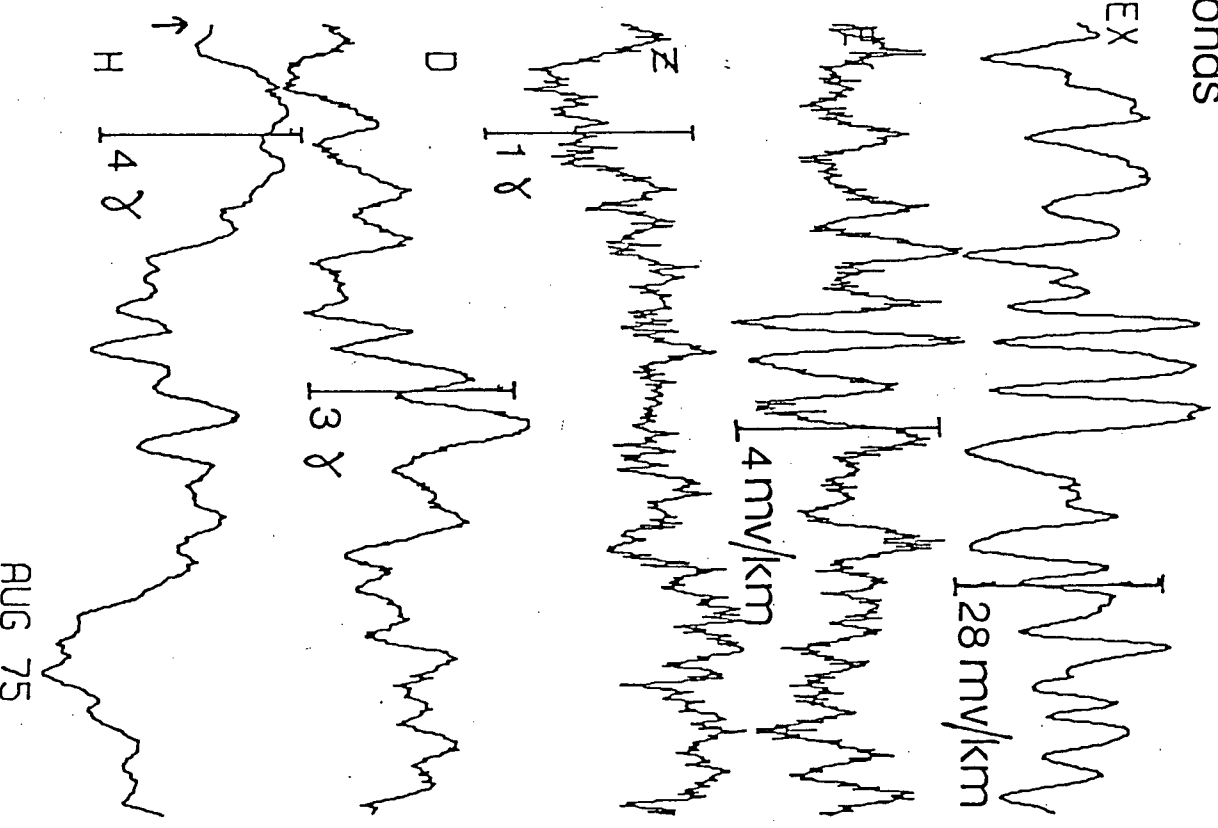
STATION: DAR : EVENT: 103



GMT:- 14:57:14 20 AUG 75

100 seconds

STATION: DAR : EVENT: 104



AUG 75

FIG. 10 Block diagram representation of the digitisation process.

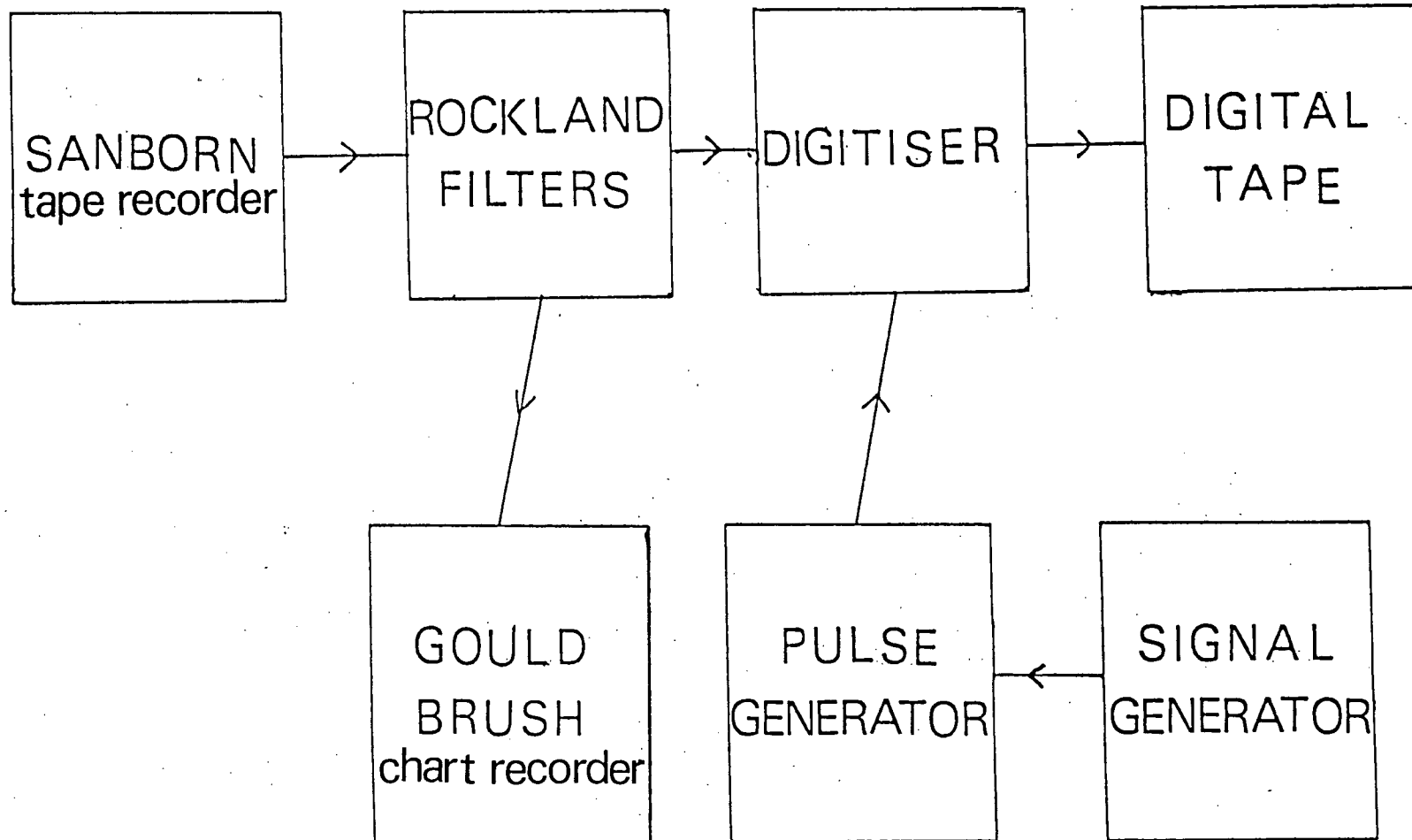


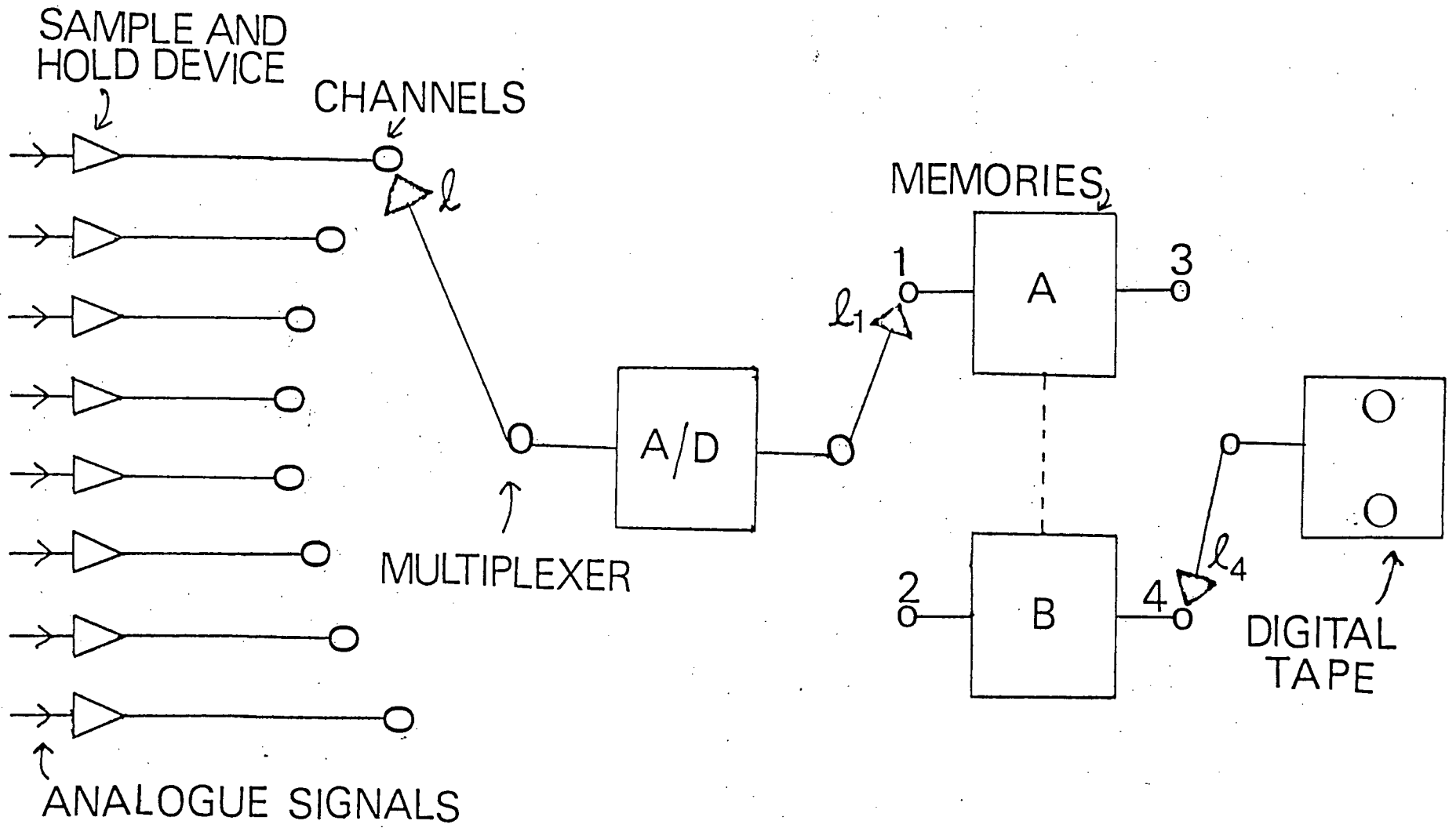
Fig. 11 shows a block diagram of the digitiser (Analogic AN 5800 series plus Kennedy 8108). The sample-and-hold device simultaneously samples all the input analogue signals. At the preset time intervals, the multiplexer, ℓ picks sequentially the contents of the channels in the form of a voltage and passes these to the Analogue-to-Digital converter (A/D) which then stores them in the memory in contact with it. The A/D consists of 14 bits + 2 flag bits, viz, 0-13 for data, 14 for missed data and 15 for zero channel. The digitiser has a dynamic range of ± 10 volts. Each of the memories A and B holds 256 samples or words (equivalent to a block of data). At any particular time, one memory is being filled with data samples while the other writes on the tape. The samples are written on the tape as half words, that is, 2 bytes per word.

In this thesis, each digitised one-hour section constituted a "data file". For the data analysis, 28 data files were used (13 at PEM, 7 at ALT and 8 at DAR).

The multiplexed data were demultiplexed on an IBM 370/168 computer using a program of W.B. Cumming. The data were then cleaned of unwanted spikes and pulses using "Digalt" (a U.B.C. Computing Centre supported program). At any point where a spike was found, the data value was set equal to the mean of the two flanking points.

The mean and the linear trends in the time series were then removed. Linear trend may arise from instrumentation drift or long-term changes in the geomagnetic field, such as diurnal variations. The series were then cosine-belled and padded with zeros to make the total data length a power of two before the Fast Fourier Transform (FFT) was taken.

FIG. 11 Diagrammatic representation of the digitiser. A/D is the analogue-to-digital converter.



4.3 DATA ANALYSIS

The general nature of the electric and magnetic variations is depicted in Figs. 7 to 9. It is assumed that the selected sections of the variations possess the properties of weakly stationary time series hence permitting power spectral techniques to be used. Using the FFT periodogram technique, the power spectra of each data file were estimated. A Parzen window was used for smoothing in the frequency domain. If the window is very wide, the long period data will be poorly resolved; on the other hand, if the window is very narrow, stability of the spectral estimate will be poor. To balance the above effects, three different window sizes were used in the data analysis of each data file — these will be referred to from now on as W1 (for the long period range, about 110 to 600 seconds), W2 (for the intermediate period range, about 45 to 60 seconds) and W3 (for the short period range, 10 to 60 seconds). These windows were normalised and their resolutions and variances corresponded to those given by equivalent maximum lags of 35%, 20% and 10% of data length respectively.

In terms of the power in each component, the apparent resistivity, ρ_a can be written as

$$\rho_a = 0.2 T \frac{P_{EX}}{P_D}$$

or

$$\rho_a = 0.2 T \frac{P_{EY}}{P_H}$$

(4.1.)

where P stands for power

The coherence between any two signals x and y (a measure of the correlation between the two signals) is given by

$$\text{Coh}_{xy}(f) = \frac{P_{xy}(f)}{P_{xx}(f) P_{yy}(f)} \quad (4.2)$$

where P_{xy} is the smoothed cross-power spectrum of x and y and P_{xx} and P_{yy} are the smoothed power spectra of x and y respectively. The magnitude of Coh_{xy} is usually designated the coherence. Its phase is the phase angle between the two signals. For perfectly coherent signals $|\text{Coh}_{xy}| = 1.0$. Spurious signals, which may be considered as noise, will lower the coherence between the electric and magnetic components.

Using the above relations, the coherence and phase angle between the orthogonal electric and magnetic components and the apparent resistivities were calculated for each data file at each frequency. At each station and for each window size, the averages of these quantities were then found using only the data showing a coherence of 0.70 or higher.

The vertical magnetic component Z can be expressed linearly in terms of the horizontal components H and D at each frequency as (Everett and Hyndman, 1967)

$$Z = aH + bD \quad (4.3)$$

where a and b are complex coefficients. These coefficients can be viewed as operating on the horizontal magnetic field and tipping part of it into the vertical. For this reason, (a, b) is called the "tipper" or Z -transfer function. For two dimensional structures, the tipper indicates the magnitude, direction and depth of lateral conductivity changes. For each data file, the Z -transfer function was calculated at each frequency and the averages for each station were found.

From equation (2.1) we can write

$$\left(\frac{E}{H}\right)^2 = \frac{5\rho_a}{T}$$

For a homogeneous, horizontally stratified and isotropic earth, the above equation can be written as

$$\left(\frac{E}{H}\right)^2 = A + \left(\frac{B}{T}\right) \quad (4.4)$$

where A and B are constants for each layer. The plot of $(E/H)^2$ against frequency will therefore give straight line segments corresponding to each horizontal layer. In terms of the power in the electric and magnetic components, (4.4) becomes

$$\frac{P_E}{P_H} = A + \left(\frac{B}{T} \right) \quad (4.5)$$

From equations (2.2) and (4.4), it can be easily shown that the depth of penetration of plane EM waves at any point on the straight line segments is given by

$$P = \left(\frac{1}{2\pi} \right) \sqrt{2T(A + B)} \quad (4.6)$$

where T is the period value at the point in question. Using the average powers at each station, P_{EX}/P_D and P_{EY}/P_H have been calculated at each frequency, but the plots of these are not presented in the thesis. Although these quantities show a fairly large scatter, their plots do show straight line segments. It should be remarked that the layer resistivities and thicknesses estimated from the straight line segments were very helpful in finding a mathematical model to fit the experimental apparent resistivity curves at the stations.

The standard impedance ratio or power attenuation ratio (Caner et al., 1967) is given by

$$M_H = (P_Z/P_H)_{\text{station}} / (P_Z/P_H)_{\text{reference station}} \quad (4.7)$$

This normalised dimensionless attenuation factor is fairly independent of geomagnetic latitude effects. Its variation with frequency, in the absence of anomalous fields, characterises the differences in the horizontal conductivity structure. Using the mean smoothed powers and with PEM as the reference station, the power attenuation ratios at ALT and DAR have

been calculated at each frequency. M_H is usually evaluated using simultaneous data. In this project however, the data are not all simultaneous since only PEM and either ALT or DAR have been operated at the same time.

Figs. 12 to 14 show the mean smoothed power spectra of the electric and magnetic components at the various stations. On these plots, the solid lines without symbols correspond to W1, those with stars correspond to W2 and those with crosses correspond to W3. The peak power seems confined within the period band 35 to 135 seconds. Fig. 15 shows the mean EX/D and EY/H coherence plots for each station. From the coherence and power spectra plots, it can be seen that the frequency bands showing power peaks also indicate corresponding coherence peaks.

FIG. 12 Mean smoothed power spectra of the electric and magnetic components at Alta Lake. For a clear visual presentation, the logarithms of $(P_{EX} \times 10^{2.4})$, $(P_{EY} \times 10^{2.4})$, (P_Z) , $(P_D \times 10^2)$ and (P_H) have been plotted, where P stands for power. The solid lines without symbols correspond to W1, those with stars correspond to W2 and those with crosses correspond to W3, where W stands for the smoothing window. The unit of power for the electric and magnetic components is $(\text{mv/km})^2$ and γ^2 respectively.

ALT

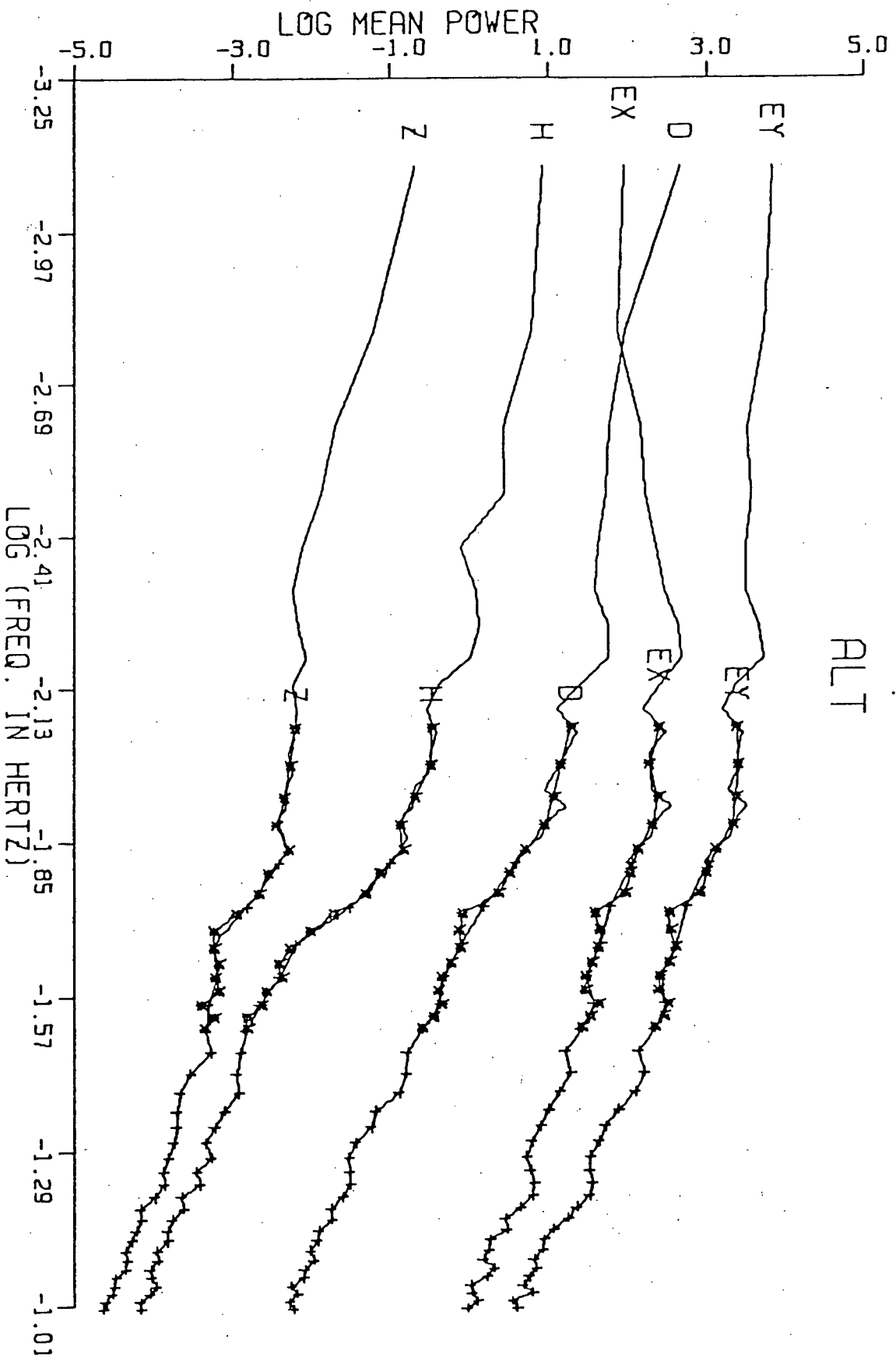


FIG. 13 Mean smoothed power spectra of the electric and magnetic components at Pemberton. For a clear visual presentation, the logarithms of ($P_{EX} \times 10^4$), ($P_{EY} \times 10^3$), (P_Z), ($P_D \times 10^2$) and ($P_H \times 10$), where P stands for power. The solid lines without symbols correspond to W1, those with stars correspond to W2 and those with crosses correspond to W3, where W stands for the smoothing window. The unit of power for the electric and magnetic components is $(\text{mv/km})^2$ and γ^2 respectively.

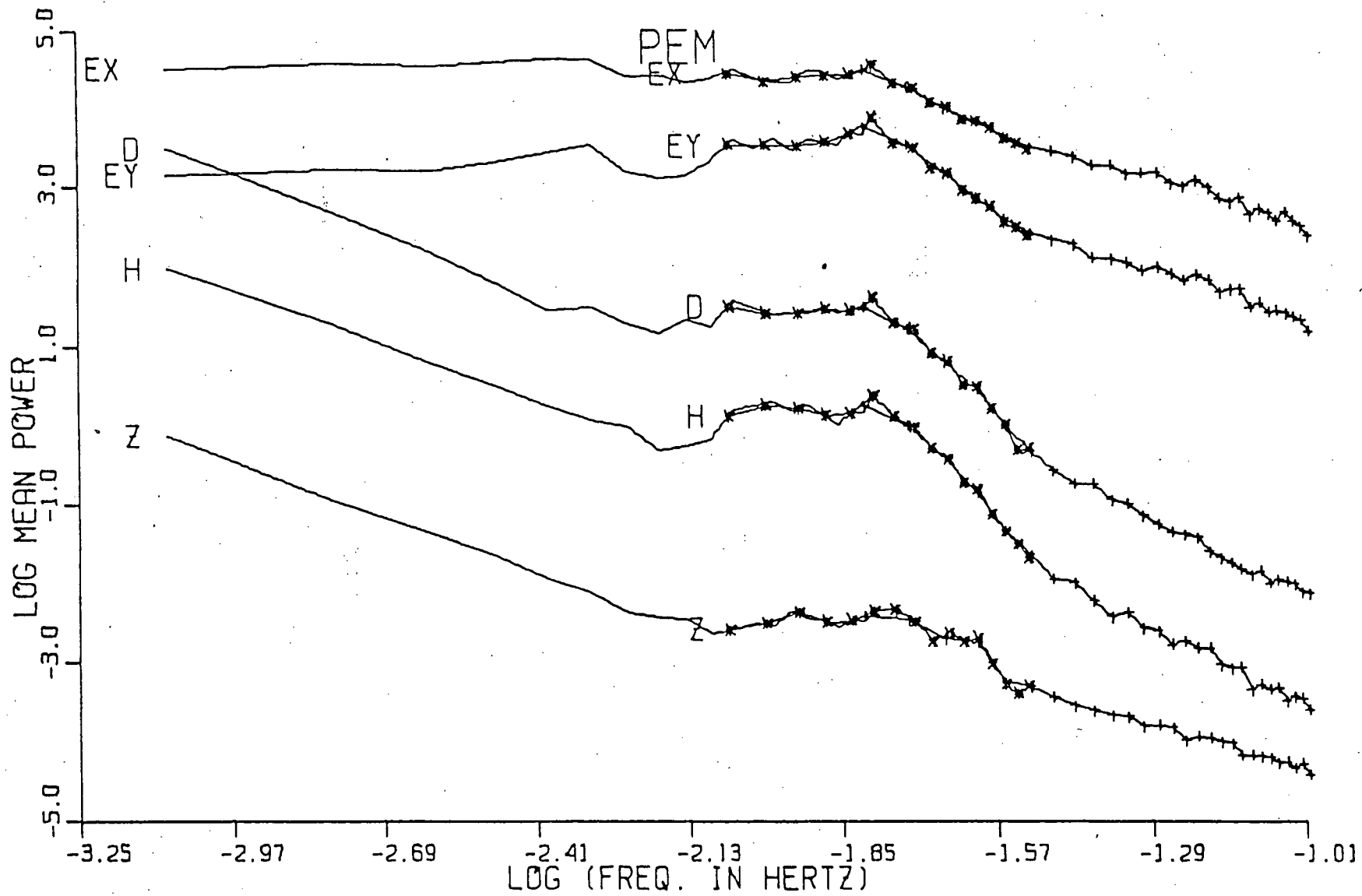


FIG. 14 Mean power spectra of the electric and magnetic components at D'Arcy. For a clear visual presentation, the logarithms of $(P_{EX} \times 10^3)$, $(P_{EY} \times 10^3)$, (P_Z) , $(P_D \times 10^4)$ and $(P_H \times 10)$ have been plotted, where P stands for power. The solid lines without symbols correspond to W1, those with stars correspond to W2 and those with crosses correspond to W3, where W stands for the smoothing window. The unit of power for the electric and magnetic components is $(\text{mv}/\text{km})^2$ and γ^2 respectively.

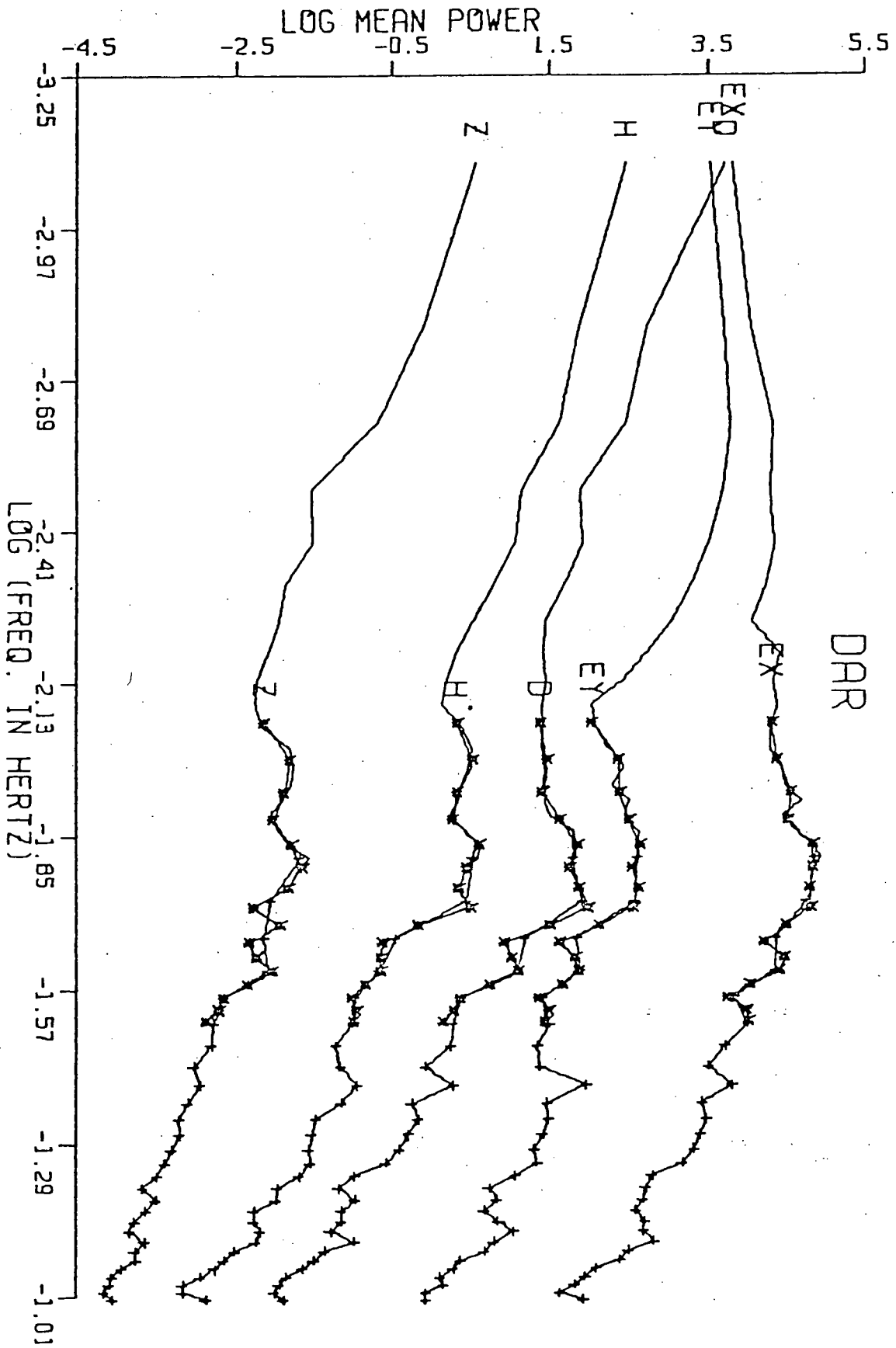
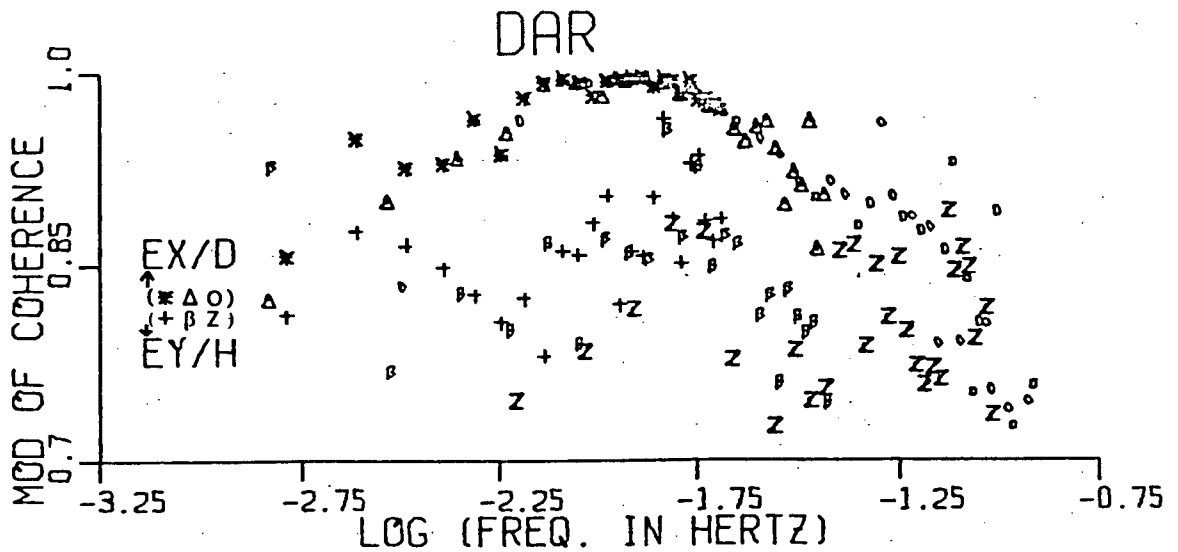
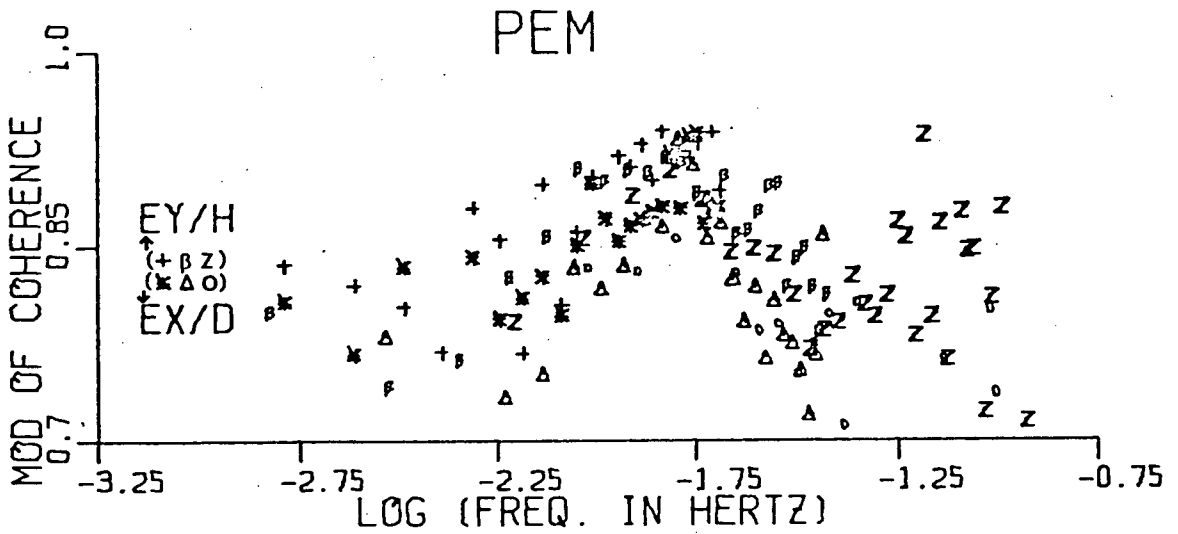
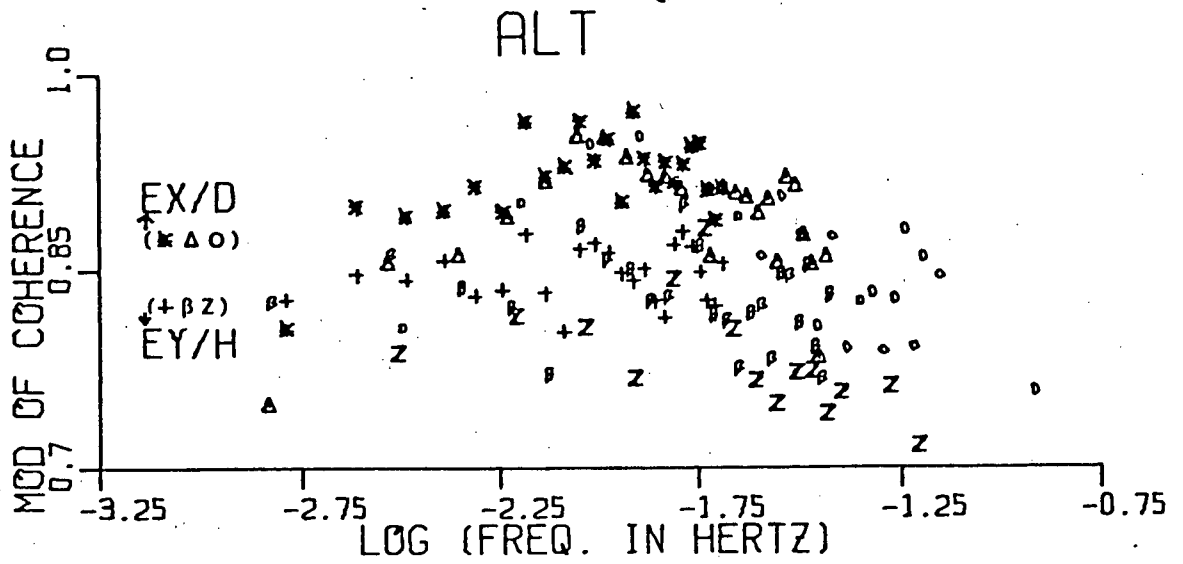


FIG. 15 Mean coherence between the orthogonal electric and magnetic components at each station. The symbols $+$ and $*$ correspond to W1, β and Δ correspond to W2, Z and O correspond to W3, where W stands for the smoothing window.



CHAPTER FIVE

INTERPRETATION AND CONCLUSIONS

5.1 GENERAL INTRODUCTION

In any geophysical method, the next step after the data analysis is the determination of the different physical parameters. This can be done by comparing the experimental curves with a set of master curves which have been drawn for simple theoretical structures. When a close fit is obtained between the experimental and master curves, the parameters of the mathematical model are assumed to estimate the real earth parameters for the area in question. This type of indirect interpretational approach may give ambiguous results. A brief discussion of the ambiguities involved in interpretational geophysical work has been given by Roy (1962). In spite of the possible ambiguities, the curve matching technique is a powerful geophysical tool and is used in the present data interpretation since more sophisticated techniques are beyond the scope of the preliminary interpretation presented in this thesis.

The curve matching technique is based on the law of similitude (Stratton, 1941). This law states that the necessary and sufficient condition for the impedance value at a frequency f_1 for a geological section whose parameters are σ_1 (conductivity) and h_1 (linear dimension) to be the same at a frequency f_2 for another geological section whose parameters are σ_2 and h_2 is that

$$\sigma_1 f_1 h_1^2 = \sigma_2 f_2 h_2^2$$

that is,

$$\sigma_f h^2 = \text{constant}$$

Fig. 16 shows master curves of apparent resistivity for two-layer earth models (after Yungul, 1961). Fig. 17 shows MT two-layer standard phase angle curves (after Cagniard, 1953).

5.2 DETERMINATION OF RESISTIVITY DISTRIBUTION

From the phase angle plots (Figs. 18 to 20), it can be generalised that at the short period end, the phase angles increase with increasing period. At the long period end, the phase angles decrease with increasing period. By visual comparison with the master curves (Fig. 17), it can be seen that the above result is indicative of the presence of a less resistive layer beneath a more resistive upper layer. A similar model is implied by the decrease of apparent resistivity with increasing period (see Fig. 16). Both factors indicate the presence of two or more layers.

From the apparent resistivity plots (Figs. 21 to 23), it can be seen that two distinct curves can be drawn, one resulting from EX and D components and the other from EY and H components. This in effect indicates that either there is an anisotropic conductivity or there is a lateral conductivity change or both. This apparent discrepancy between the EX/D and EY/D curves will be discussed later.

By considering the EX/D and EY/H apparent resistivity curves individually, a layered earth model interpretation has been done at each station using the curve matching technique as described in Appendix C. Due to the complexity of the experimental curves, the available published apparent resistivity curves could not be used. This is because they have assumed more resistive sub-layers, particularly the basement layer. Hence, to carry out the interpretation, several apparent

FIG. 16 Two-layer standard resistivity curves (after Yungul, 1961).

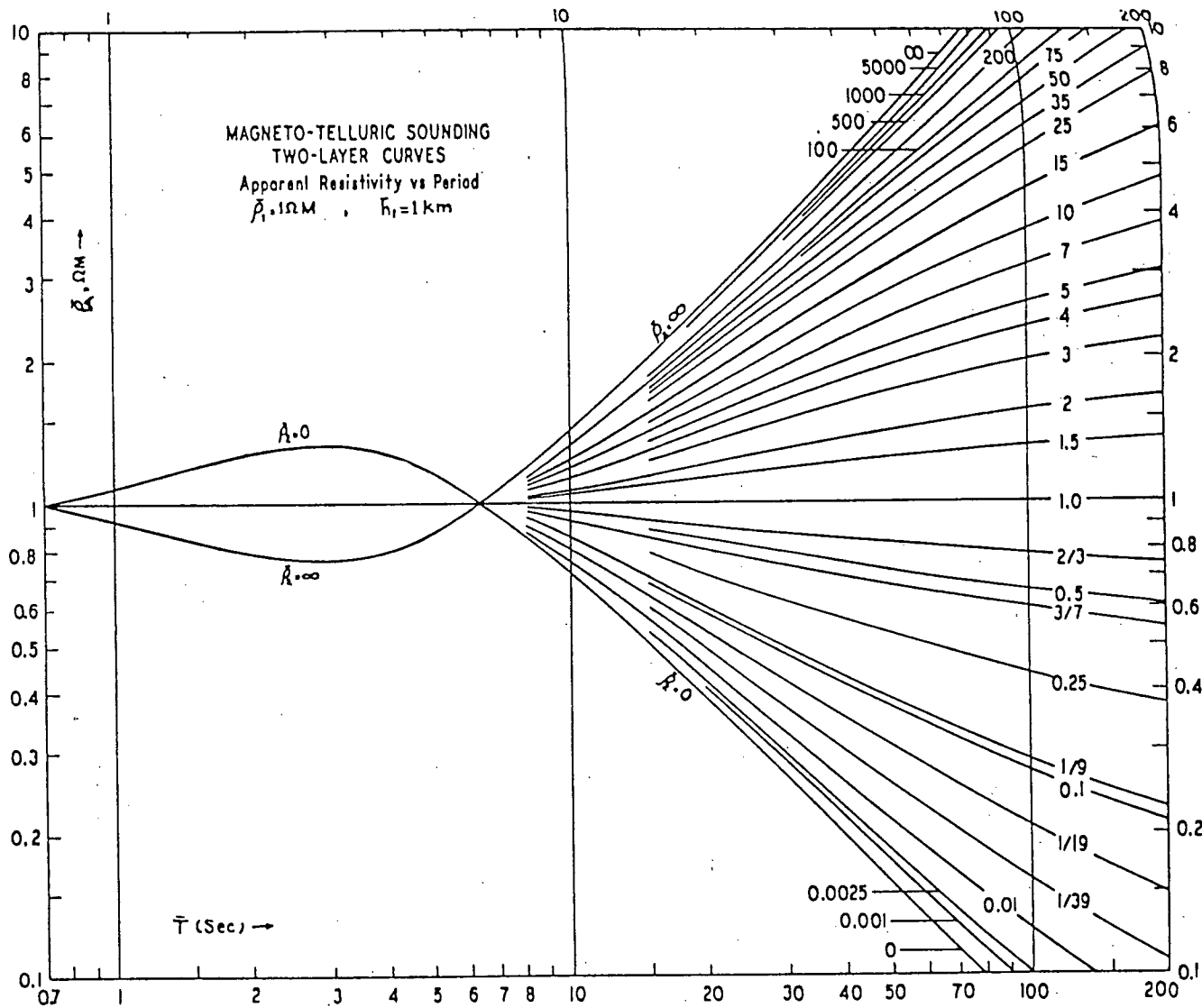


FIG. 17 Two-layer standard phase angle curves (after Cagniard, 1953).

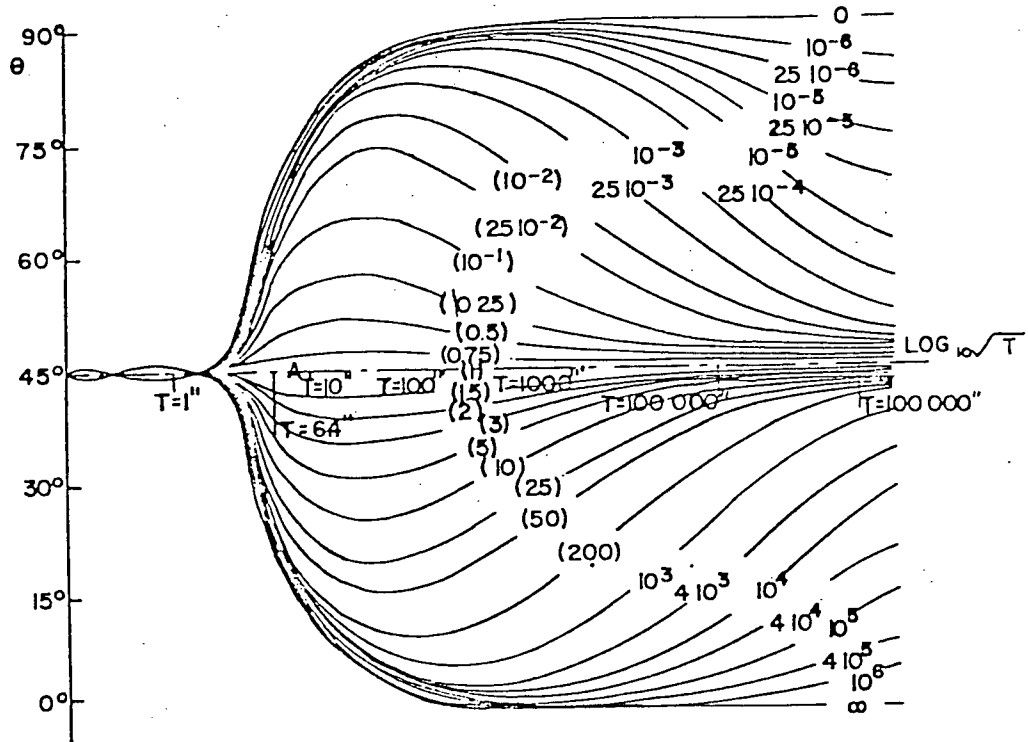


FIG. 18 Phase angles between the orthogonal electric and magnetic components at Alta Lake. The symbols \dagger and $*$ correspond to W1, β and Δ correspond to W2, Z and O correspond to W3, where W stands for the smoothing window.

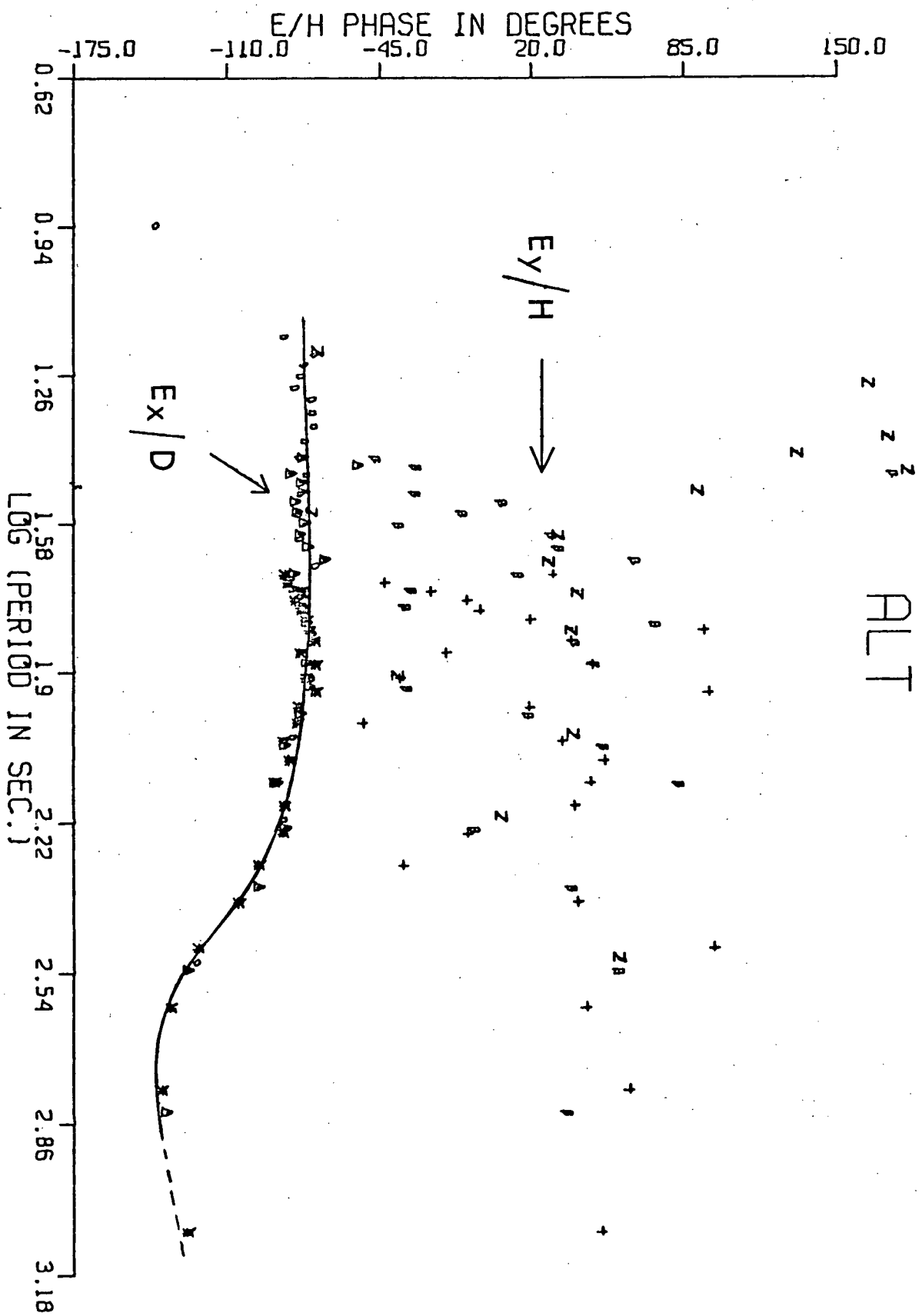


FIG. 19 Phase angles between the orthogonal electric and magnetic components at Pemberton. The symbols $+$ and $*$ correspond to W1, β and Δ correspond to W2, Z and O correspond to W3, where W stands for the smoothing window.

PEM

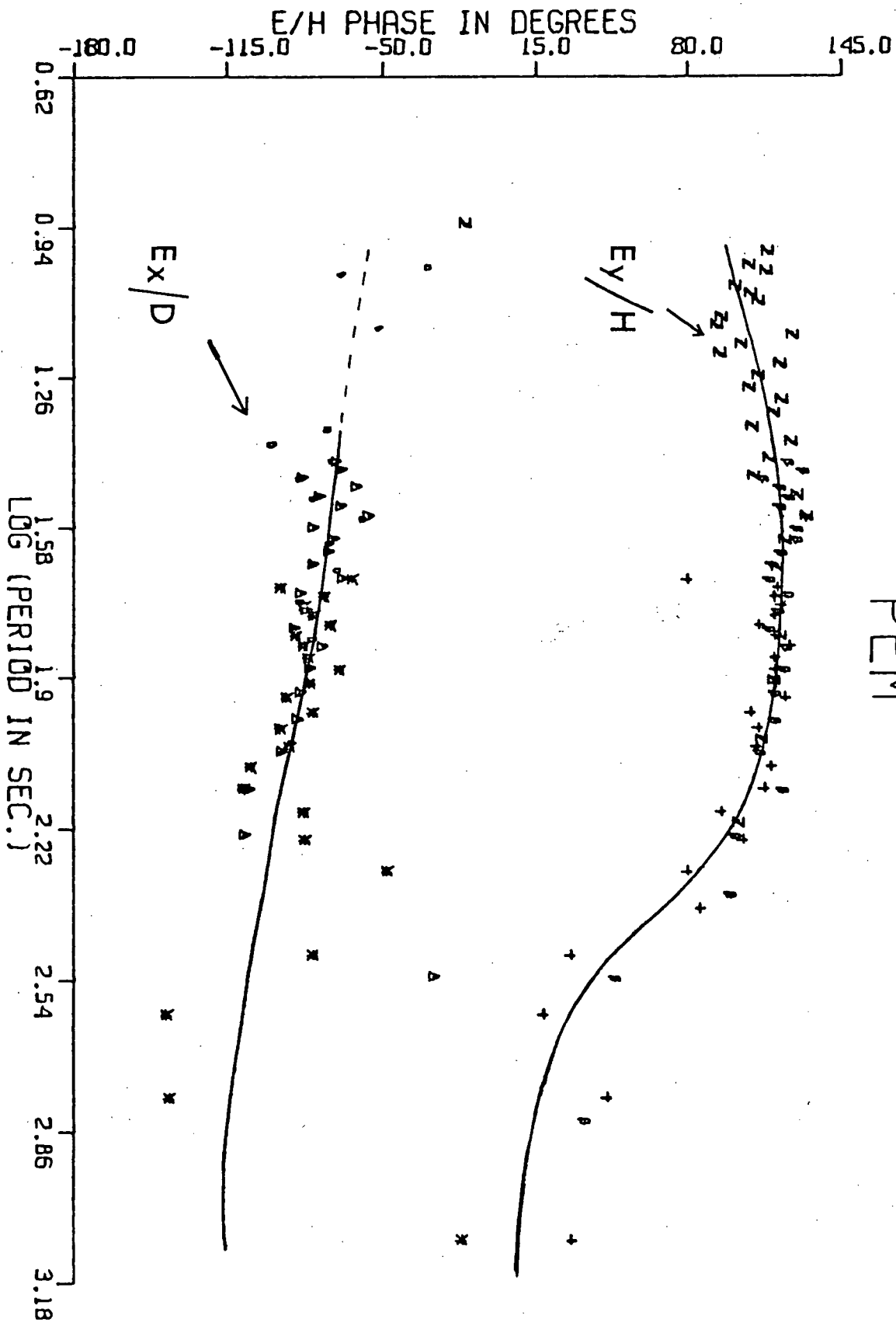


FIG. 20 Phase angles between the orthogonal electric and magnetic components at D'Arcy. The symbols $+$ and \times correspond to W1, β and Δ correspond to W2, Z and O correspond to W3, where W stands for the smoothing window.

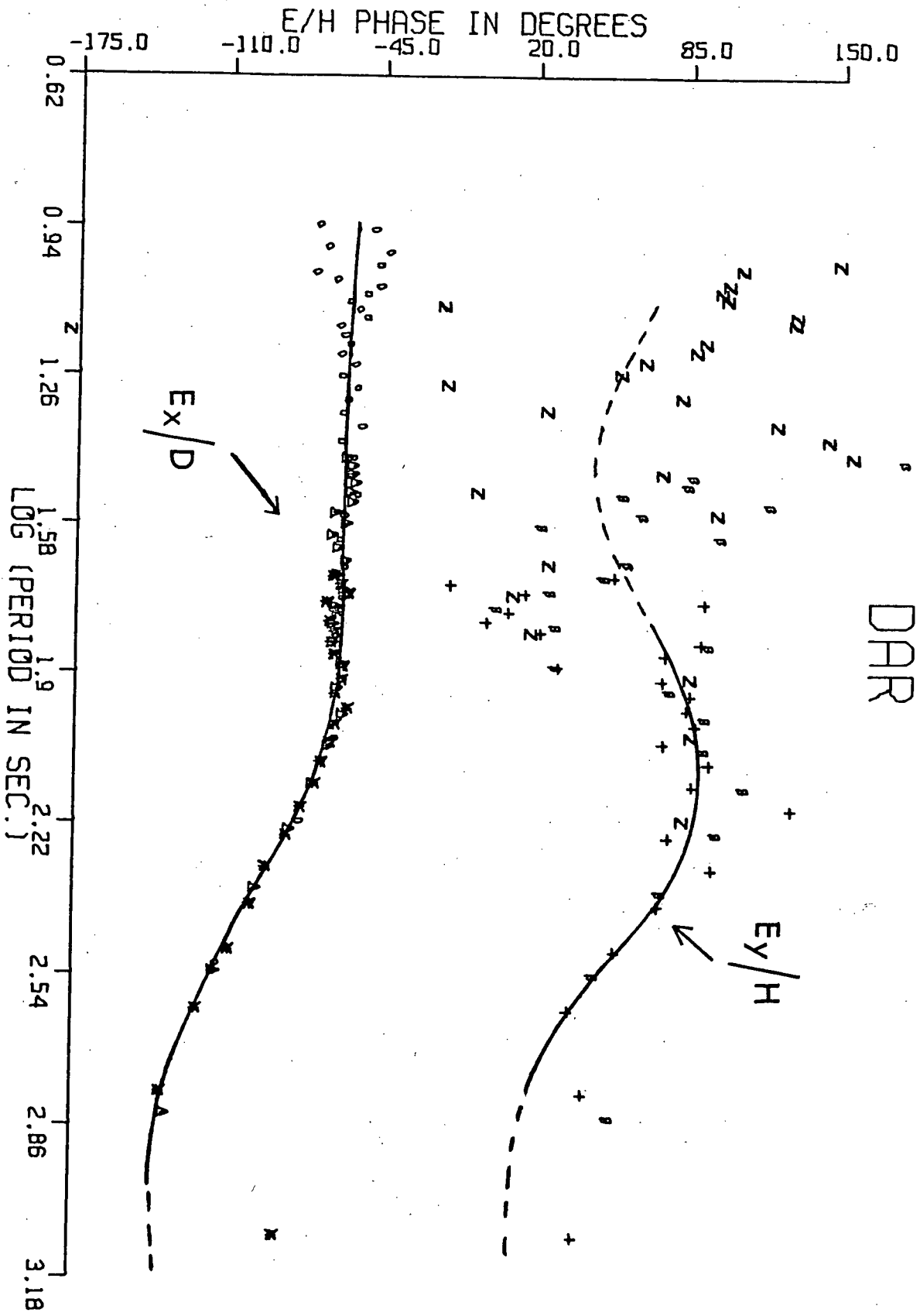


FIG. 21 Apparent resistivity curves at Alta Lake. The symbols + and ✕ correspond to W1, β and Δ correspond to W2, Z and O correspond to W3, where W stands for the smoothing window. The vertical bars represent one standard deviation.

ALT

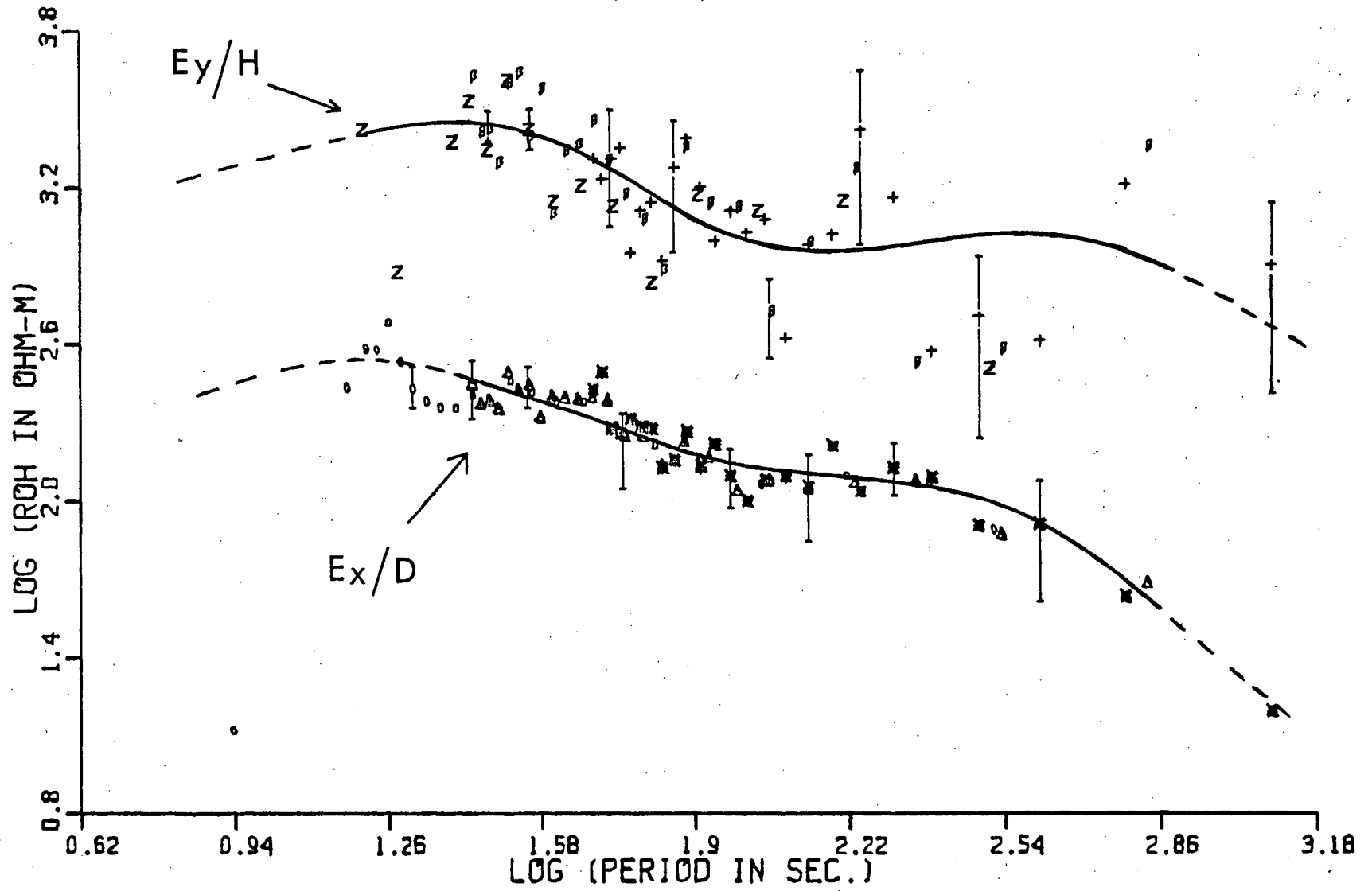


FIG. 22 Apparent resistivity curves at Pemberton. The symbols $+$ and $*$ correspond to W1, β and Δ correspond to W2, Z and O correspond to W3, where W stands for the smoothing window. The vertical bars represent one standard deviation.

PEM

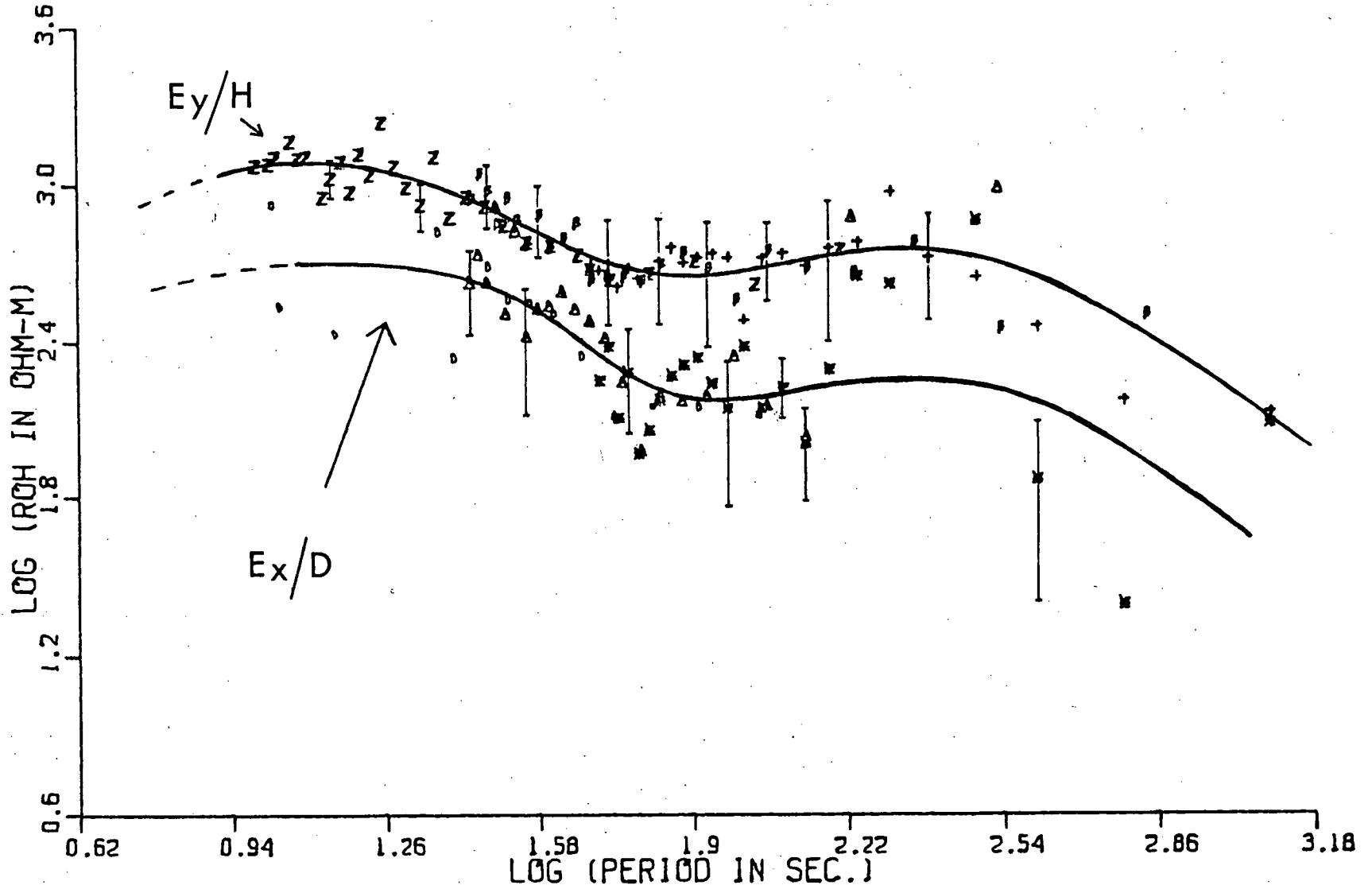
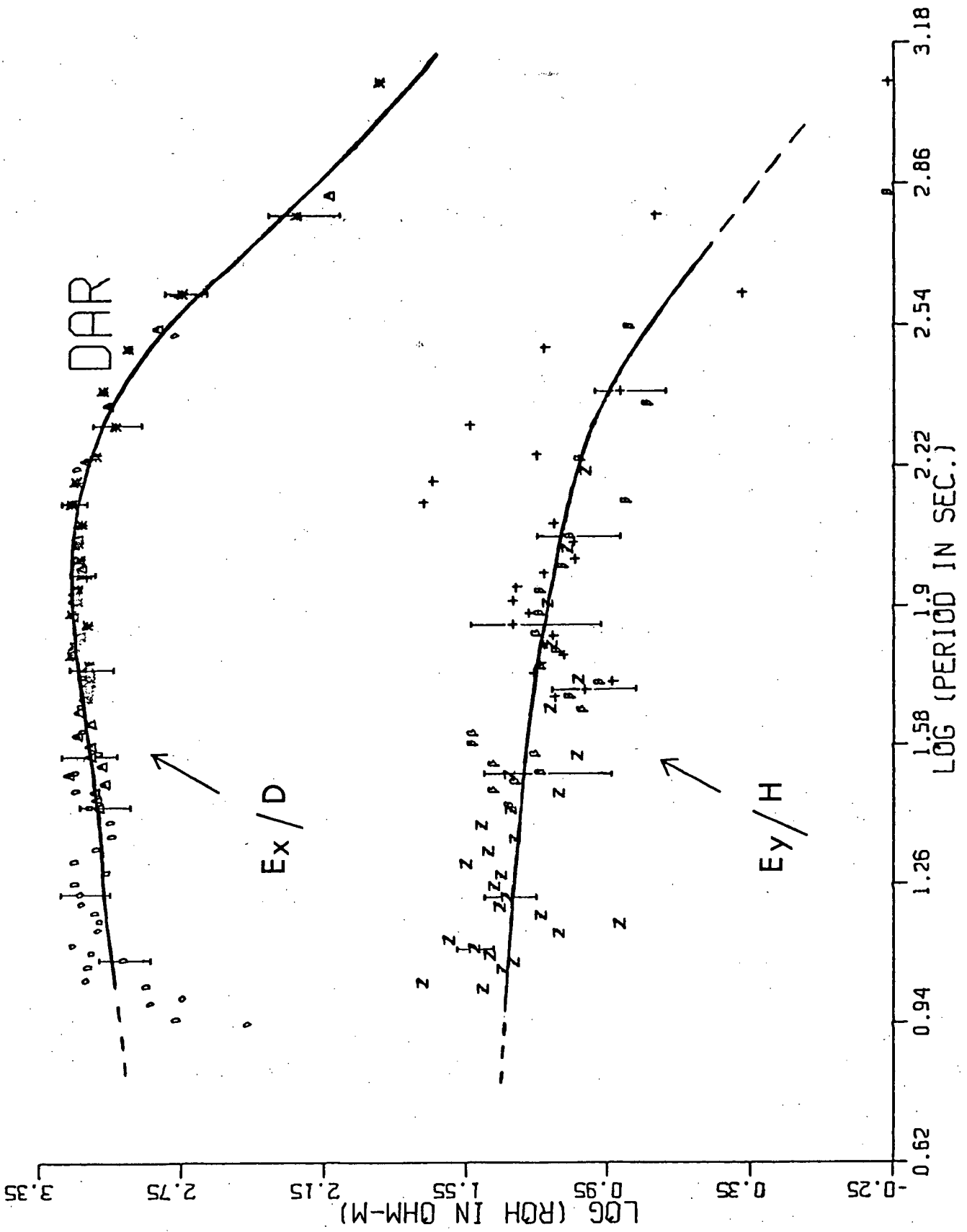


FIG. 23 Apparent resistivity curves at D'Arcy. The symbols + and * correspond to W1, β and Δ correspond to W2 and Z and O correspond to W3, where W stands for the smoothing window. The vertical bars represent one standard deviation.



resistivity type curves were computed using the program of Hasegawa (1962). A brief note on this program is given in Appendix D. Only those model curves which show a good degree of fit with the experimental data are presented here. Fig. 24 to 26 show such curves based on five-layer models as well as the experimental data at each station. Tables 4a, b, c show these model curve parameters.

The parameter estimates obtained from the model curve best fitting the experimental data at each station are as follows (e.g., ρ_1 , refers to the resistivity of layer 1 and the numbering increases from the top layer downwards):

Station: ALT

EX/D resistivity data:

Layer thickness (km)		Layer resistivity (ohm-m)	
h_1	40	ρ_1	270
h_2	18	ρ_2	22
h_3	400	ρ_3	2200
h_4	40	ρ_4	2700
h_5	∞	ρ_5	2

The chosen best fitting model curve is curve 7. Curves 9 and 10 give a better fit than curve 7 at the long period end, but a poorer fit at the intermediate period band where there are more data points. A better fit at the short period band can be obtained by shifting the model curves down slightly. This will result in a decrease of the above parameter estimates by about 5 to 10 per cent.

FIG. 24 Computed apparent resistivity model curves (solid lines) drawn on the experimental data (symbols) at Alta Lake.

ALT

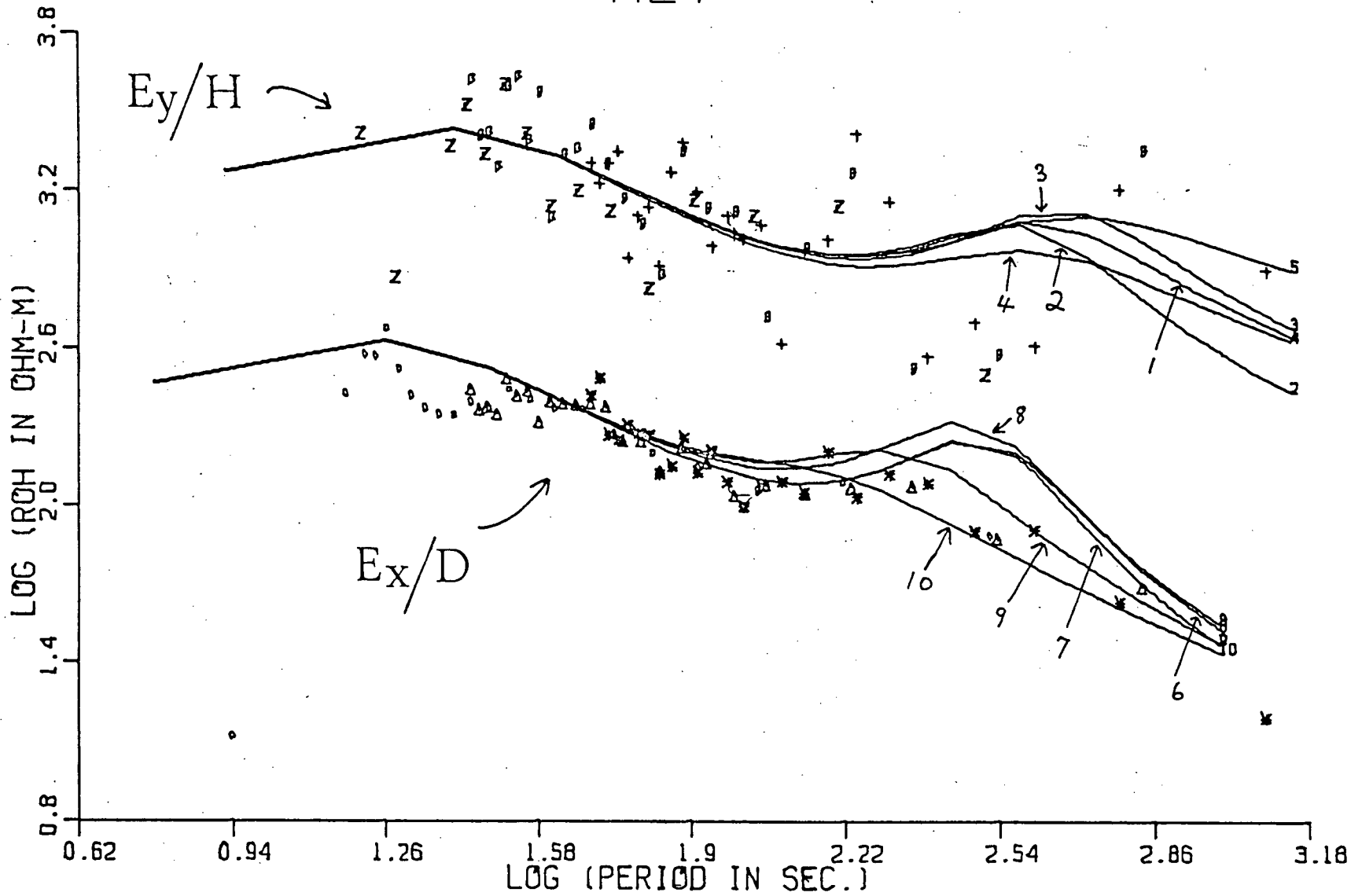


FIG. 25 Computed apparent resistivity model curves (solid lines) drawn on the experimental data (symbols) at Pemberton.

PEM

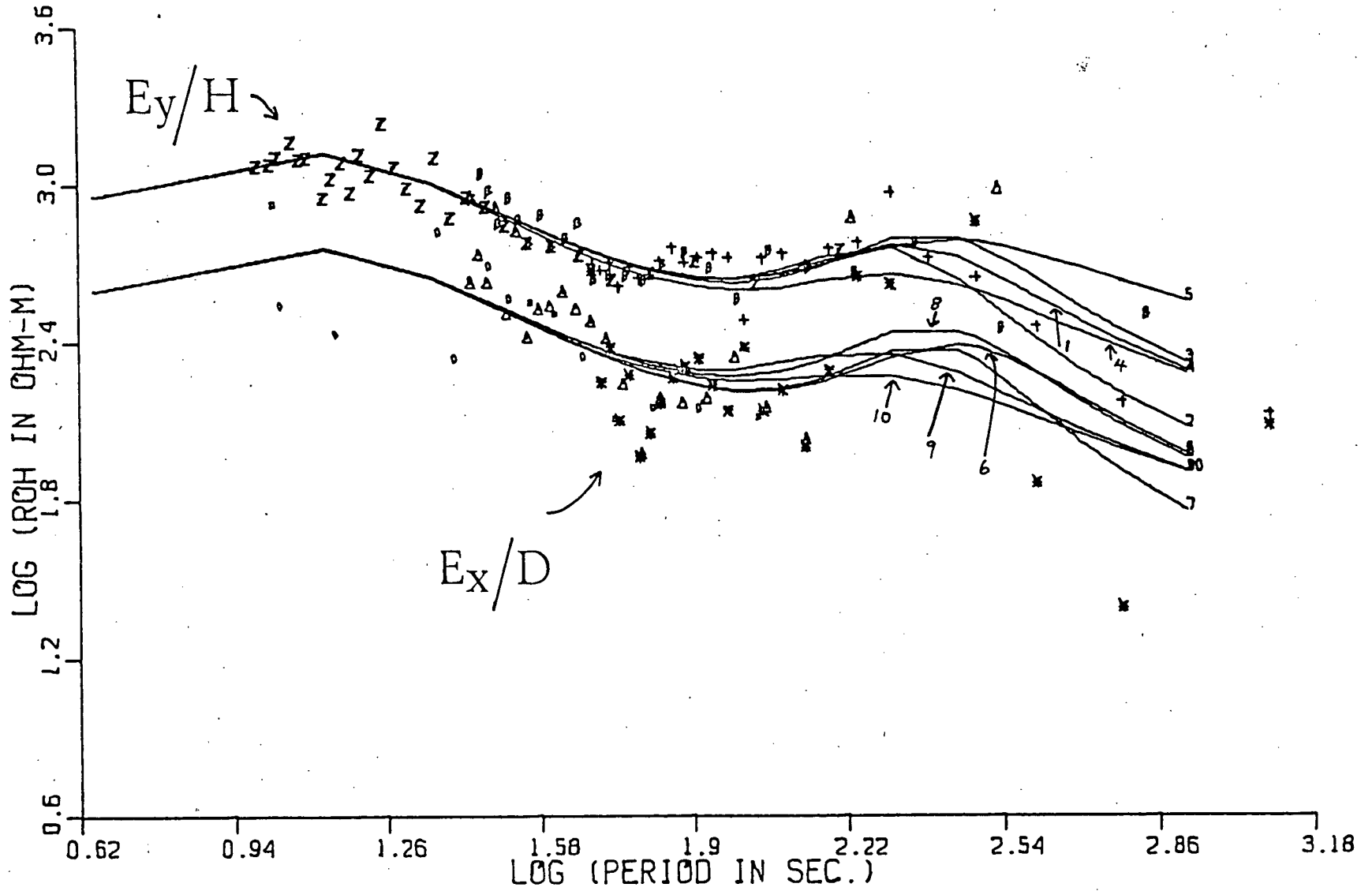


FIG. 26 Computed apparent resistivity model curves (solid lines) drawn on the experimental data (symbols) at D'Arcy.

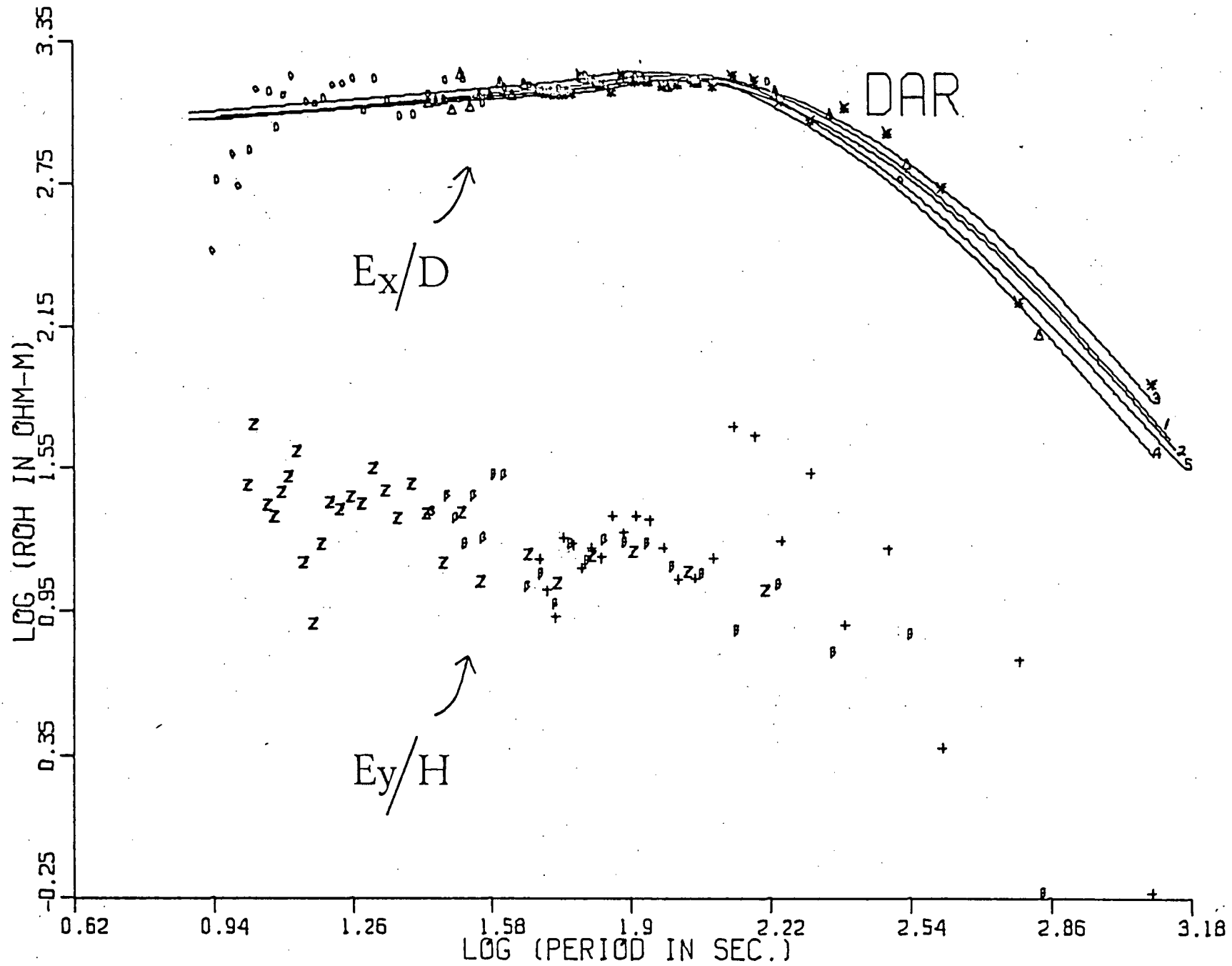


Table 4a Model curve parameters used at Alta Lake

Model	h_1	h_2	h_3	h_4	e_1	e_2	e_3	e_4	e_5
1	1.0	0.45	10.0	1.0	1.0	0.09	8.5	10.0	0.05
2	1.0	0.45	10.0	1.0	1.0	0.09	8.5	10.0	0.02
3	1.0	0.45	10.0	1.0	1.0	0.09	8.0	10.0	0.05
4	1.0	0.45	10.0	1.0	1.0	0.08	9.0	10.0	0.05
5	1.0	0.45	9.0	1.0	1.0	0.09	8.0	10.0	0.12
6	1.0	0.45	10.0	1.0	1.0	0.08	8.0	10.0	0.008
7	1.0	0.45	10.0	1.0	1.0	0.08	8.0	10.0	0.005
8	1.0	0.45	10.0	1.0	1.0	0.09	8.0	10.0	0.01
9	1.0	0.45	10.0	1.0	1.0	0.09	9.0	10.0	0.01
10	1.0	0.45	9.0	1.0	1.0	0.09	9.5	10.0	0.01

Coordinates used in estimating the first layer parameters of the real earth are:

$$\begin{array}{lll}
 T = 5.5 & e = 300 & \text{(EX/D data)} \\
 \text{and } T = 8.4 & e = 1720 & \text{(EY/H data)}
 \end{array}$$

Table 4b Model curve parameters used at Pemberton

Model	h_1	h_2	h_3	h_4	ρ_1	ρ_2	ρ_3	ρ_4	ρ_5
1	1.0	0.45	10.0	1.0	1.0	0.09	8.5	10.0	0.05
2	1.0	0.45	10.0	1.0	1.0	0.09	8.5	10.0	0.02
3	1.0	0.45	10.0	1.0	1.0	0.09	8.0	10.0	0.05
4	1.0	0.45	10.0	1.0	1.0	0.08	9.0	10.0	0.05
5	1.0	0.45	9.0	1.0	1.0	0.09	8.0	10.0	0.12
6	1.0	0.45	10.0	1.0	1.0	0.08	8.0	10.0	0.05
7	1.0	0.45	10.0	1.0	1.0	0.08	8.0	10.0	0.02
8	1.0	0.45	10.0	1.0	1.0	0.09	8.0	10.0	0.05
9	1.0	0.45	10.0	1.0	1.0	0.09	9.0	10.0	0.05
10	1.0	0.45	9.0	1.0	1.0	0.08	9.0	10.0	0.05

Coordinates used in estimating the first layer parameters of the real earth are:

$T = 4.5$ $\rho = 363$ (EX/D data)
 $T = 4.5$ $\rho = 831$ (EY/H data)

Table 4c Model curve parameters used at D'Arcy

Model	h_1	h_2	h_3	h_4	ρ_1	ρ_2	ρ_3	ρ_4	ρ_5
1	1.0	0.05	11.0	0.05	1.0	1.05	8.0	13.0	0.01
2	1.0	0.05	10.0	0.05	1.0	1.05	7.0	12.0	0.01
3	1.0	0.05	11.0	0.05	1.0	1.05	7.0	12.0	0.01
4	1.0	0.05	10.0	0.05	1.0	1.05	7.0	11.0	0.01
5	1.0	0.05	9.0	0.05	1.0	1.05	5.0	7.0	0.01

Coordinates used in estimating the first layer parameters of the real earth are:

$$T = 11.0 \quad \rho = 280 \quad (\text{EX/D data})$$

EY/H resistivity data:

Layer thickness (km)		Layer resistivity (ohm-m)	
h_1	120	ρ_1	1720
h_2	54	ρ_2	155
h_3	1200	ρ_3	14620
h_4	120	ρ_4	17200
h_5	∞	ρ_5	85

Curve 1 has been used in estimating the layer parameters.

Any of the five model curves could have been chosen and they give approximately the same parameter estimates. This is because there are very few data points at the long period end.

Station: PEM

EX/D resistivity data:

Layer thickness (km)		Layer resistivity (ohm-m)	
h_1	40	ρ_1	363
h_2	18	ρ_2	29
h_3	400	ρ_3	2900
h_4	40	ρ_4	3630
h_5	∞	ρ_5	7

Curve 7 has been used in estimating the layer parameters.

There are very few data points at the short and long period bands and hence any of the curves are appropriate. They give roughly the same parameter estimates.

EY/H resistivity data:

Best fitting model curve is curve 1.

Layer thickness (km)		Layer resistivity (ohm-m)	
h_1	61	1	831
h_2	27	2	75
h_3	610	3	7063
h_4	61	4	8310
h_5		5	41

Station: DAR

EX/D resistivity data:

Layer thickness (km)		Layer resistivity (ohm-m)	
h_1	56	1	280
h_2	3	2	294
h_3	616	3	1960
h_4	3	4	3360
h_5		5	3

All the curves fit the experimental data at the short and intermediate periods, but curve 3 shows the best fit at the long period band and hence has been used in estimating the layer parameters.

The curves give roughly the same parameter estimates.

EY/H resistivity data:

These data could not be modelled because of the large scatter in them.

Although a five-layered mathematical model as shown above provides a suitable fit to the experimental data at the stations, it should be remarked that at ALT and PEM the third and fourth layers will be practically indistinguishable. Similarly, at DAR the second and fourth layers will not be practically resolved since there is insufficient contrast between either layer and the one immediately above. Thus, the

real earth structure at ALT and PEM corresponds to four layers. That at DAR corresponds to three layers. Fig. 27 shows the proposed, two-dimensional conductivity model for the whole area.

On the basis of the above structure, the apparent discrepancy between the EX/D and EY/H data can be explained by the fault zone near PEM which in this preliminary interpretation has been considered vertical. The wider displacement between the EX/D and EY/H curves at DAR as compared to ALT is due to the fact that ALT is nearer the fault zone than DAR. It should be noted that the general structural trend of the Pemberton area is NW and hence EX is more nearly normal to the structure than EY. This is because EX is in the geomagnetic NS direction and the magnetic declination is about 23°E . Thus, EX/D data results have been used in Fig. 27 since they will characterise any lateral structural change better than EY/H.

The Z-transfer function plots at each station (Figs. 28 to 30) show a fairly large scatter, particularly at the short periods. On the average, the magnitude of the Z-transfer function is small. The nature of this function is quite similar at all the stations at the long periods. This indicates that inhomogeneity does not exist at large depths.

In Fig. 31a, which shows the power ratios Z/H at each station, it can be seen that at the long period (low frequency) end these ratios are quite similar at all the stations and are generally less than 0.2. These ratios are greater than 0.5 at the short period end. The increase in Z/H at the short periods is probably due to cultural noise. The power attenuation ratio plots (with PEM as reference) in Fig. 31b show a fairly large scatter and are less than unity at the short and long periods but higher in the intermediate band (about 30 to 120 seconds). The power attenuation ratios are slightly higher at DAR than at ALT indicating that the Z power increases slightly from ALT towards

FIG 27 The derived MT model for the Pemberton area.

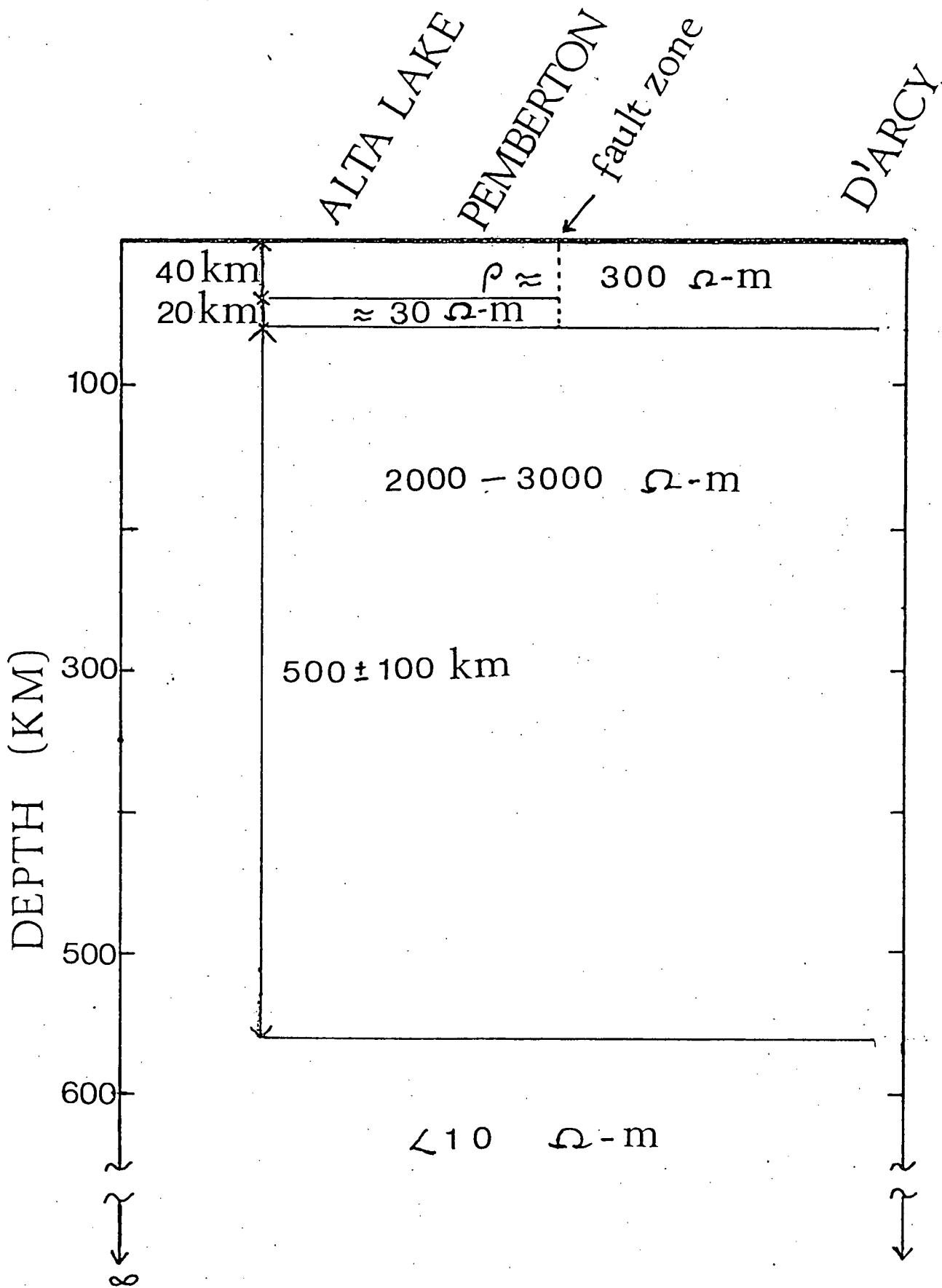
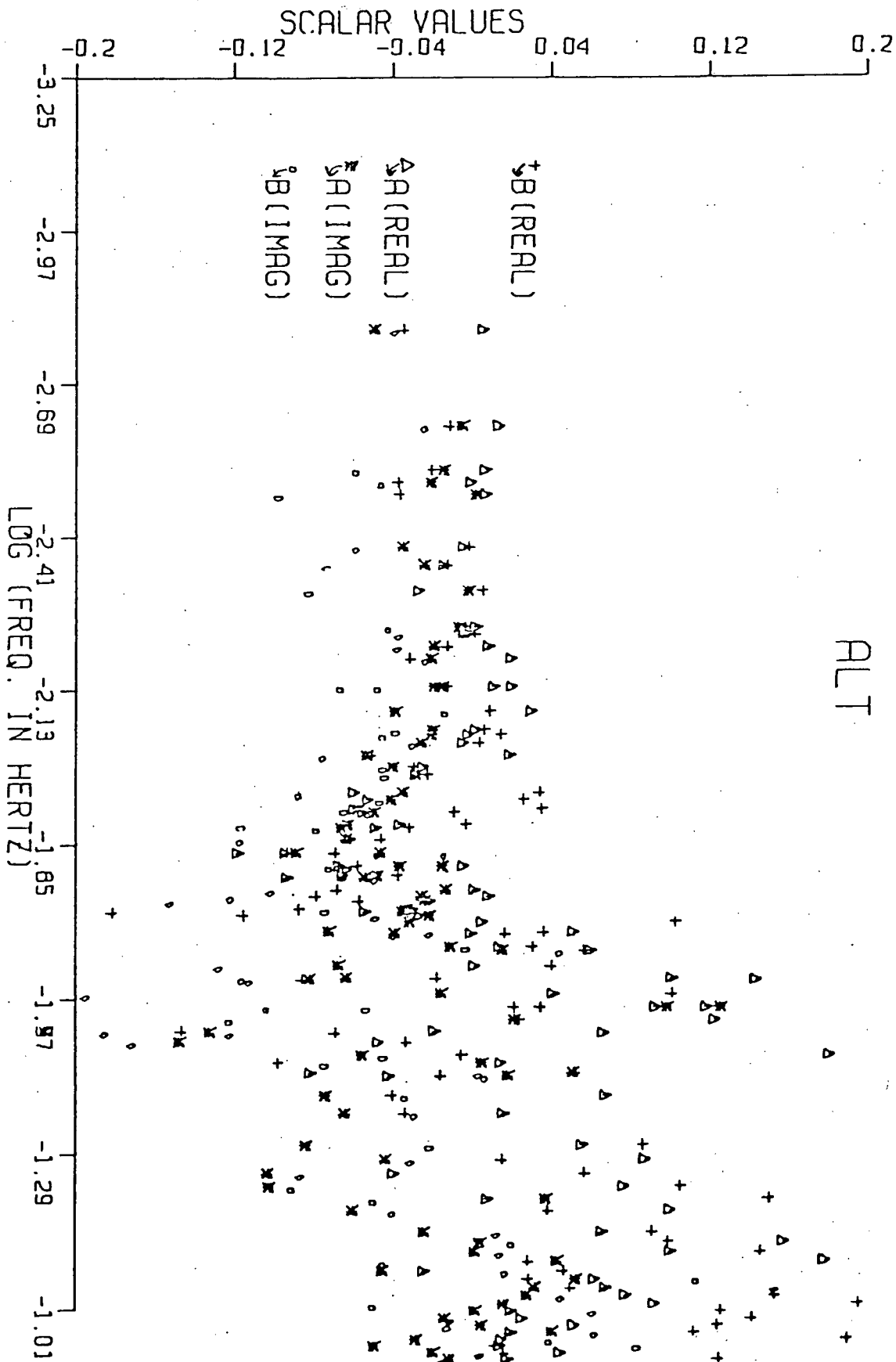
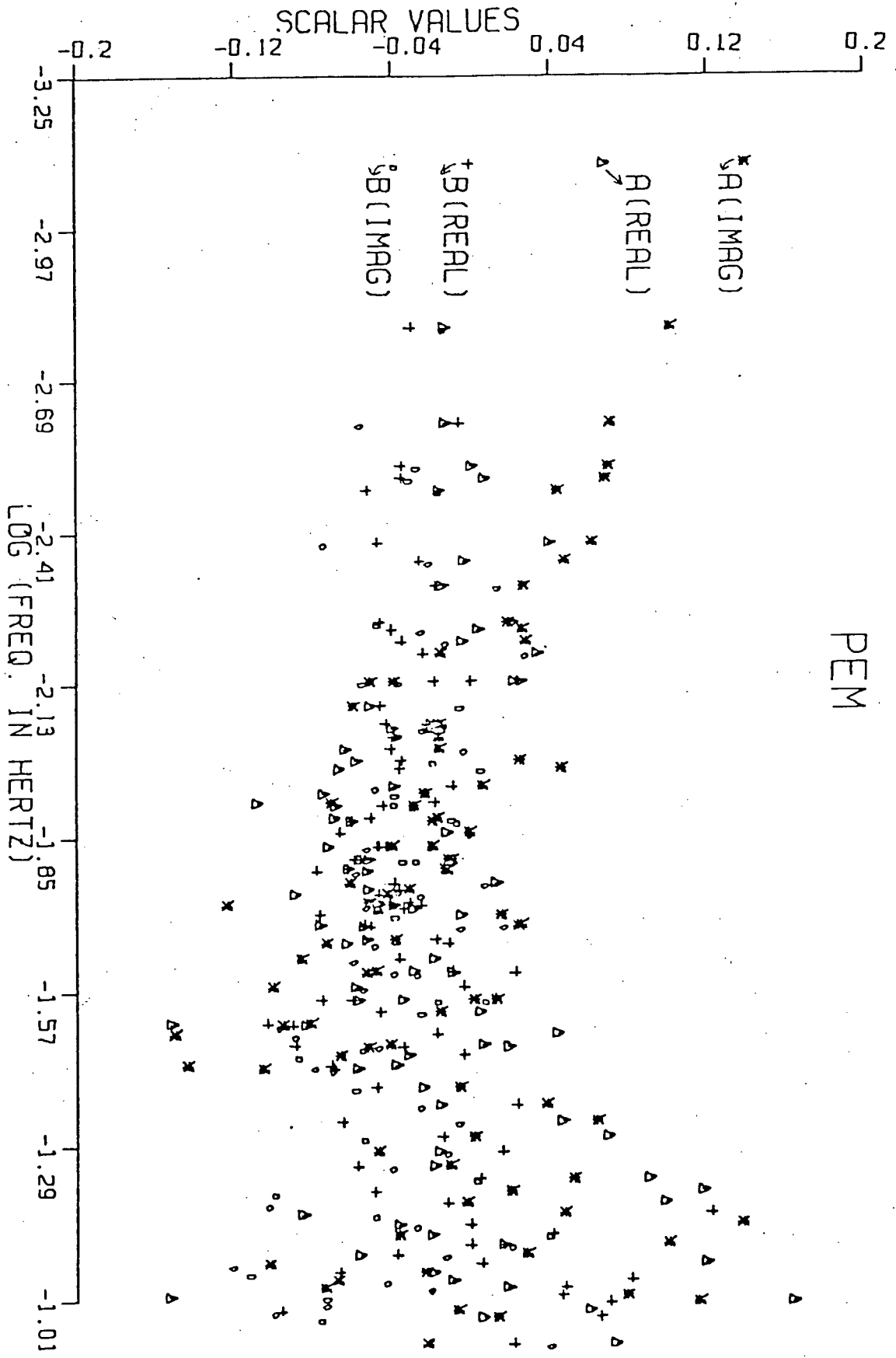


FIG. 28 Z - transfer function at Alta Lake.



ALT

FIG. 29 Z - transfer function at Pemberton.



PEM

FIG. 30 Z - transfer function at D'Arcy.

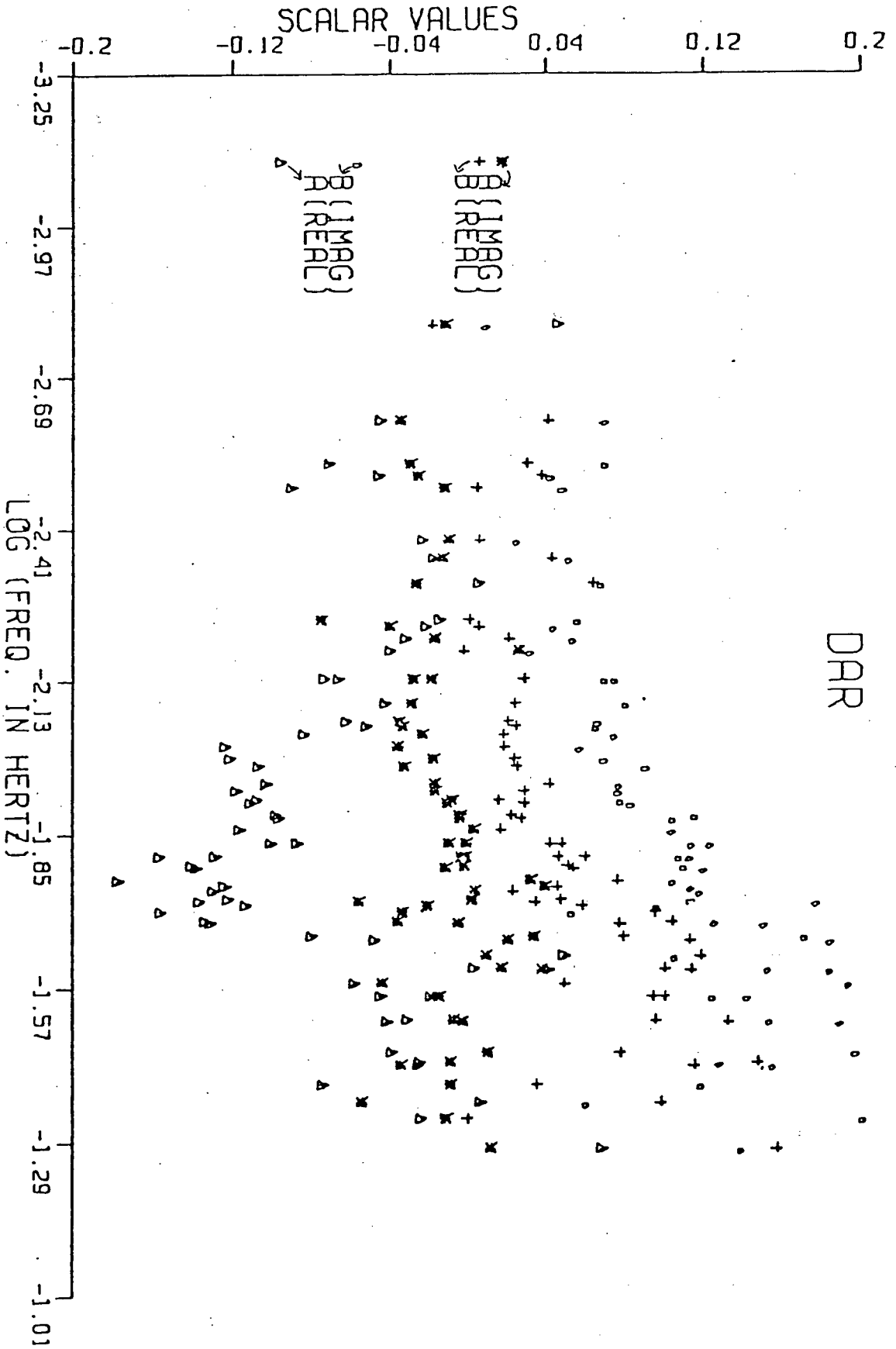


FIG. 31A Power ratios, Z/H at each station.

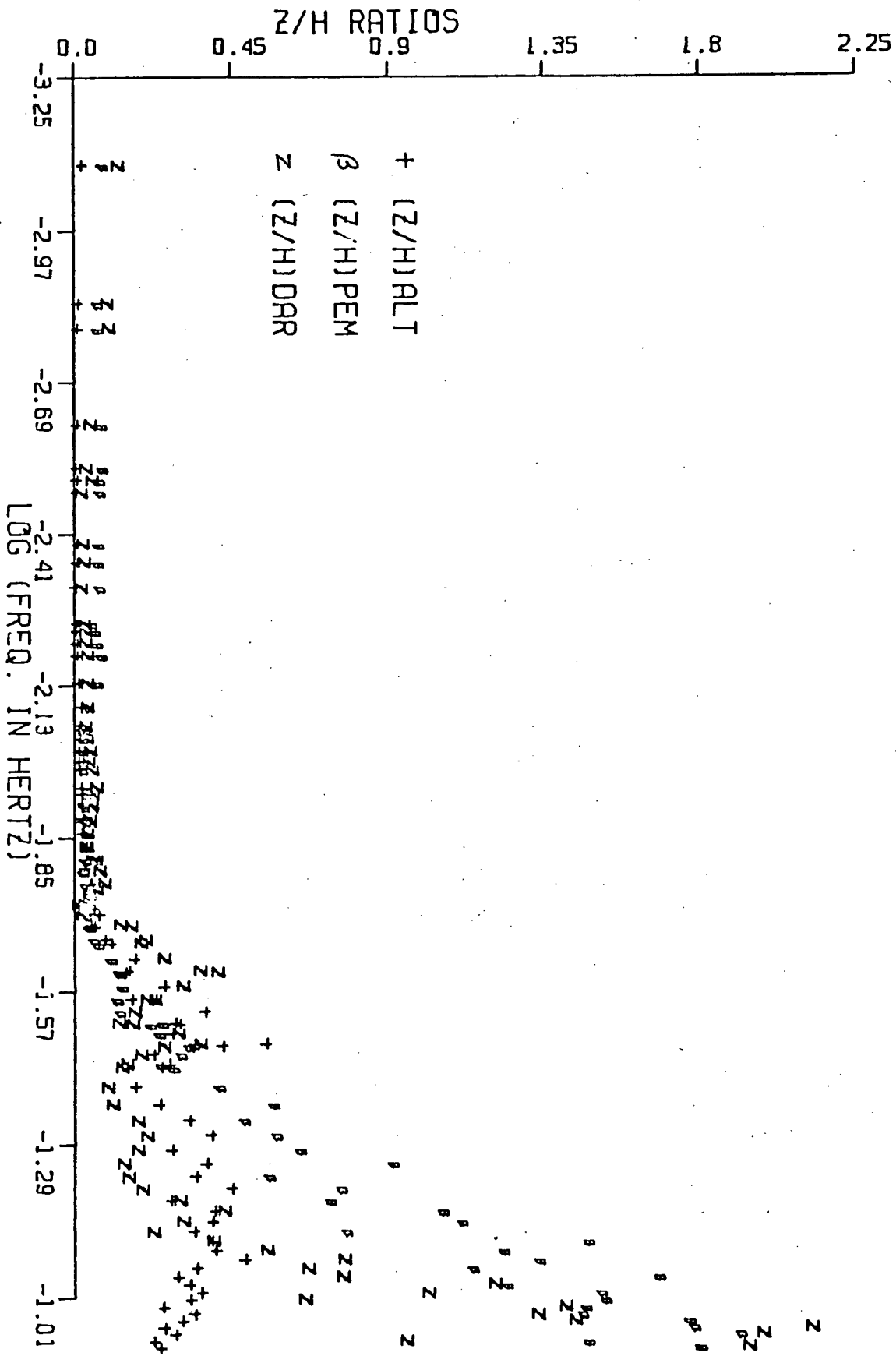
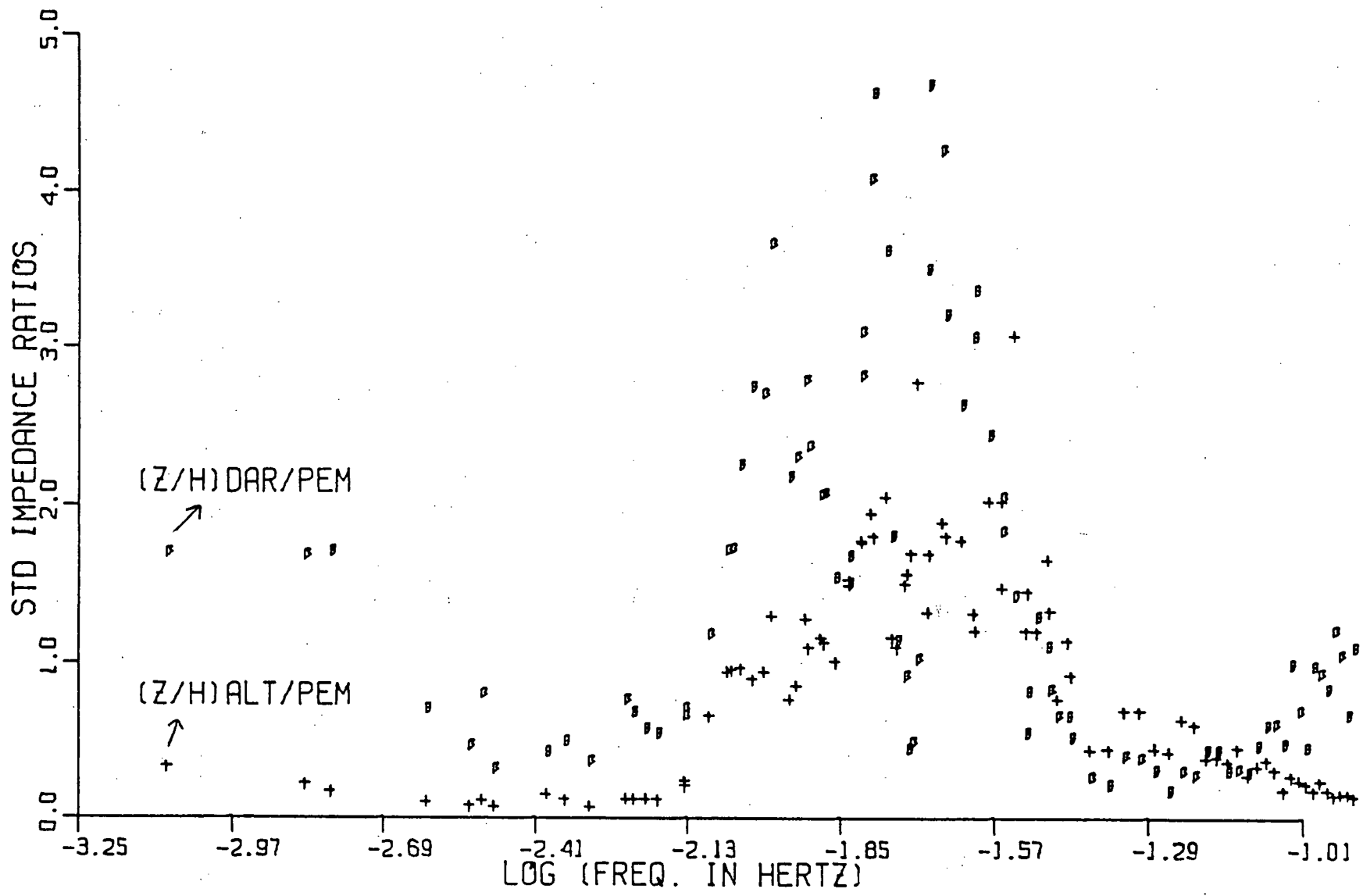


FIG. 31B Power attenuation (standard impedance) ratios.



DAR. The same result may be inferred from the plot of the ratios of the Z power at ALT and DAR to that at PEM (Fig. 31c). From the relative H power ratios (a plot of these is not presented) between stations, it was observed that:

at the long periods	H_{ALT}	>	H_{DAR}	>	H_{PEM}
at the intermediate periods	H_{ALT}	<	H_{PEM}	<	H_{DAR}
and at the short periods	H_{DAR}	>	H_{ALT}	>	H_{PEM}

This H variation cannot be explained by the small geomagnetic latitude differences between the stations, however, it is consistent with the derived MT model (Fig. 27).

From all of the above, it can be inferred that there is a structural change near PEM which does not persist at large depths. The nature of the variation of the Z and H power, particularly the latter, with period indicates a more complex structural change than the vertical fault considered in the MT model, possibly a sloping interface.

It should be noted that the exact nature and extent of the deduced fault zone are not delineated in this work. The latter involves more sophisticated techniques (e.g. modelling the Z-transfer function) beyond the scope of the present preliminary investigation. The domain of the effect of the fault zone is within the intermediate period range (about 30 to 120 second).

5.3 CONCLUSIONS

It is worthwhile to compare the present results with the MT results of Caner and Auld (1968) for Victoria, British Columbia and Caner et al. (1969) in the Intermontane Belt of the Canadian Cordillera. The results of the latter at Penticton and Grand Forks indicate a resistive crustal upper layer, 250 ohm-m or higher with no upper limit and a thickness of 15 km, a conductive second layer of 10 ohm-m resistivity and 20 to 40 km in thickness and a basement of 30 to 50 ohm-m resistivity (Fig. 32A). Thus, it can be seen that our model differs significantly from that of Caner et al. (1969) because a thick and highly resistive layer between the second layer and the basement is present in the Pemberton area. Our model compares more favourably with the MT model for Victoria (Caner and Auld, 1968). This latter model shows a conductive layer of thickness about 10 km and 100 - 125 ohm-m resistivity at a depth of approximately 65 km; below this layer is a high resistivity zone of the order of 4000-5000 ohm-m (Fig. 32B). This high resistivity zone is very similar to that found in the Pemberton area.

It should be noted that very little is presently known about the tectonics of the Pemberton area and on account of the rugged terrain, gravity work has not yet been done. Thus, it is difficult to determine whether the thick highly resistive layer in our MT model is consistent with present or past tectonics in the area. However, Hyndman (1976) has reported high heat flow inland in southwestern British Columbia which he attributes to present (or recent) subduction of the oceanic Juan de Fuca plate under the continent. The observed high resistivities with depth at Victoria and in the Pemberton area may be related to this plate wedged beneath the region.

FIG. 31c Ratios of the power in the Z components at Alta Lake and D'Arcy to that at Pemberton. These are $Z(\text{ALT})/Z(\text{PEM})$ and $Z(\text{DAR})/Z(\text{PEM})$ respectively.

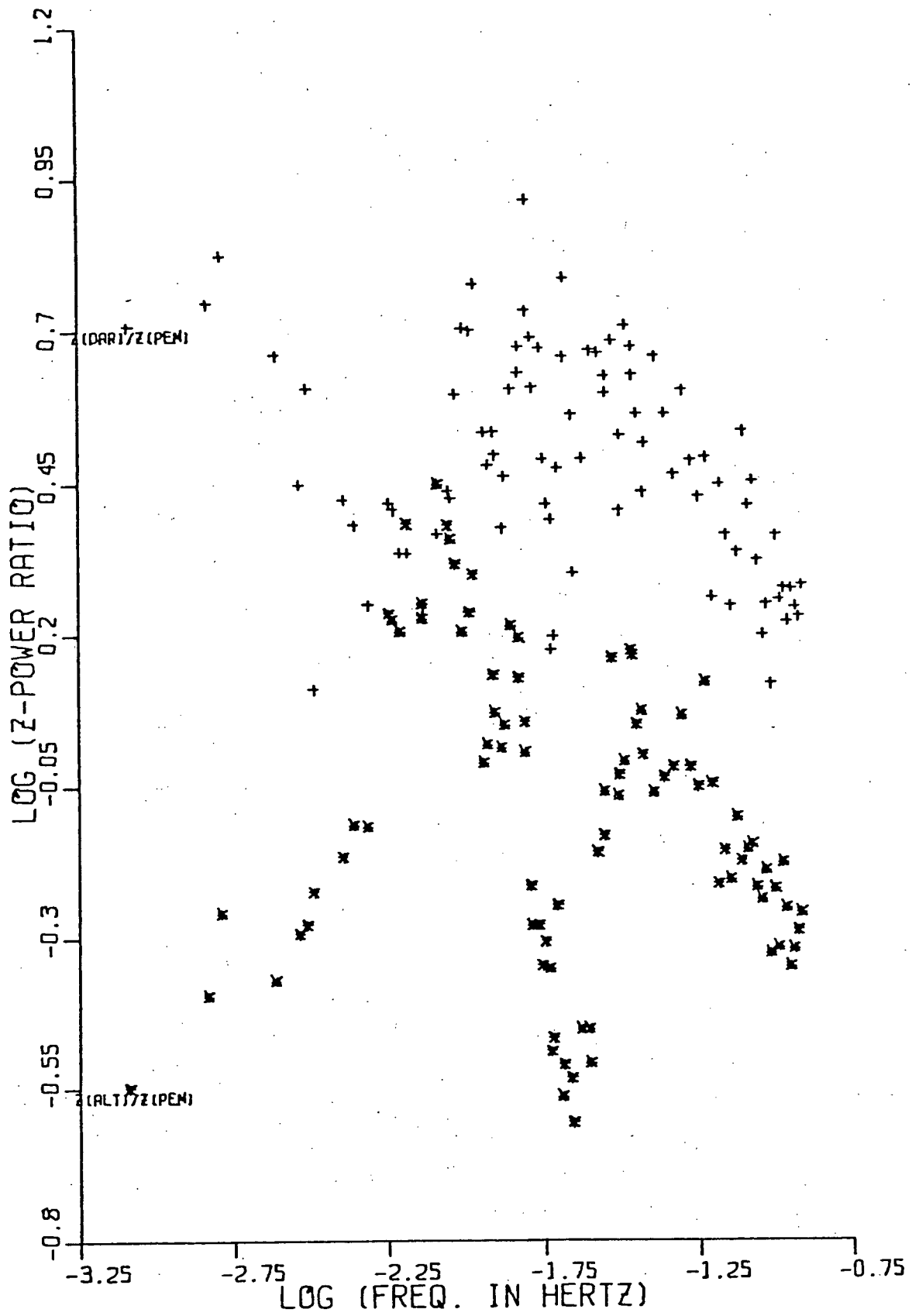
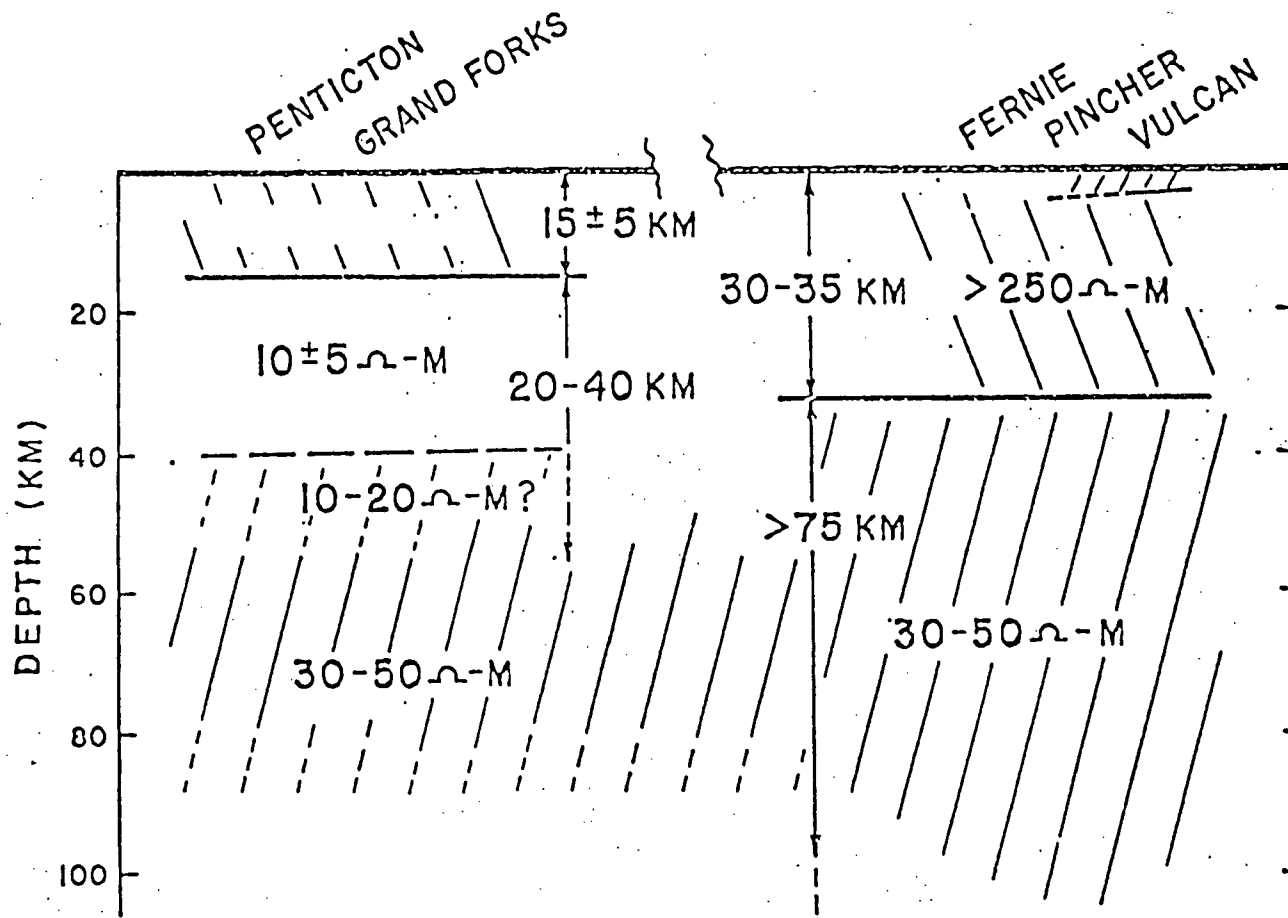
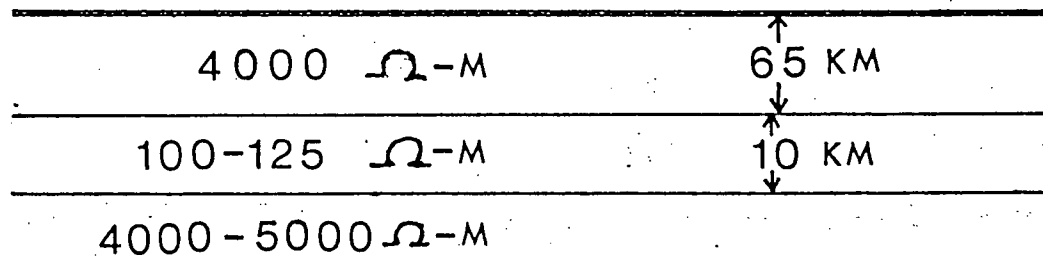


FIG. 32 (A) MT structural model of Western Canada by Caner et al. (1969)
(B) MT structural model for Victoria by Caner and Auld (1968)

(A)



(B)



The results obtained from the earth model best fitting the apparent resistivity data in the region investigated in this project can be summarised as follows:

(1) A resistive crustal upper layer is inferred. Its resistivity is of the order of 300 ohm-m and its thickness is about 40 km under ALT and PEM and about 60 km under DAR.

(2) The resistive crust at ALT and PEM is underlain by a more conductive material of resistivity about 30 ohm-m and a thickness of approximately 20 km. There is no trace of this layer at DAR. The resistivity value of this layer is of the same order of magnitude as the values usually reported from regions of geothermal investigations.

(3) The next layer at all the stations is highly resistive, of the order of 2000 to 3000 ohm-m and a thickness of 500 ± 100 km. This is underlain by a highly conductive basement, about 10 ohm-m or less.

(4) From the power attenuation ratios and the relative Z power ratios between stations, it is inferred that the Z power increases slightly from ALT towards DAR. This is in accordance with expectation. Z should be more attenuated at ALT and PEM than at DAR because of the presence of the conductive second layer at ALT and PEM. Also, Z at PEM should be higher than ALT because of the presence of the fault zone near PEM.

(5) From the Z-transfer function and the power attenuation ratios, it is inferred that any inhomogeneity does not persist to large depths.

(6) From their southern seismic refraction profile running from Nitinat to Greenbush (less than 100 km south of our MT profile),

Berry and Forsyth (1975) have reported that the crust along the eastern edge of the Coast Range Plutonic Complex is 33 km thick. Thus, our MT results seem to indicate a resistivity change close to the crust and upper mantle boundary. The highly resistive layer (greater than 2000 ohm-m) in the upper mantle is quite similar to the reported MT results by Caner and Auld (1968) and Nienaber et al. (1973).

From the overall results, it is evident that there is a resistivity change across the structural boundary of the Pemberton volcanic belt. In this work, this conductivity change has been designated as a vertical fault. We have thus delineated some of the structural control in the Pemberton area. Although some of the discrepancy between the EX/D and EY/H apparent resistivity curves may be due to near surface inhomogeneities and the physical topography of the area, the bulk of this difference can be explained by the presence of the fault zone near PEM.

It is quite gratifying to note that the results of the simple layered earth interpretation presented here are similar to those of Caner and Auld (1968), but only have some resemblance to those of Caner et al. (1969) as shown above. Our stations are geographically located between those of Caner and Auld (1968) and Caner et al. (1969).

SUGGESTIONS FOR FURTHER WORK

On the basis of this study I would suggest that

- (1) A detailed structural geological study as well as a petrological study of the area be undertaken.
- (2) A detailed resistivity investigation be undertaken near PEM to determine the nature and extent of the structural change deduced in the present work.
- (3) MT/GDS work be done in at least two stations, one north of DAR and the other south of ALT, to determine the conductivity structure beyond the area investigated here.

By integrating all the above results together, it is anticipated that a detailed structural model can be constructed. This will significantly aid in the investigation of both known and unknown geothermal areas.

BIBLIOGRAPHY

- Baker, W. G. and Martyn D. F.,
The conductivity of the ionosphere, *Nature*, 170, p. 1090,
1952.
- Berdichevsky M. N.,
Electric prospecting by the telluric current method,
Gostoptekhizdot, Moscow, 1960.
- Berry M. J. and Forsyth D. A.,
Structure of the Canadian Cordillera from seismic refraction
and other data, *Can. J. Earth Sci.*, 12, 182-208, 1975.
- Bostick F. X. and Smith H. W.,
Investigation of large-scale inhomogeneities in the earth by
the magnetotelluric method, *Proc. Inst. Radio Eng.*, 50,
2339-2346, 1962.
- Cagniard L.,
Basic theory of the magnetotelluric method of geophysical
prospecting, *Geophysics*, 18, 605-635, 1953.
- Cairnes C. E.,
Pemberton Area, Lillooet District, B.C., GSC summary reports
1924A, 76-79, 1924.
- Campbell W. H.,
Geomagnetic pulsations, article in *Physics of geomagnetic
phenomena*, Academic Press, New York, 1967.
- Camsell C.,
Reconnaissance along the Pacific Great Eastern Railway
between Squamish and Lillooet, GSC summary reports 1917B,
12B-28B, 1917.
- Caner B.,
Electrical conductivity structure of the lower crust and
upper mantle in Western Canada, Ph. D. thesis, Univ. of
British Columbia, 1969.
- Caner B. and Auld D. R.,
Magnetotelluric determination of upper mantle conductivity
structure at Victoria, British Columbia, *Can. J. Earth Sci.*,
12, 1209-1220, 1968.
- Caner B., Camfield P. A., Andersen F. and Niblett E. R.,
A large-scale magnetotelluric survey in Western Canada,
Can. J. Earth Sci., 6, 1245-1261, 1969.

- Caner B., Cannon W. H. and Livingstone C. E.,
Geomagnetic depth-sounding and upper mantle structure in the
Cordillera region of western North America, *J. Geophys. Res.*,
72, 6335-6351, 1967.
- Caner B. and Dragert H.,
Instrumentation for wide-frequency-band (0.01 - 100
millihertz) Geomagnetic induction work, *Zeitschrift für,
Geophysik* (now called *J. Geophys.*), Band 38, 121-132,
1972.
- Cantwell T.,
Detection and analysis of low frequency magnetotelluric
signals, Ph. D. thesis, M. I. T., Cambridge, Mass., 1960.
- Chetaev D. N.,
The determination of the anisotropy coefficient and the
angle of inclination of a homogeneous anisotropic medium,
by measuring the impedance of the natural electromagnetic
field, *Bull. (Izv.) Acad. Sci. USSR, Geophys. Ser. No. 4*,
617-619, 1960.
- D'Erceville I. and Kunetz G.,
The effect of a fault on the earth's natural electromagnetic
field, *Geophysics*, 27, 651-665, 1972.
- Dosso H. W.,
Analogue model measurements for electromagnetic variations
near vertical faults and dykes, *Can. J. Earth Sci.*, 3,
287-303, 1966a.
- Dragert H.,
Broad-band geomagnetic depth-sounding along an anomalous
profile in the Canadian Cordillera, Ph. D. thesis,
Univ. of British Columbia, 1973.
- A field evaluation of Caner's Broad-Band geomagnetic
induction instrumentation, *J. Geophys.*, 40, 121-129,
1974.
- Everett J. E. and Hyndman R. D.,
Geomagnetic variations and electrical conductivity in
southwestern Australia, *Phys. Earth Planet. Int.*, 1,
24-34, 1967.

- Grant F. S. and West G. F.,
Interpretation theory in applied geophysics, McGraw-Hill
Book Co., 1965.
- Hasegawa H.,
Magnetotelluric studies in Central Alberta, M. Sc. thesis,
Univ. of Alberta, 1962.
- Jacobs, J. A.,
Physics and Chemistry in space, Vol. 1, Springer-Verlag,
1970.
- Jacobs, J. A., Kato Y., Matsushita S. and Troitskaya V. A.,
Classification of geomagnetic pulsations, J. Geophys.
Res., 69, 180-181, 1964.
- Jacobs J. A. and Sinno K.,
Occurrence frequency of geomagnetic micropulsations, Pc.
J. Geophys. Res., 65, 107-133, 1960a.
- World-wide characteristics of geomagnetic micropulsations,
Geophys. J., 3, 333-353, 1960b.
- Jones D. S.,
The theory of electromagnetism, Ch. 6, Macmillan Co.,
New York, 1964.
- Kato Y. and Kikuchi T.,
On the phase difference of earth currents induced by
changes of the earth's magnetic field, Parts I and II,
Sci. Reports of Tohoku Univ., Ser. 5, Geophys. J.
139-145, 1950.
- King P. B.,
Tectonic map of North America: U. S. Geological Surv.,
1969.
- Kovtun A. A.,
The magnetotelluric investigation of structures inhomogeneous
in layers, Bull. (Izv.) Acad. Sci. USSR, Geophys. Ser.
No. 11, 1663-1667, 1961.
- Madden T. and Nelson P.,
A defence of Cagniard's magnetotelluric method, Project
NR-371-401, Geophys. Lab., M. I. T., 1964.

- Mann, J. E. (Jr.)
Magnetotelluric theory of sinusoidal interface, J. Geophys. Res., 69, 3517-3524, 1964.
- The importance of anisotropic conductivity in magnetotelluric interpretation, J. Geophys. Res., 70, 2940-2942, 1965.
- Mathews W. H.,
Geology of the Mount Garibaldi map-area, southwestern B.C., Canada. Pt2: Geomorphology and Quaternary volcanic rocks: Geol. Soc. Amer. Bull., 69, 1974-198, 1958.
- Monger J. W. H., Souther J. G. and Gabrielse H.,
Evolution of the Canadian Cordillera: A plate-tectonic model, Amer. J. Sci., 272, 577-602, 1972.
- Nasmith H., Mathews W. H. and Rouse G. E.,
Bridge River ash and some other recent ash beds in British Columbia, Can. J. Earth Sci., 4, 163-170, 1967.
- Ney C. S.,
Geological and Geochemical Report on the VAN Claims, British Columbia: B. C. Department of Mines Assessment Report, open file, 1968.
- Nienaber W., Auld D. R. and Dosso H. W.,
Analysis of Anisotropic Magnetotelluric Measurements at Victoria, B. C., Can. J. Earth Sci., 10, 557-570, 1973.
- Nourry G. R.,
Interplanetary magnetic field, solar and geomagnetic micropulsations, Ph. D. thesis, Univ. of British Columbia, 1976.
- O'Brien D. P. and Morrison H. F.,
Electromagnetic fields in an N-layer anisotropic half-space, Geophysics, 32, 668-677, 1967.
- Pokityanski I. I.,
On the application of the magnetotelluric method to anisotropic and inhomogeneous masses, Bull. (Izv.) Acad. Sci. USSR, Geophys. Ser. No. 11, 1607-1613, 1961.
- Price A. T.,
The theory of magnetotelluric methods when the source field is considered, J. Geophys. Res., 67, 1907-1918, 1962.
- Price R. A. and Douglas R. J. W.,
Variations in tectonic styles in Canada, Geol. Assoc. of Canada Special Paper No. 11, 1972.

- Quon C.,
Electromagnetic fields of elevated dipoles on a two-layer earth, M. Sc. thesis, Univ. of Alberta, 1963.
- Rankin D.,
The magnetotelluric effect of a dyke, *Geophysics*, 27, 666-676, 1962.
- Rankin D., Garland G. D. and Vozoff K.,
An analogue model for the magnetotelluric effect, *J. Geophys. Res.*, 70, 1939-1945, 1965.
- Raspopov O. M.,
Possible excitation mechanism of type Pi 2 geomagnetic field pulsations, *Geomagn. and Aeronomy*, 8, 257-260, 1968.
- Reddy I. K.,
Magnetotelluric sounding in Central Alberta, Ph. D. thesis, Univ. of Alberta, 1970.
- Rikitake T.,
Electromagnetic induction within the earth and its relation to the electrical state of the earth's interior, *Bull. Earthq. Res. Inst. Tokyo*, 28, 45-98, 1950.
- Changes in earth currents and the relation to the electrical state of the earth's crust, *Bull. Earthq. Res. Inst. Tokyo*, 29, 270-275, 1951.
- Roy A.,
Ambiguity in geophysical interpretation, *Geophysics*, 27, 90-100, 1962.
- Schelkunoff S. A.,
Electromagnetic waves, Ch. 4, D. Van Nostrand Co., New York, 1943.
- Sinha A. K. and Bhattacharya P. K.,
Electric dipole over an anisotropic and inhomogeneous earth, *Geophysics*, 32, 652-667, 1967.

Souther J. G.,

Acid volcanism and its relationship to the tectonic history of the Cordillera of B. C., Canada, Bull. Volcanol., 30, 161-176, 1967.

Tectonic implications of volcanism in the Cordillera of North America (Abs.), Univ. of Alaska, Geophys. Inst., Inaugural Symposium Geophys. and Geol. of Bering Sea region, 1970a.

Volcanism and its relationship to recent crustal movements in the Canadian Cordillera, Can. J. Earth Sci., 7, No. 2, 553-568, 1970b.

Geothermal Power, the Canadian Potential, Geoscience Canada, 14-20, 1976.

Srivastava S.P.,

Method of interpretation of magnetotelluric data when source field is considered, J. Geophys. Res., 70, 945-954, 1965.

Magnetotelluric two and three layer master curves, Publ. Dominion Obs. Ottawa, Vol. 35, No. 7, 1967.

Stratton J. A.,

Electromagnetic theory, McGraw-Hill Book Co., New York, 1941.

Tikhonov A. N.,

Determination of the deep state of the earth's crust, Dok. Akad. Nauk. USSR, 73, No. 2, 295-297, 1950.

Trigg D. F.,

An automatic zero suppression circuit, Rev. of Sci. Instr., 41, 1298-1302, 1970.

Trigg D. F., Serson P. H. and Campfield P. A.,

A solid-state electrical recording magnetometer, Publ. Earth Phys. Branch, Ottawa, 41, No. 5, 67-80, 1971.

Troitskaya V. A.,

Micropulsations and the state of the magnetosphere, article in Solar-Terrestrial Phys., Academic Press, London, 1967.

Vladimirov N. P.,

The feasibility of using the earth's natural electromagnetic field for geological surveying, Bull. (Izv.) Acad. Sci. USSR, Geophys. Ser. No. 1, 139-141, 1960.

- Volker H.,
Observations of geomagnetic pulsations Pc 3, 4 and Pi 2 at different latitudes, *Ann. Geophys.* 24, 245-252, 1968.
- Vozoff K.,
The magnetotelluric method in the exploration of sedimentary basins, *Geophysics*, 37, 98-141, 1972.
- Wait J. R.,
On the relation between telluric currents and the earth's magnetic field, *Geophysics*, 19, 281-285, 1954.
- Theory of magnetotelluric fields, *J. Res. National Bureau Std.*, Vol. 66D, No. 5, 509-541, 1962.
- Weaver J. T.,
The electromagnetic field within a discontinuous conductor with reference to geomagnetic micropulsations near a coast line, *Can. J. Phys.*, 41, 484-495, 1963.
- Wright J. A.,
Anisotropic apparent resistivities arising from non-homogeneous two dimensional structures, *Can. J. of Earth Sci.*, 7, 527-531, 1970.
- Yungul S. H.,
Magnetotelluric sounding three-layer interpretation curves, *Geophysics*, 26, 465-473, 1961.

Appendix A

Basic magnetotelluric theory

In this section, the basic MT equation of Cagniard (1953) is derived.

The following assumptions are made in the derivation of the equation:

- (1) Micropulsations are plane electromagnetic waves.
- (2) The incident waves are normal to the earth's surface.
- (3) The earth is a homogeneous, isotropic and source-free half-space (Fig. 33)
- (4) The electric field is plane polarised in the x -direction and the magnetic field in the y -direction.
- (5) A time factor of the form $\exp(-i\omega t)$ is used.

For an isotropic medium, the time independent field equation

(SI units) is

$$\nabla^2 \underline{E} + \omega^2 \mu \epsilon \left(1 + \frac{i\sigma}{\omega \epsilon} \right) \underline{E} = 0 \quad (A1)$$

In the earth, for MT frequencies of interest,

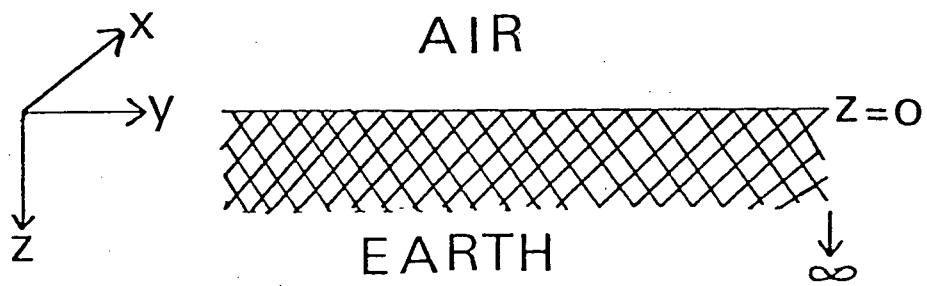
$$\frac{\sigma}{\omega \epsilon} \gg 1$$

— this implies that the displacement currents are negligible compared to the conduction currents.

Thus, (A1) reduces to

$$\nabla^2 \underline{E} = -i\omega \mu \sigma \underline{E} \quad (A2)$$

FIG. 33 Model of source-free, homogenous and isotropic half-space.



Under the stated assumptions above, (A2) becomes

$$\frac{d^2 E_x}{dz^2} = K^2 E_x \quad (A3)$$

where $K^2 = -i\omega\sigma\mu$ (A4)

Also from Maxwell's equations

$$\text{Curl } \underline{E} = i\omega\mu \underline{H}$$

implying that

$$H_y = \frac{1}{i\omega\mu} \frac{d}{dz} E_x \quad (A5)$$

Since the fields originate from a source above the earth's surface, then all the field quantities must remain finite at $z = \infty$. Hence, the solution of (A3) is

$$E_x = N e^{-Kz} \quad (A6)$$

From (A4), (A5) and (A6)

$$\begin{aligned} \frac{E_x}{H_y} &= -\frac{i\omega\mu}{K} \\ &= i\sqrt{i\omega\mu/\sigma} \\ &= i\sqrt{2\pi i\mu/\sigma} T \end{aligned} \quad (A7)$$

where T is the period of the EM waves, μ is the permeability and σ is the conductivity. The intrinsic impedance (Schelkunoff, 1943) of the medium is given by

$$\left. \frac{E_x}{H_y} \right|_{z=0}$$

and it has the expression given in (A7). From (A7), it can be seen that in the case of an isotropic, homogeneous half-space, the magnetic field lags behind the electric field by $\pi/4$ radians and that the intrinsic impedance is a function of the period, T , of the waves and also depends on the conductivity of the medium. The resistivity of the medium in SI unit can be obtained from (A7) as a function of period:

$$\rho = \frac{1}{\sigma} = \left| \frac{E_x}{H_y} \right|^2 \frac{T}{2\pi\mu}$$

Similarly

$$\rho = \left| \frac{E_y}{H_x} \right|^2 \frac{T}{2\pi\mu} \quad (A8)$$

Thus, if the medium resistivity is uniform, the expressions on the right-hand side of (A8) must be constant. The basic equation obtained by Cagniard (1953) for the MT method using practical EM system of units is

$$\rho = 0.2 T \left| \frac{E_x}{H_y} \right|^2 \quad (A9)$$

where

ρ = apparent resistivity (ohm-m),

E_x = variation in the horizontal electric field (mv/km),

H_y = variation in the horizontal magnetic field (γ),

T = period (seconds).

It should be noted that (A8) and (A9) are identical as long as the appropriate units in either system are adhered to.

The depth of penetration or skin depth, P is equal to $1/\text{Real } K$. Hence, from (A4) P (in metres) is given by

$$P = \sqrt{\frac{2}{\mu\omega\sigma}} = \sqrt{\frac{T\rho}{\pi\mu}} \quad (A10)$$

In the practical EM units, P (in kilometres) is given by

$$P = \frac{1}{2\pi} \sqrt{10\rho T} \quad (A11)$$

Appendix B

MT fields over an n-layered,
homogeneous and isotropic earth

The real earth is far from being an isotropic half-space and hence, the MT equation applicable to an n-layered earth was developed by Berdichevsky (1960). Following a similar formalism used by Reddy (1970), the apparent resistivity for an n-layered isotropic half-space can be obtained as follows:

Consider the n-layered earth model shown in Fig. 34 with coordinate axes as shown where $z = 0$ corresponds to the earth's surface. Each of the parallel layers is assumed to be isotropic, with ϵ and μ constant and the bottom layer (n^{th}) is assumed to extend to infinity, that is, a semi-infinite layer. Considering layer L and assuming plane EM waves impinging on the source-free earth, then equation (A3) takes the form (a time factor $\exp(-i\omega t)$ is assumed as in Appendix A):

$$\frac{d^2 E_{x,L}}{dz^2} = K_L^2 E_{x,L} \quad (\text{B1})$$

$$\text{where } K_L^2 = -i\omega\sigma_L\mu \quad (\text{B2})$$

and σ_L is the conductivity of the L^{th} layer.

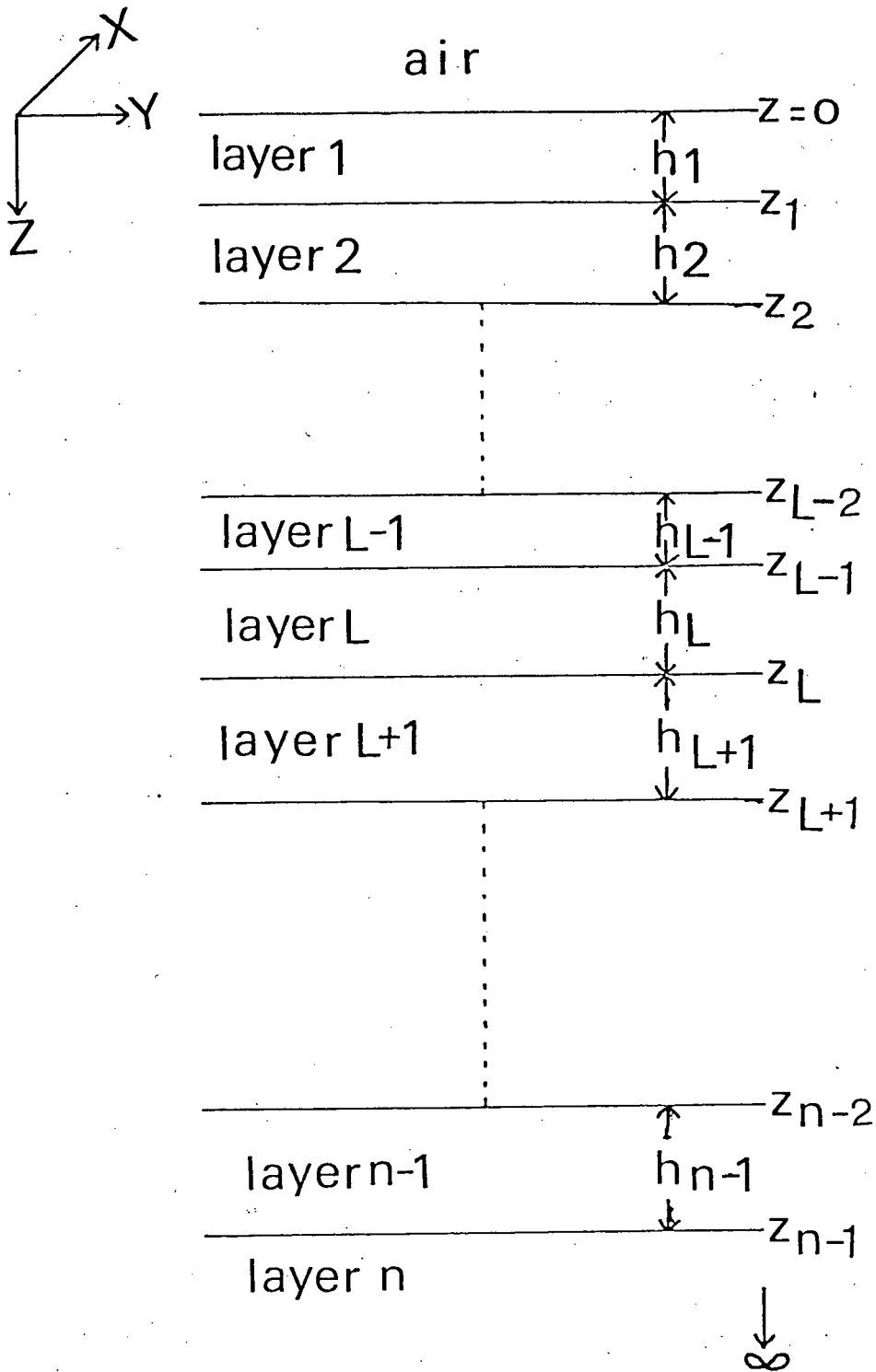
According to Jones (1964), the solution of (B2) will be of the form:

$$E_{x,L} = A_L e^{K_L(z-z_{L-1})} + B_L e^{-K_L(z-z_{L-1})} \quad (\text{B3})$$

where A_L , B_L are constants which may be complex. Making use of (A5), the horizontal component of the magnetic field can be obtained

$$\text{from (B3) as } H_{y,L} = \frac{K_L}{i\omega\mu} \left[A_L e^{K_L(z-z_{L-1})} - B_L e^{-K_L(z-z_{L-1})} \right] \quad (\text{B4})$$

FIG. 34 Isotropic n-layered earth model showing layer thickness and resistivity notation used in the theoretical formulation.



At each of the layer boundaries, the tangential components of the electric and magnetic fields must be continuous. Thus, the continuity of E_x and H_y on $Z=Z_{L-1}$ will result in the following equations:

$$E_{x,L-1} = E_{x,L} \quad \text{evaluated at } z = z_{L-1},$$

that is,

$$A_{L-1} e^{K_{L-1} h_{L-1}} + B_{L-1} e^{-K_{L-1} h_{L-1}} = A_L + B_L \quad (\text{B5})$$

and $H_{y,L-1} = H_{y,L}$ evaluated at $z = z_{L-1}$, that is,

$$(A_{L-1} e^{K_{L-1} h_{L-1}} - B_{L-1} e^{-K_{L-1} h_{L-1}}) K_{L-1} = (A_L - B_L) K_L \quad (\text{B6})$$

From (B5) and (B6) it can be shown that

$$A_{L-1} = \frac{1}{2} e^{K_{L-1} h_{L-1}} \left[\left(1 + \frac{K_L}{K_{L-1}}\right) A_L + \left(1 - \frac{K_L}{K_{L-1}}\right) B_L \right] \quad (\text{B7})$$

and

$$B_{L-1} = \frac{1}{2} e^{K_{L-1} h_{L-1}} \left[\left(1 - \frac{K_L}{K_{L-1}}\right) A_L + \left(1 + \frac{K_L}{K_{L-1}}\right) B_L \right] \quad (\text{B8})$$

Since the n^{th} layer extends to infinity ($h_n \rightarrow \infty$), it is required that both the electric and magnetic fields remain finite at infinity. This is equivalent to saying that the waves are travelling only in the positive z -direction. Hence A_n must be taken as zero and B_n can be chosen arbitrarily. Let $B_n = 1$. Consequently, A_{n-1} and B_{n-1} become respectively

$$A_{n-1} = \frac{1}{2} \left(1 - \frac{K_n}{K_{n-1}}\right) e^{-K_{n-1} h_{n-1}}$$

and

$$B_{n-1} = \frac{1}{2} \left(1 + \frac{K_n}{K_{n-1}} \right) e^{-K_{n-1}h_{n-1}} \quad (\text{B9})$$

From the recursion relations B7 and B8, the A_i and B_i can then be determined in all shallower layers. Thus, finally the constants A_1 and B_1 corresponding to the first layer can be obtained as

$$A_1 = \frac{1}{2} e^{-K_1 h_1} \left[\left(1 + \frac{K_2}{K_1} \right) A_2 + \left(1 - \frac{K_2}{K_1} \right) B_2 \right] \quad (\text{B10})$$

and

$$B_1 = \frac{1}{2} e^{K_1 h_1} \left[\left(1 - \frac{K_2}{K_1} \right) A_2 + \left(1 + \frac{K_2}{K_1} \right) B_2 \right] \quad (\text{B11})$$

The continuity of the fields at the air-earth interface ($z = 0$) results in the following equations:

$$E_{x,1} = E_{x,0} = A_1 + B_1 \quad (\text{B12})$$

$$H_{y,1} = H_{y,0} = \frac{K_1}{i\omega\mu} (A_1 - B_1) \quad (\text{B13})$$

From (B12) and (B13), the intrinsic impedance, Z_I of the n-layered earth model is

$$Z_I = \frac{E_x}{H_y} \Big|_{z=0} = \frac{i\omega\mu}{K_1} \frac{A_1 + B_1}{A_1 - B_1} \quad (\text{B14})$$

and the apparent resistivity, ρ^a can be expressed as

$$\begin{aligned} \rho^a &= \frac{T}{2\pi\mu} \left| \frac{E_x}{H_y} \right|^2 \\ &= \frac{T}{2\pi\mu} |Z_I|^2 \end{aligned} \quad (\text{B15})$$

where all the quantities are in SI units.

From a consideration of non-planar waves incident on the earth's surface, Wait (1954) has pointed out that for MT periods longer than 10 seconds and earth conductivity of about 10^{-3} mho/metre, it is probable that the spatial variations of the electric and magnetic fields in a horizontal distance of about 35 km is appreciable since the sources (micropulsations) of the variations of the earth's magnetic field are at heights of the order of 100 km as evidenced from rocket measurements (Baker and Martyn, 1952) and hence necessitate corrections to Cagniard's analysis. The relevant distance varies as $\sqrt{T/\sigma}$ and is of the order of the skin depth in the ground.

From a consideration of the influence of the spatial dimensions of the source field, Price (1962) has shown that for a homogeneous earth of conductivity σ (using practical EM units)

$$\frac{E_x}{H_y} = \frac{i\omega}{\theta}$$

where $\theta^2 = \nu^2 + 4\pi i\sigma\omega$ and ν is the separation constant whose dimension is the inverse of length. In SI units, his result will be of the form:

$$\frac{E_x}{H_y} = \frac{i\omega\mu}{\theta} \quad (B16)$$

where $\theta^2 = \nu^2 + i\omega\mu\sigma$ (B17)

He defined $2\pi/\nu$ as the wavelength of the inducing field. For $\nu=0$, the source is infinitely large corresponding to Cagniard's plane wave solution. Price estimated the smallest and largest values of ν which can occur by equating $2\pi/\nu$ to the circumference of the earth and to 4 times the height of ionospheric currents respectively. He concludes that the range of ν in the fields of natural geomagnetic fluctuations is from $1.6 \times 10^{-9} \text{ cm}^{-1}$ (global fields) to $1.6 \times 10^{-7} \text{ cm}^{-1}$ (local fields). Using dipole sources, Quon (1963) has confirmed this

estimate for the upper limit of ν . Price has pointed out that the depth of penetration will not be significantly affected by the scale of the inducing field if ν is too small compared with $(4\pi\sigma\omega)^{\frac{1}{2}}$ in practical EM units.

Thus, when the source dimensions are taken into account

(B14) is modified as

$$\begin{aligned} Z_{I,S} &= \frac{E_x}{H_y} \Big|_{z=0} \\ &= \frac{i\omega\mu}{\theta} \frac{A_1 + B_1}{A_1 - B_1} \end{aligned} \quad (\text{B18})$$

where θ from (B17) above can be written as

$$\theta = \frac{1}{\sqrt{2}} \left[\left\{ (b^4 + \nu^4)^{1/2} + \nu^2 \right\}^{1/2} + i \left\{ (b^4 + \nu^4)^{1/2} - \nu^2 \right\}^{1/2} \right] \quad (\text{B19})$$

where $b^2 = \mu\omega\sigma$

In this case, the apparent resistivity is

$$\rho_s^a = \frac{I}{2\pi\mu} \left| Z_{I,S} \right|^2 \quad (\text{B20})$$

s in these equations indicates that the influence of the source field is taken into account.

As pointed out by Grant and West (1965), with the exception of water ($\epsilon/\epsilon_0 \doteq 80$) for most rocks and minerals, $\epsilon \doteq 9\epsilon_0$ ($\doteq 8 \times 10^{-11}$ farad per metre) and $\mu \doteq \mu_0$ ($\doteq 1.3 \times 10^{-6}$ henry per metre), where ϵ_0 , μ_0 are permittivity and permeability of empty space. Hence, in all the above equations (Appendices A and B), ϵ can be replaced by ϵ_0 and μ by μ_0 .

It should be noted that anisotropic conductivity and inhomogeneity form an important part of a model for MT interpretation. The anisotropic and inhomogeneous MT theories are not presented in this thesis because these are not specifically used in the present preliminary data interpretation — the n-layered MT theory has been used. For the interpretation of MT data involving anisotropy and inhomogeneity, the standard procedure is to use tensor analysis. This technique is now well developed and for details, the reader is referred to Cantwell (1960), Chetaev (1960), Kovtun (1961), Pokityanski (1961), Bostick and Smith (1962), Weaver (1963), Mann (1964, 1965), Sinha and Bhattacharya (1967) and O'Brien and Morrison (1967).

Appendix C

MT curve matching technique

The procedure of interpreting MT experimental curves using the curve matching technique can be briefly explained as follows:

Consider a standard layered earth model with parameters $\bar{\rho}_1, \bar{\rho}_2, \bar{\rho}_3, \bar{h}_1$ and \bar{h}_2 and let the apparent resistivity at a certain period, \bar{T} be $\bar{\rho}_A$. Let the corresponding parameters for a real earth be denoted by $\rho_1, \rho_2, \rho_3, h_1, h_2, T$ and ρ_A respectively, such that they are related to the standard model by the proportionality factors ρ, h and t in the following way:

$$\begin{aligned} \rho_1 / \bar{\rho}_1 &= \rho_2 / \bar{\rho}_2 = \rho_3 / \bar{\rho}_3 = \rho \\ h_1 / \bar{h}_1 &= h_2 / \bar{h}_2 = h \\ T / \bar{T} &= t \end{aligned} \quad (C1)$$

To satisfy the law of similitude we must have

$$h^2 = \rho t \quad (C2)$$

Once the law of similitude is satisfied, it follows that

$$\rho_A = \rho \bar{\rho}_A \quad (C3)$$

The experimental apparent resistivities are calculated and plotted against period on a logarithmic paper (log-log) using the same scales as the standard curves. By means of translational motions along both axes, a match between the experimental curve, $\rho_A(T)$ and a certain standard curve, $\bar{\rho}_A(\bar{T})$ is obtained. The parameters of the real earth can then be obtained as follows:

(i) Two-layer case

According to (C3), the horizontal line $\bar{P}_A = 1$ reads ρ_1 on the experimental ρ_A - axis and from (C1) $\rho_2 = \bar{\rho}_2 \bar{\rho}_1$, where $\bar{\rho}_2$ is indicated on the standard curve. The vertical line $\bar{T} = 1$ reads T_1 on the experimental T -axis and hence, from (C1)

$$h_1 = \sqrt{\rho_1 T_1}$$

On the other hand, if the vertical line $\bar{T} = 10$ is used and this reads T_{10} then

$$h_1 = \sqrt{\rho_1 T_{10}/10}$$

(ii) Three-layer case

ρ_1, ρ_2 and h_1 are obtained as in the two-layer case. The values of $\bar{\rho}_3, \bar{h}_2$ are indicated on the standard curve and hence from (C1)

$$\rho_3 = \bar{\rho}_3 \rho_1$$

and

$$h_2 = \bar{h}_2 h_1$$

The determination of the layer parameters in the n-layer case follows a similar pattern.

Appendix D

Brief note on Hasegawa's MT program (1962)

(1) It is a 5-layer MT interpretation program based on Cagniard's theory. Finite source dimension effects are neglected.

(2) Periods (seconds), layer thicknesses (km) and layer resistivities (ohm-m) are the inputs to the program and the calculated apparent resistivities are output.

(3) To prevent array overflow on the computer, it is best to specify the parameters of the first layer to be unity and the parameters of the other layers expressed relative to these. This will allow more flexibility.

(4) The program can be used for 3- and 4-layer MT interpretations by specifying the resistivities of the dummy layers to be approximately equal to the adjacent real layers (within about 5%) and their thicknesses to be about 5% of the adjacent ones. This eliminates the risk of getting a zero divisor which will cause the termination of the program on the computer.

It should be noted that the program accepts only non-zero and finite parameters.